5-3-2012

International Joint Conference On Emerging Intelligent Sustainable Technologies

Prof. Srikanta Patnaik Mentor
IRNet India, patnaik_srikanta@yahoo.co.in

International Joint Conference

On

EMERGING INTELLIGENT SUSTAINABLE TECHNOLOGIES

(EISTCON-2012)

VOLUME-2

3rd & 4th May, 2012

Organised By:

Department Of Electrical & Electronics Engineering

Dayananda Sagar College of Engineering

Bangalore-560078, India

&

Interscience Research Network (IRNet)

Bhubaneswar, India

Mail To: irnet.chapter@gmail.com

Venue:

Dayananda Sagar College of Engineering

Shavige Malleswara Hills, Kumaraswamy Layout, Bangalore-560078

About: EISTCON-2012

There is no second thought that the academic and industrial scenario of 21st century is a sphere of knowledge driven by cutting edge technologies. It appears like Sky is the limit for the aspiring generation. The scope of today's amazing technology enables us to diffuse the ideas and transform the living conditions. The prospering dream to master over economic resources available the mankind has developed and categorised a concrete knowledge system that gives solutions and support to socio-economic and techno structural problems of our loving and enriching society. Some disciplines have their own theoretical foundations and some are derived. The growing interdependence of differentiating knowledge from several domains is leading an interdisciplinary approach or a holistic approach in analysing technical or social problems. . The thrust is to propagate new research and learning from experts, practitioners and avid scholars and improving the field of study for future development. The broad framework in which the conference is manifested is to augment and cater to the purpose of those silent laboratories and their relentless insistence for coming out with flying colours. The conference also honours to the most valued and contributing articles through its **"Young Investigator Award"** scheme. The areas covered under the conference are as follows:

- Stream-1: Electrical Engineering
- Stream-2: Electronics & Communication Engineering
- Stream-3: Computer Science Engg. & Information Technology

Stream-1: Electrical Engineering

The conference invites papers from all areas under the broad spectrum of power system planning, coordination, marketing, safety, stability, security, optimality, economy, reliability and their applications. The areas are as follows:

- Power system modeling, simulation and analysis
- Power system stability, dynamics and control
- Power generation, transmission and distribution
- FACTS & HVDC
- Smart Grid Technology
- Parallel Processing in Power Systems
- High voltage engineering and insulation coordination
- Distributed generation systems, micro grid operation and wind power systems
- Power Quality and demand side management
- Power system protection and digital relaying
- Energy management policy planning and decision making
- Network restructuring and marketing strategy
- Power system optimization
- State estimation and security analysis
- Reliability analysis
- Modeling uncertainties and contingencies
- Fault detection and diagnosis
- Deregulation of electricity market

- Distribution automation
- Machines, power electronics and drives
- Computer applications in power systems
- Soft computing applications in power systems
- Power system communication
- Renewable Energy Sources & Management
- Hybrid energy systems
- Power system instrumentation
- Energy conservation and management
- Fuel cells and batteries
- Nuclear power alternatives
- Remote sensing, telemetry, and signal processing
- Application of Nano-Technology
- Use of super conductors in power systems
- Energy efficient protocols, tools and gadgets
- Microprocessor/Microcontroller based applications
- Supervisory control and data acquisition

Stream-2: Electronics & Communication Engineering:

The conference covers all aspects of theory and design of circuits, systems and devices for electronics, signal processing, and communication, including:

- Signal and System theory, Digital signal processing
- Network theory and Circuit design
- Information theory, Communication theory and techniques, Modulation, Source and Channel coding
- Switching theory and techniques, Communication protocols
- Optical communications
- Microwave theory and techniques, Radar, Sonar
- Antennas, wave propagation
- Measurement and instrumentation; Circuit design, Simulation and CAD
- Signal and Image processing, Coding; Microwaves, Antennas and Radio propagation
- Optoelectronics; TV and Sound broadcasting; Telecommunication networks; Radio and Satellite communications; Radar, Sonar and navigation systems; Electromagnetic compatibility.

Stream-3: Computer Science Engineering. & Information Technology:

The conference aims to bring together developers, users, academicians and researchers in the information technology and computer science for sharing and exploring new areas of research and development and to discuss emerging issues faced by them.

- Algorithms Artificial Intelligence
- Automated Software Engineering
- Bioinformatics and Scientific Computing
- Biomedical Engineering
- Compilers and Interpreters
- E-commerce and E-governance
- Event Driven Programming
- Expert Systems
- High Performance Computing
- Human Computer Interaction

- Computational Intelligence
- Computer Animation
- Computer Architecture & VLSI
- Computer Architecture and Embedded Systems
- Computer Based Education
- Computer Games
- Computer Graphics & Virtual Reality
- Computer Graphics and Multimedia
- Computer Networks,Modeling & Data Communication
- Computer Security / Simulation/ Vision
- Computer-aided Design/Manufacturing
- Computing Ethics/ Practices & Applications
- Control Systems
- Data Communications / Compression/ Encryption.
- Data Mining
- Database Systems
- Digital Library
- Digital Signal and Image Processing
- Digital System and Logic Design
- Distributed and Parallel Processing
- Distributed Systems
- Information Retrieval Systems
- Internet and Web Applications
- Knowledge Data Engineering
- Mobile Computing
- Multimedia Applications
- Natural Language
- Processing Neural Networks
- Parallel and Distributed Computing
- Pattern Recognition
- Performance Evaluation
- Programming Languages
- Reconfigurable Computing Systems
- Robotics and Automation Security & Cryptography
- Software Engineering & CASE
- System Security
- Technology in Education Technology
- Management Theoretical Computer Science
- Ubiquitous Computing
- Wireless Sensor Networks
- Wireless Communication and Mobile Computing

COMMITTEE MEMBERS

Program Chair /Chief Mentor:

Dr. K. Shanmukha Sundar
Prof & HOD.
Electrical & Electronics Engineering Department,
Dayananda Sagar College of Engineering
Bangalore-560078, India
E-mail: bonniekhs@gmail.com

Prof. (Dr.) Srikanta Patnaik
President, IRNet India and Chairman IIMT
Intersceince Campus, Bhubaneswar
Email: srikantapatnaik@hotmail.com

Program Co-Chairs:

Dr.B. N. Sarkar
Additional Directro(Retd),CPRI,
Bangalore,India

Secretary IRNet:

Prof. Pradeep Kumar Mallick
Department of Computer Science
IIMT, Bhubaneswar
Email:pradeepmallick84@gmail.com
Mobile No: 08895885152

Conference Secretary:

Dr. Vasantha Kumar.S
EEE Department, DSCE,Bangalore

Conference Coordinator:
Suchana Mishra
EEE Department, DSCE, Bangalore

Program Coordinator:

Balaji Ramakrishna
EEE Department, DSCE,Bangalore

Madhura .S
EEE Department, DSCE,Bangalore

Technical Committee:

Dr. B. R. Lakshmikantha,
Principal, Dayananda Sagar Academy of Technology
Bangalore- 560082,India

Dr. B. N. Sarkar
Add Director (Retd),CPRI,Bangalore
Dr. Ravishankar Dixit
Prof & HOD, EEE Dept., BMSCE,Basavana Gudi
Bangalore

Dr. H. M. Ravikumar
Prof &HOD, EEE Dept.
NITTE Meenakshi Institute of Technology
Yelahanka, Bangalore - 560 064.

Dr. Pradeepkumar Dixit
MSRIT, Bangalore,India

Dr. K. L. Putta Buddhi
Professor,SJCE, Mysore

Smt. R. V. Parimala
Asst. Professor, DSCE,Bangalore

Smt. P. Usha
Asst. Professor, DSCE,Bangalore

Dr. B. K. Keshavan
Prof & HOD,EEE Dept.,
PESIT, Bangalore

Dr. Basavaraj Banakar
Vice Principal, Prof & HOD , GITAM University,Hyderabad

Post Conference Coordinator:
Miss. Ujjayinee Swain
IRNet , Bhubaneswar,India
Mob:08763722892

Head System & Utilities:
Prof. Sanjay Sharma
IIMT, Bhubaneswar
Mr. Sharath Kumar
EEE Department, DSCE,Bangalore

Publicity Committee:
Mr. Manjunatha Babu
EEE Department,DSCE,Bangalore
Mr. Rajaram
EEE Department,DSCE,Bangalore
Prof. Sushanta Kumar Panigrahi
IIMT, Bhubaneswar
Prof. Mritunjay Sharma
IIMT, Bhubaneswar

Organizing Committee:

Bibhu Prasad Mohanty
Pritika Mohanty
Bijan kumar Barik
Ganeswar Mishra

First Impression : 2012

International Joint Conference

On

EMERGING INTELLIGENT SUSTAINABLE TECHNOLOGIES

(EISTCON-2012), Volume-II

DISCLAIMER

The authors are solely responsible for the contents of the papers complied in this volume. The publishers or editors do not take any responsibility for the same in any manner. Errors, if any, are purely unintentional and readers are requested to communicate such errors to the editors or publishers to avoid discrepancies in future.

ISBN : 978-93-81693-76-6

Published by :

IPM PVT. LTD., Interscience Campus
At/PO.: Kantabada, Via: Janla, Dist: Khurda, Pin- 752054
Publisher's Website : www.interscience.in
E-mail: ipm.bbsr@gmail.com

Typeset & Printed by :
IPM PVT. LTD.

TABLE OF CONTENTS

Editorial

In the pursuit of scientific excellence human society is accelerating the pace of technological developments in every discipline. In the 21st century the most critical concern of every research is to address the environmental and sustainability issues. Specifically in the areas like Power and Electronics engineering where energy is an integral component of analysis, scholars and practitioners must exhibit a thrust on energy aspect of their research interest. The major drivers of a new paradigm can be attributed to:

- Environmental pressures
- Customer pressures
- Financial pressures
- Technology developments

There are several reason why the traditional technologies are not appropriate anymore for current usage:

- Do not meet current environmental pressures
- Cannot readily meet customer pressures
- Are no longer the most appropriate solutions for developing countries
- Have long term paybacks which do not meet current financial restraints
- Do not allow for innovative solutions

The new electricity production technologies consist of:

- Development of gas infrastructures
- Application of gas fired generation closer to loads
- Combined heat and power Embedded generation
- Development of micro turbines
- Advancement of fuel cell technologies
- Development of renewable sources
- Development of energy storage technologies
- Development of photovoltaic technologies
- Nuclear generation

For a technological point of view it means that a user centric approach is needed (smart grid). Furthermore to enable secure and sustainable solutions integration of utility infrastructures and super grids are needed. For the next decades a detailed asset management needs to be done in order to determine the efficient investments, sustainable utilization and precise removal to have an effective hybrid network consisting of old and new technologies. Another aspect that needs to be discussed is energy conservation which refers to the preservation of fossil energy sources (oil and gas). For that restrictions need to be imposed. Also it needs to be pointed out that we are trying to conserve raw materials and the environment. Saving of energy will only assist but will not be part of energy conservation.
From a material point of view it will require a greater cooperation between technology equipment and material developers, identification of idealized material requirement for new technologies and a decrease of development periods. The following aspects for material developments need to be considered:

- High temperature superconducting compounds
- Polymers
- Ceramics
- Semiconductors

- Liquid insulation
- Gas insulation etc

The word Computing has obtained a different connotation in the context of advance studies in Computer Science. As the computational complexities are increasingly influence the researchers in several multidisciplinary studies the approach should to develop advanced techniques in easing an user-friendly end product. In the latter half of the twentieth century witnessed incremental innovations in the field of computational science. The growth of such a distinctive field dates back to 1960 when John McCarthy opined "computation may someday be organized as a public utility". The present scenario of computer vision and cloud characteristics were explicitly described by the scholarly bibliography by Canadian technologist Douglass Parkhill's "The Challenges of the Computer Utility". Other scholars have shown that cloud computing's roots go all the way back to the 1950s when scientist Herb Grosch (the author of Grosch's law) postulated that the entire world would operate on dumb terminals powered by about 15 large data centers.

The mission of Roadmap of future is to provide a practical, independent and objective analysis of pathways to achieve low-carbon economies in the world in line with the energy security, environmental and economic goals.

The conference is designed to stimulate the young minds including Research Scholars, Academicians, and Practitioners to contribute their ideas, thoughts and nobility in these emerging disciplines. Even a fraction of active participation deeply influences the magnanimity of this international event. I must acknowledge your response to this conference. I ought to convey that this conference is only a little step towards knowledge, network and relationship

I sincerely thank to the board of editors for their generous gifts of time, energy and intellect. I salute to the technical committee, organizing committee and publishing house for their unbroken professional commitments in bringing this proceeding.

I hope this gracious piece of effort will earn a significant appreciation from the readers to whom I owe indebtedness. I must welcome constructive feedbacks for future development.

With Warm Regards

Editors
Prof. (Dr.) Srikanta Patnaik
President, IRNet India and Chairman IIMT
Intersceince Campus, Bhubaneswar
Email: srikantapatnaik@hotmail.com

&

Dr. K. Shanmukha Sundar
Prof & HOD.
Electrical & Electronics Engineering Department,
Dayananda Sagar College of Engineering
Bangalore-560078, India
E-mail: bonniekhs@gmail.com

Preparation and Characterization of P3HT-PCBM Organic Solar Cells

Anubhav Gupta[1], Praveen S[1], Abhishek Kumar[1], Priyanka Shree[1], Suchana Mishra[1] & C.M.Joseph[2]

[1]Department of Electrical & Electronics Engineering, Dayananda Sagar College of Engineering, Bangalore -560 078,
[2]Department of Physics, Dayananda Sagar College of Engineering, Bangalore – 560 078, India
E-mail: anubhavgupta1989@yahoo.com, abhi9kr@hotmail.com,
praveennair.dsi@gmail.com, priyankashree.dsi@gmail.com

Abstract - Organic solar cells using P3HT: PCBM as an active layer on ITO coated glass substrates were fabricated and characterized. Different air annealing procedures and cathode materials were tried and the characteristics were compared with that of a standard thin film polycrystalline silicon solar cell. It was found that the sample prepared with post-deposition air annealing at 130 ^{o}C improves the open circuit voltage (Voc) considerably. Besides, short circuit current (Isc) and the efficiency (η) were highest for the sample with a non annealed active layer. Series resistance (Rs) for this sample was lowest, but 10^3 times higher than that of the silicon solar cell, which in turn may have reduced the efficiency value for the organic cell compared to silicon.

Keywords *– Organic solar cells; Spin Coating; Photolithography; P3HT:PCBM blend layer; Air annealing.*

I. INTRODUCTION

With the higher consumption rate of fossil fuels, resources are about to deplete in a few decades but the demand for energy usage is continuously increasing. To meet the higher energy demands, different renewable sources are been used with more focus on solar energy because of its unbound availability. The solar energy is harvested using solar cells. The first type of solar cells manufactured were the silicon based solar cells which had an efficiency of 27% theoretically and 24% practically. The silicon based cells make use of photovoltaic effect. Such cells are also known as PV cells. There are different types of solar cells: crystalline silicon based and polycrystalline thin film and bulk and organic. With the bridging of practical and theoretical values of efficiency for silicon based cells, the demand for another type of solar cells augmented. The organic solar cells were first fabricated and demonstrated by C.W. Tang [1]. The organic solar cells with different organic compounds were fabricated and characterized in the succeeding years. So far, an efficiency of 5-6% has been achieved [2-5].

Organic materials find application in numerous electronic devices also. When used as an active element in optoelectronic devices it is called as Organic Light Emitting Diode (OLED) while with transistors as Organic Field Effect Transistors (OFET) [6-9]. An organic cell is fabricated by depositing different layers on a glass substrate. The cells can be of different types such as single layer, double layer, blend layer and laminated layer type [5]. Each of these has its own advantages and disadvantages. Different procedures are also used to fabricate a cell; for solid source, we can use vacuum evaporation technique. For liquid organic material which is the source in the current work, we use a spin coating method. Detailed studies on the preparation procedures and annealing conditions of devices are published elsewhere [10-14].

Here, we have used a polymer based organic solar cell. Out of many commercially available compounds, we have used PEDOT (polyethylene dioxythiophene) and PSS (poly styrene sulfonic acid) as a conducting layer over ITO (Indium tin oxide) coated glass substrate while a blend of P3HT (poly (3-hexylthiophene)) and PCBM ([6, 6]-phenyl-C_{61}-butyric acid methyl ester) is used as the active material. . P3HT acts as the *p*-type donor polymer and PCBM as the *n*-type acceptor in the active layer. Although, there are four different architectures- single layer, blend layer, double layer and laminated device, we have used blend layer architecture due to a large interface area if the molecular mixing occurs on a scale that allows good contact between alike molecules and most excitons to reach the Donor /Acceptor interface [5]. The polymer P3HT/PCBM is preferred over other organic compounds because of its higher efficiency and low processing cost. The advantages of using polymer PV cells are that they offer mechanical flexibility, durability and unlimited potential from advances in organic chemistry. The performance of these cells is limited by low carrier mobility & short exciton diffusion lengths of polymers.

II. EXPERIMENTAL PROCEDURE

A. *Materials Used*

An ITO coated glass substrate has been used as the substrate for the polymer based organic solar cell. As a smoothening layer for hole transportation, PEDOT: PSS is used. The active material used is P3HT-PCBM blend. The active layer is a blend layer and thus is referred as blend layer architecture. The source materials of research specified above are commercially purchased from Sigma-Aldrich.

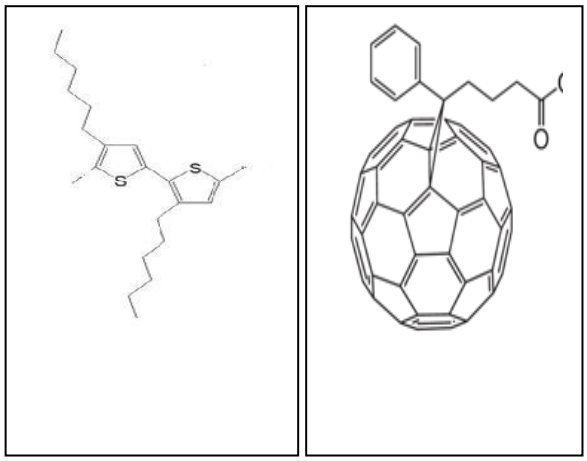

(1a) (1b)

Figure. (1a): Structure of P3HT, (1b): Structure of PCBM.

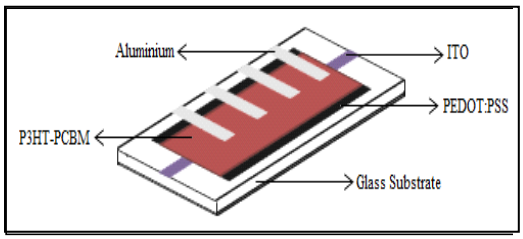

Figure 2: Architecture of P3HT: PCBM based organic solar cell fabricated.

As negative electrode, different elements have been used such as – aluminium and calcium. The organic compounds so chosen are commercially cheap as compared to other organic compounds available in the market.

B. *Fabrication Procedure*

The structure of the fabricated device is Al/ P3HT: PCBM/PEDOT: PSS/ITO/Glass. Indium Tin Oxide coated glass substrates were cleaned in an ultrasonic cleaner and patterned by photolithography. ITO was used as the anode. Each substrate was then treated with UV light to improve the wettability of diluted PEDOT: PSS in deionized water. PEDOT: PSS was then spin coated on these substrates using Holmarc spin coater and then annealed in air for 10mints. A blend of P3HT: PCBM was made in chlorobenzene in the ratio 10mg: 10mg: 1ml and filtered using a micro-syringe. Then it was spin coated on the PEDOT: PSS layer. Final contact material aluminium was thermally evaporated in a vacuum of around 2×10^{-6} Torr through a shadow mask to form the cathode. Thermal evaporation was done in a Hind Highvac vacuum coating unit.

We have prepared P3HT: PCBM solar cells with different post deposition conditions such as air annealed (130^{o}C) active layer (sample 1), Non-annealed active layer (sample 2), with Ca electrode and air annealed at 100^{o}C (sample 3). The reason for using Ca electrode is that work function of Ca is very low. This gives higher built-in voltage which will eventually help in improving the Jsc (Current Density) of the solar cell. The layer of Al is used as a protective layer to Ca to avoid its oxidation [14].

Electrical characterization of the devices was performed using a Keithley 2400 digital source meter and a solar simulator with xenon DC 350 (Autosys) operating at an intensity of 100mW/cm^2.

C. *Precautions*

The cell shall not be exposed much to air directly during the process of fabrication as they are degradable. Presence of dust particles or of any other foreign material is avoided by filtering the solutions.

III. RESULTS AND DISCUSSION

Figure 3 shows the dark characteristics of a typical non annealed P3HT: PCBM solar cell fabricated.

Shown in figure 4 is the characteristic of the P3HT: PCBM organic solar cell in the presence of light.

We have prepared P3HT:PCBM solar cells with different post deposition conditions such as air annealed

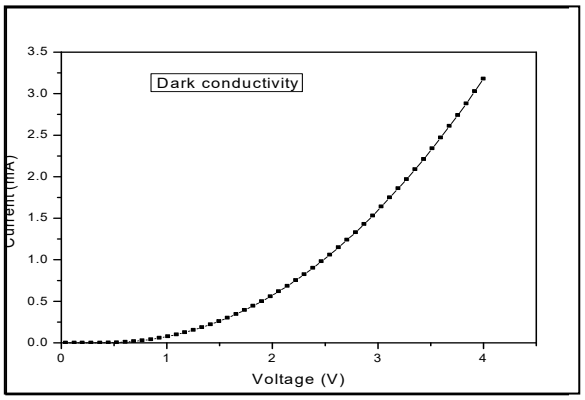

Figure 3: Dark Characteristics of Organic Solar Cell.

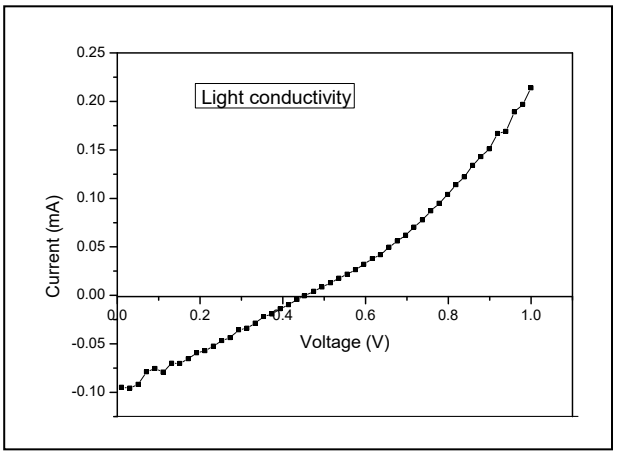

Figure 4: Light characteristics of a typical non annealed P3HT: PCBM solar cell fabricated (Sample 2).

(130^{o}C) active layer (sample 1), Non-annealed active layer (sample 2), with Ca electrode and air annealed at 100^{o}C (sample 3). All the samples were with a small active area of 0.06 cm^2. The solar cell parameters of all the fabricated devices are tabulated in the table 1.

It is found that air annealing at 130 ^{o}C improves the open circuit voltage (Voc) considerably for the deposited samples and the short circuit current (Isc) and the efficiency (η) were highest for the sample with non annealed active layer. Besides, series resistance (Rs) for this sample was lowest, but 10^3 times higher than that of the polycrystalline thin film silicon solar cell purchased. Fill factor values were almost similar for all the samples including the silicon sample. Following are the parameters calculated for the standard polycrystalline thin film silicon solar cell: Area of the active cell = 4 cm^2, V_{oc} = 0.63 V, I_{sc} = 0.04 A, FF = 0.54, η = 8.4 %. Shown in figure 5 is the *IV* characteristic of a standard thin film silicon solar cell.

A detailed study on these types of solar cells and annealing procedures like vacuum annealing for crystallization of active layers and optimum series resistance may yield organic solar cells with more efficiency and is underway in table 1s.

TABLE I. COMPARISON OF PARAMETERS OF THE P3HT: PCBM SOLAR CELL WITH A STANDARD THIN FILM SILICON SOLAR

Sample	**Device**	**Voc (V)**	**Isc (A)**	**FF**	**η (%)**	**Rs (Ω)**
1	Air annealed (130^{o}C) active layer	1.01	0.84 x 10^{-6}	0.413	0.01	6 M
2	Non-annealed active layer	0.46	100 x 10^{-6}	0.48	0.4	0.005 M
3	with Ca electrode and air annealed (100^{o}C)	0.75	1.37 x 10^{-6}	0.37	0.01	0.5 M
4	Standard thin film Silicon solar cell	0.63	0.04	0.54	8.4	5

IV. CONCLUSION

We have prepared solar cells using P3HT: PCBM active layer in different post deposition conditions. We have compared the parameters with a standard silicon solar cell. It is found that air annealing at 130 ^{o}C improves the open circuit voltage (Voc) considerably for the deposited samples and the short circuit current (Isc) and the efficiency (η) were highest for the sample with non annealed active layer. Besides, series resistance (Rs) for this sample was lowest, but 10^3 times higher than that of the silicon solar cell. A detailed study on these types of solar cells and annealing procedures like vacuum annealing for crystallization of active layers and optimum series resistance may yield organic solar cells with more efficiency.

ACKNOWLEDGMENT

We are thankful to Mrs. Gayathri A.G. (Research Assistant) for her valuable help in sample preparation. Also, we are thankful to Dr. Nethaji S. Ganesan, Principal, Dayananda Sagar College of Engineering and Dr. K. Shanmukha Sundar, Head, Department of Electrical & Electronics Engineering, Dayananda Sagar College of Engineering for providing us with the opportunity to do research on the subject matter. Support by Visvesvaraya Technological University (VTU, Belgaum) for the financial support through a grant is gratefully acknowledged. Financial support by Vision Group on Science and Technology (VGST), Department of Information Technology, Biotechnology & Science and Technology, Government of Karnataka, India through a CISE grant is also acknowledged.

REFERENCES

[1] C.W. Tang, Applied Physics Letters, Jan 1986, volume 4, issue 2, pages 183-185.

[2] Yi-Cang Lai, Tomoya Higashihara, Jumg-Ching Hsu, Mitsuru Ueda, Wen-Chang Chen, Solar Energy Materials and Solar Cells, volume 97, February 2012, pages 164-170.

[3] Yanmin Wang, Wei Wei, Xin Liu, Yijie Gu, Solar Energy Materials and Solar Cells, volume 98, March 2012, pages 129-145.

[4] Biswajit Ray, Pradeep R. Nair, Muhammad A. Alam, Solar Energy Materials and Solar Cells,

volume 95, issue 12, December 2011, pages 3287-3294.

[5] Klaus Petritsch, Organic Solar Cell Arcitectures, Thesis submitted to Technical University of Graz (Austria), 2000.

[6] Zi-En Ooi, Samarendra P. Singh, Serene L.G.Ng, Gregory K. L. Goh, Ananth Dodabalapur, Organic Electronics, volume 12, 2011, pages 1794-1799.

[7] C. M. Joseph, M.Nakamura, M. Iizuka, K. Kudo, Applied Surface Science, volume 244, issue 1-4, 2005, pages 603-606.

[8] C. M. Joseph, T. Natsume, M.Nakamura, M. Iizuka, K. Kudo, Microelectronics Journal, volume 37, 2006, pages 884-887.

[9] Tik H Lee, K. M. Lai, Louis M. Leung, Polymer, volume 50, 2009, pages 4602-4611.

[10] Paola Vivo, Johanna Jukola, Mikko Ojala, Vladimir Chukharev, Helge Lemmetyinen, Solar Energy Materials and Solar Cells, volume 92, 2008, pages 1416-1420.

[11] Su Cheol Gong, Seong Kyu Gang, Sang Ouk Ryu, Hyeongtag Geon, Hyung-ho Park, Hogung Chang, Current Applied Physics, volume 10, 2010, pages 192-196.

[12] Toshihiro Yamanari, Tetsuya Taima, Jun Sakai, Kazuiro Saito, Solar Energy Materials and Solar Cells, volume 93, 2009, pages 759-761.

[13] S. Cros, R. de Bettignies, S. Berson, Sbailly, P. Maisse, N. Lemaitre, S. Guillerez, Solar Energy Materials and Solar Cells, volume 95, 2011, pages s65-s69.

[14] Arun Tej Mallajosyula, Naveen Srivastava, S. Sundar kumar Iyer, Baquer Mazhari, Solar energy materials and solar cells, volume 94, 2010, pages 1319-1323.

◈◈◈

Inline Elasticity Measure of Textile Using ANN

[1]Santhosh K V, [2]Namratha S N & [3]Anjana Parua

[1]Department of Electrical Engineering, National Institute of Technology, Silchar, India
[2&3]Department of Instrumentation, BMSCE, Bangalore, India
E-mail : kv.santhu@gmail.com, namrathans@gmail.com

Abstract- In this paper, we propose a technique to measure the Elasticity Modulus of the textile material using flex LVDT. Elasticity modulus is measured indirectly by measuring stiffness of the material first. The material whose stiffness is to be measured is subjected to a known force and the deflection caused in the material due to applied load is measured using the LVDT. Here the whole measurement is done dynamically without halting the manufacturing line of process. The output of LVDT is AC voltage. AC-DC converter is used to convert the AC output voltage of LVDT to DC output voltage. This is cascaded to the ANN block programmed on the LabVIEW platform. The results show that the proposed technique has achieved its proposed objectives.

Keywords-*LVDT; LabVIEW; stiffness measure; Elasticity Modulus, Artificial Neural Network.*

I. INTRODUCTION

Elastic modulus is a property of the constituent material; stiffness is a property of a structure. That is, the elasticity modulus is an intensive property of the material. The stiffness of a structure is of principal importance in many engineering applications, so the modulus of elasticity is often one of the primary properties considered when selecting a material. A high modulus of elasticity is sought when deflection is undesirable, while a low modulus of elasticity is required when flexibility is needed. The measure of elasticity modulus cannot be done directly; we can find the elasticity modulus by measuring the stiffness of the material. The stiffness of a body is a measure of the resistance offered by an elastic body to deformation. For an elastic body with a single Degree of Freedom (for example, stretching or compression of a rod), the stiffness is defined as force per displacement produced by the force along the same degree of freedom [1]-[3].

There are many techniques to measure the elasticity of textile but all these are offline process and most of them derive the elasticity modulus from the material of the cloth or some are derived from tensile strength of the thread bused to spun the textile.

The present paper proposes a technique used to measure the elasticity of textile online using LVDT to measure deflection of the textile for applied load. Thus, stiffness and elasticity modulus of textile is calculated.

The paper is organised as follows: After introduction in section –I. Section-II discusses with the block diagram of the proposed technique, a brief description on sensor is given in section III. The output of the sensor is AC voltage; A brief discussion on data conversion i.e. AC-DC converter, is done in section IV, section V deals with the problem statement. Section VI deals with problem solution and finally, results and conclusion is given in section VII.

II. BLOCK DIAGRAM OF MEASURING SYSTEM

The block diagram representation of the proposed elasticity measuring technique is given in Fig.1

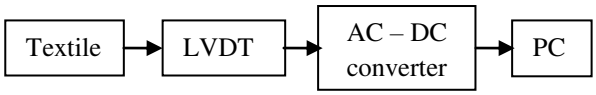

Figure. 1 Block diagram of proposed system

III. LVDT

LVDT is used to measure linear displacement. LVDT operates on the principle of a transformer. As shown in Fig. 2, an LVDT consists of a coil assembly and a core. The coil assembly is typically mounted to a stationary form, while the core is secured to the object whose position is being measured. The coil assembly consists of three coils of wire wound on the hollow form. A core of permeable material can slide freely through the center of the form. The centre coil is the primary, which is excited by an AC source as shown. Magnetic flux produced by the primary is coupled to the two secondary coils placed on both sides of primary coil, inducing an AC voltage in each secondary coil [4]-[6].

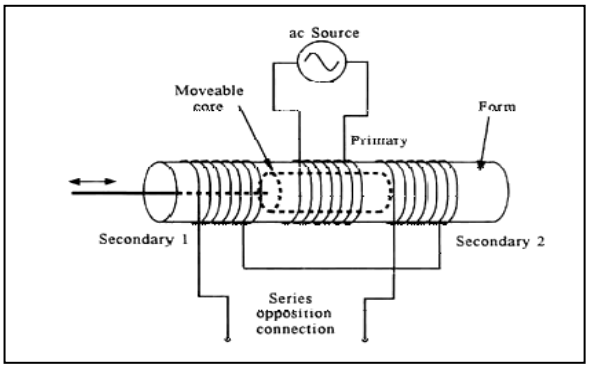

Figure 2. LVDT schematic diagram

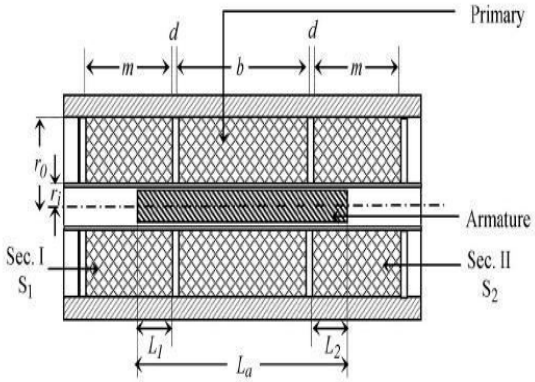

Figure. 3 Cross-section of LVDT

Figure. 4 Image of experimental setup

Figure 4 shows the experimental model used for the proposed measurement technique. The textile fabric whose stiffness or elasticity is to be measured is made to roll on to the roller. The roller are arranged in a way that the textile is held tight Now, a weigh ball is applied on the centre of the textile causing slag on the textile proportional to the properties of textile like stiffness and elasticity modulus.

IV. AC-DC CONVERTER

LVDT's output signal is converted by a 'LTC1967 true RMS to DC converter' to a DC signal that is linearly proportional to the displacement of the LVDT core. The LTC1967 is a true RMS-to-DC converter that uses an innovative delta-sigma computational technique. The benefits of the LTC1967 proprietary architecture are higher linearity & accuracy, bandwidth independent of amplitude and improved temperature behavior when compared to conventional log-antilog RMS-to-DC converters [7].

V. PROBLEM STATEMENT

Once signal is acquired from the AC-DC converter using DAQ card. LabVIEW is programmed to achieve the following:

(i) Display the actual stiffness of textile used

(ii) Display the elasticity of textile used

VI. PROBLEM SOLUTION

The signal from the AC-DC converter is connected to the DAQ card connected to the PC programmed using LabVIEW. LabVIEW is a graphical language used for control and automation. LabVIEW consists of two parts called the front panel and block diagram windows. The front panel to the vi consist of two numerical indicators which display the actual quantities of stiffness and elasticity modulus as shown in Fig.5.

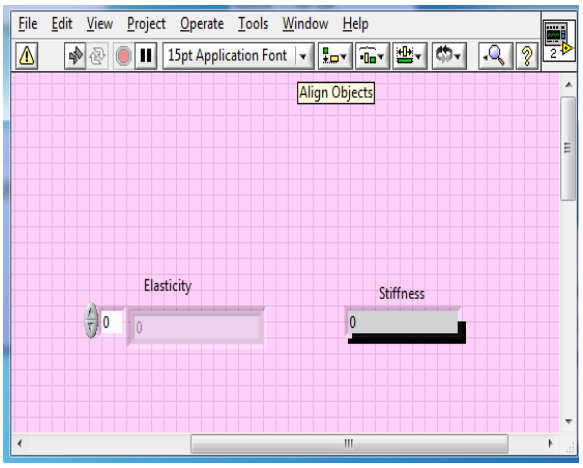

Figure. 5 Front panel view

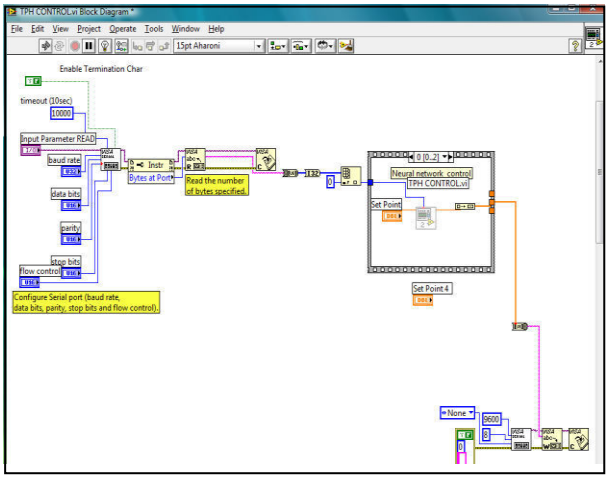

Fig 5: Block diagram view

Fig. 6 shows the block diagram vi for the proposed technique. The block diagram consists of a DAQ input acquire corresponding to output of LVDT. This signal is further processed using the concept of neural network to display the stiffness and elasticity modulus of the textile. The neural vi is designed using the back-propagation algorithm to calculate the stiffness and elasticity modulus of textile [8]-[9].

A: BACK-PROPOGATION ALGORITHM

The back-propagation learning algorithm can be divided into two phases: propagation and weight update [10]-12].

Phase 1: Propagation

Each propagation involves the following steps:

1. Forward propagation of a training pattern's input through the neural network in order to generate the propagation's output activations.
2. Backward propagation of the propagation's output activations through the neural network using the training pattern's target in order to generate the deltas of all output and hidden neurons.

Phase 2: Weight update

For each weight-synapse:

1. Multiply its output delta and input activation to get the gradient of the weight.
2. Bring the weight in the opposite direction of the gradient by subtracting a ratio of it from the weight.

This ratio influences the speed and quality of learning; it is called the learning rate. The sign of the gradient of a weight indicates where the error is increasing; this is why the weight must be updated in the opposite direction. Repeat the phase 1 and 2 until the performance of the network is good enough.

The training data for the network would be the set point data given by the user.

Table-1 summarizes the require data for training.

OPTIMIZED PARAMETERS OF THE NEURAL NETWORKS MODEL		
No of neurons in	1st layer	6
Transfer function of	1st layer	Logsig
	Output layer	linear
MSE	Training	4.42E-09
	Validation	3.265E-08
	Test	2.993E-08
R	Training	0.9999900
	Validation	0.9999960
	Test	0.9999990

Mean Squared Error (MSE) is the average squared difference between outputs and targets. Lower values are better. Zero means no error. Regression (R) values measure the correlation between outputs and targets. An R value of 1 means a close relationship, 0 a random relationship. With these details the network is trained.

The output of the neural network model is connected to the numerical indicators to display the stiffness and elasticity modulus of textile.

VII. RESULT AND CONCLUSION

The system after being trained by neural network using back-propagation was subjected to test and following results were plotted.

Parameter		Actual	Measured value
1	Stiffness	0.66 N/m	0.66 N/m
2	Stiffness	0.62 N/m	0.62 N/m
3	Stiffness	0.89 N/m	0.89 N/m
4	Stiffness	1.3 N/m	1.3 N/m
5	Elasticity Modulus of nylon	3.8 GPa	3.8 GPa
6	Elasticity Modulus of polystyrene	3.1 GPa	3.1 GPa
7	Elasticity Modulus of cotton	5.3 GPa	5.3GPa
8	Elasticity Modulus of jute	18.2 GPa	18.2 GPa

The result show that the technique produces accurate results.

REFERENCES

[1] N.J. Abbott, "The Measurement of Stiffness in Textile Fabrics", Textile Research Journal, vol. 21, No. 6 pp 435-441, June 1951.

[2] Martin Wenham, "Stiffness and flexibility", *200 science investigations for young students*, p. 126, ISBN 9780761963493, 2001.

[3] Hugo Partsch, Bernhard partsch, Walter Braun, "Interface Pressure and Stiffness of ready made Compression Stockings: Comparison of in vivo and in vitro Measurements", Journal of Vascular Surgery, vol 44, Issue 4, pp 809-814, october 2006.

[4] H. K. P. Neubert. Instrument Transducers: An Introduction to Their Performance and Design. 2nd edition New Delhi, India, Oxford University Press, 2003.

[5] Bela G Liptak. Instrument Engineers Handbook-Process Measurement and Analysis. 4th Edition, CRC Press, 2003.

[6] DVS Murty. Transducers and Instrumentation. PHI publication India, 2003.

[7] Charles Kitchin, Lew Counts, RMS To DC Conversion Application Guide, 2nd Edition, Analog Devices, 2000.

[8] National Instruments, LabVIEW help manuals

[9] Mahesh.L.Chugani, "LabVlEW Signal Processing", Prentice-Hall India, 1998.

[10] Stuart Russell and Peter Norvig, Artificial Intelligence A Modern Approach, 3rd Edition, Prentice Hall New York, 2009.

[11] T Poggio, F Girosi, "Networks for approximation and learning," Proc. IEEE 78(9), pp. 1484-1487, 1990.

[12] Jeng-Bin Li, Yun-Kung Chung, A Novel Back propagation Neural Network Training Algorithm Designed by an Ant Colony Optimization, IEEE/PES Transmission and Distribution Conference & Exhibition: Asia and Pacific Dalian, China 2005.

◈◈◈

Rotor Speed Estimation for Vector Controlled Induction Motor Drive using Sliding Mode Observer

Shinde S. N & D. S. More

Department of Electrical Engineering, Walchand College of Engineering, Sangli, India.
E-mail : mail.sshinde@gmail.com & dsm.wce@gmail.com

Abstract - The term sensorless vector control means vector control without any speed sensor. Sensorless vector control drives have main benefits over vector control drives as reliability and low cost. In this paper a sliding-mode observer for the speed-sensorless vector control of induction motors is proposed. The observer estimates the motor speed, the rotor flux from measured terminal voltages and currents. The nonlinear sliding-mode technique provides very good performance for full range of speed and robustness in motor losses and load variations. In this paper speed of induction motor is estimated using sliding mode observer and system is simulated using MATLAB. Simulation results of estimated speed are correct.

Keywords*: sensorless, speed estimation, modelling, parameter estimation, induction motor.*

I. INTRODUCTION

In recent years, the vector control theory has been receiving much attention because of the better steady and dynamic performance over conventional control methods in controlling motors torque and speed. In various vector control schemes, the speed sensorless vector control has been a relevant area of interest for many researchers due to its low drive cost, high reliability and easy maintenance.[1] There are two main parameters which are required in speed sensorless vector control of induction motor, those are, the motor flux and speed estimation. These parameters are necessary for establishing the outer speed loop feedback and also in the flux and torque control algorithms.

In order to get good performance of sensorless vector control, different speed estimation methods have been proposed. Such as direct calculation method, model reference adaptive system (MRAS), Observers (extended Kalman filter, luenberger, etc), Estimators using artificial intelligence etc [1,2]. Out of various speed estimation methods, MRAS-based speed sensorless estimation has been commonly used in AC speed regulation systems due to its good performance and ease of implementation.

In a MRAS system, rotor flux-linkage components, Ψ_{dr}^{s}, Ψ_{qr}^{s} of the induction machine (which are obtained by using measured quantities, e .g. stator voltages and currents) are estimated in a reference model and are then compared with, Ψ_{dr}^{s}, Ψ_{qr}^{s} estimated by using an adaptive model [3]. Then effort is made to reduce this error to zero using adaptive mechanism.

Most of these conventional methods use PI controllers with complicated gain calculations. These gains have the best performance for a specific load. Also, knowledge of the motor - load inertia and friction is very important. In the case of a variable load, the PI controllers can't have the same behaviour over the full speed range. Also implementation of small gains in a fixed point DSP is very difficult and a high accuracy is needed. As a result, the use of a PI controller ensures the best performance for constant load or low- or high-speed operation.

Lately, an adaptive sliding-mode observer for speed sensorless control has been proposed [3]. This observer seems to have a very good performance over the full speed range because of the sliding-mode technique, however, in this technique; the calculation of several observer gains is needed.

In this paper, a sliding-mode observer is presented for speed sensorless motor drive systems. The proposed observer estimates the motor speed, the rotor flux. Also, only one observer gain is needed. Behaviour and robustness of proposed observer has been tested using simulation.

II. MODELLING OF INDUCTION MOTOR

In order to decouple the torque producing and flux producing components of input voltages and currents to the induction motor, Modelling of induction motor is done in stationary reference frame [4].

$$\frac{d\Psi_{dr}}{dt} = \Psi'_{dr} = -n\Psi_{dr} - \omega_r \Psi_{qr} + nL_m i_{ds} \qquad (1)$$

$$\frac{d\Psi_{qr}}{dt} = \Psi'_{qr} = -n\Psi_{qr} + \omega_r \Psi_{dr} + nL_m i_{qs} \quad (2)$$

$$\frac{di_{ds}}{dt} = i'_{ds} = \beta n\Psi_{dr} + \beta\omega_r \Psi_{qr} - \gamma i_{ds} + \frac{1}{\sigma L_s} u_{ds} \quad (3)$$

$$\frac{di_{qs}}{dt} = i'_{qs} = \beta n\Psi_{qr} - \beta\omega_r \Psi_{dr} - \gamma i_{qs} + \frac{1}{\sigma L_s} u_{qs} \quad (4)$$

The meaning of the above symbols and the definition of the constant values are given in Appendix A.

For sensorless control it is necessary to make a simultaneous observation of the rotor flux and rotor speed. The proposed observer belongs to the category of closed loop systems and its design [5] is the following:

$$\frac{d\hat{\Psi}_{dr}}{dt} = \hat{\Psi}'_{dr} = -n\hat{\Psi}_{dr} - \hat{\omega}_r \hat{\Psi}_{qr} + nL_m i_{ds} \quad (5)$$

$$\frac{d\hat{\Psi}_{qr}}{dt} = \hat{\Psi}'_{qr} = -n\hat{\Psi}_{qr} + \hat{\omega}_r \hat{\Psi}_{dr} + nL_m i_{qs} \quad (6)$$

$$\frac{d\hat{\imath}_{ds}}{dt} = \hat{\imath}'_{ds} = \beta n\hat{\Psi}_{dr} + \beta\hat{\omega}_r \hat{\Psi}_{qr} - \gamma \hat{\imath}_{ds} + \frac{1}{\sigma L_s} u_{ds} \quad (7)$$

$$\frac{d\hat{\imath}_{qs}}{dt} = \hat{\imath}'_{qs} = \beta n\hat{\Psi}_{qr} - \beta\hat{\omega}_r \hat{\Psi}_{dr} - \gamma \hat{\imath}_{qs} + \frac{1}{\sigma L_s} u_{qs} \quad (8)$$

Where, $\hat{\imath}_{ds}$ and $\hat{\imath}_{qs}$ are the estimated stator current components, $\hat{\Psi}_{dr}$ and $\hat{\Psi}_{qr}$ are the estimated rotor flux components and $\hat{\omega}_r$ is the estimated value of the motor speed. Using the following definitions:

$$\overline{i_{ds}} = \hat{\imath}_{ds} - i_{ds}, \ \overline{i_{qs}} = \hat{\imath}_{qs} - i_{qs}, \ \overline{\omega_r} = \hat{\omega}_r - \omega_r \quad (9)$$

$$\overline{\Psi_{dr}} = \hat{\Psi}_{dr} - \Psi_{dr} \qquad \overline{\Psi_{qr}} = \hat{\Psi}_{qr} - \Psi_{qr} \quad (10)$$

That expresses the mismatch between estimated and real components; a new system can be developed as follows:

$$\bar{i}'_{ds} = -\gamma\overline{i_{ds}} + \beta n\overline{\Psi_{dr}} + \beta\omega_r \overline{\Psi_{qr}} + \beta\,\overline{\omega_r}\,\hat{\Psi}_{qr} \quad (11)$$

$$\bar{i}'_{qs} = -\gamma\overline{i_{qs}} + \beta n\overline{\Psi_{qr}} - \beta\omega_r \overline{\Psi_{dr}} - \beta\,\overline{\omega_r}\,\hat{\Psi}_{qr} \quad (12)$$

$$\overline{\Psi}'_{dr} = -n\overline{\Psi_{dr}} - \overline{\omega_r}\,\hat{\Psi}_{qr} - \omega_r \overline{\Psi_{qr}} \quad (13)$$

$$\overline{\Psi}'_{qr} = -n\overline{\Psi_{qr}} + \overline{\omega_r}\,\hat{\Psi}_{dr} + \omega_r \overline{\Psi_{dr}} \quad (14)$$

III. CURRENT MISMATCH STABILITY ANALYSIS OF OBSERVER

Let us define the following positive Lyapunov function:

$$I = \frac{1}{2}(\bar{i}^2_{ds} + \bar{i}^2_{qs}) \geq 0 \quad (15)$$

Its derivative $I' = \bar{i}'_{ds}\,\overline{i_{ds}} + \bar{i}'_{qs}\,\overline{i_{qs}}$ after substitution from (11) and (12) can be written as follows:

$$I' = -2\gamma I - \beta\omega_r(\hat{s_n} - s_n) - \beta\overline{\omega_r}\,\hat{s_n} + \beta n s_c \quad (16)$$

Where, $\hat{s_n} = \overline{i_{qs}}\,\hat{\Psi}_{dr} - \overline{i_{ds}}\,\hat{\Psi}_{qr}$

$S_n = \overline{i_{qs}}\,\Psi_{dr} - \overline{i_{ds}}\,\Psi_{qr}$

$S_c = \overline{i_{ds}}\,\overline{\Psi_{dr}} + \overline{i_{qs}}\,\overline{\Psi_{qr}}$

The current mismatch dynamics are stable if the conditions $I' < 0$ and $I' \geq 0$ are true. The sufficient condition $I' < 0$ can be written as follows:

$$\omega_r(\hat{s_n} - s_n) + \overline{\omega_r}\hat{s_n} > \frac{-2\gamma}{\beta} I + n\, s_c \quad (17)$$

If the following equation is selected:

$$\hat{\omega}_r = K\,\mathrm{sgn}(\hat{s_n}) \quad (18)$$

then is sufficient to state:

$$K|\hat{s_n}| > \omega_r |s_n| + \delta \geq \omega_r s_n + \delta \quad (19)$$

Where, $\delta = -\frac{2\gamma}{\beta} I + n s_c$

If K is big enough, (18) holds and estimated current values $\hat{\imath}'_{ds}$ and $\hat{\imath}'_{qs}$ will converge to the real ones i_{ds}, i_{qs} ($\overline{i_{ds}} \to 0$, $\overline{i_{qs}} \to 0$, $\hat{s_n} \to 0$).

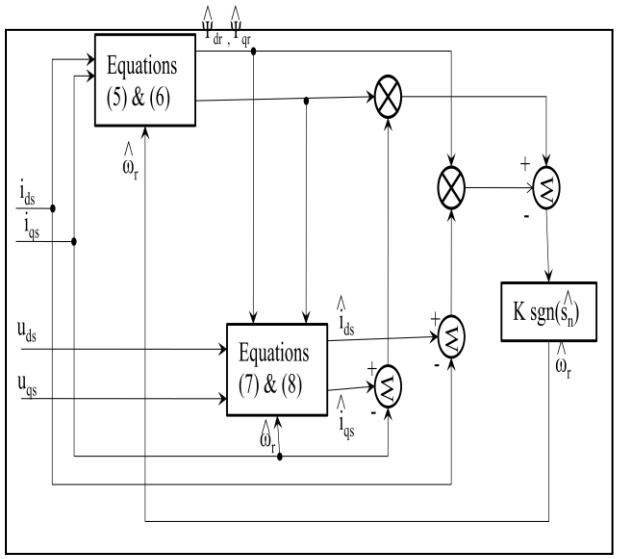

Fig. 1 Block diagram of the proposed observer.

IV. SIMULATION AND RESULTS

Speed estimation block in simulation is constructed using equations 5, 6 and 7, 8 are respectively used for speed estimation in sliding mode observer. Sliding mode

observer system shown in fig 2 is simulated using MATLAB.

The speed, current and rotor flux responses are observed under various operating conditions such as constant speed, step change in reference speed etc.

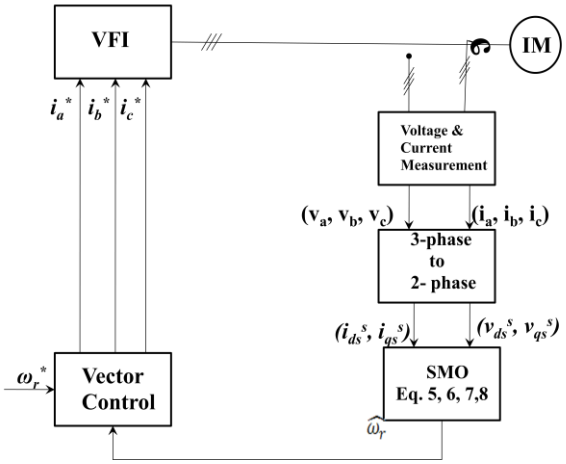

Fig. 2 Block diagram of speed sensorless vector control

Fig. 3a and 3b shows the actual and estimated speed and estimated fluxes respectively. When 100 rpm reference speed is applied to induction motor.

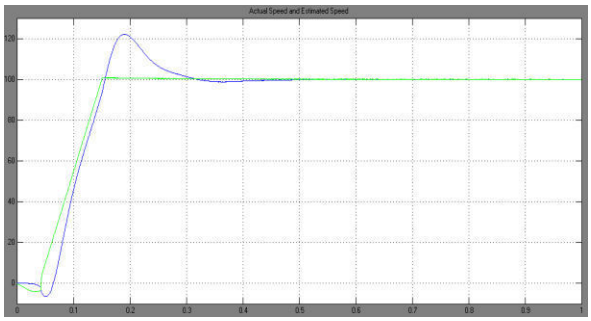

Fig. 3a actual speed and reference speed for 100 rpm

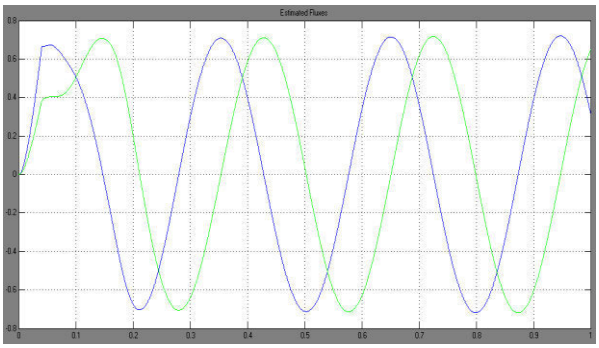

Fig. 3b Estimated fluxes at 100rpm

Fig. 4a and 4b shows the actual and estimated speed and estimated fluxes respectively. When 1000 rpm pulsed reference is applied to induction motor.

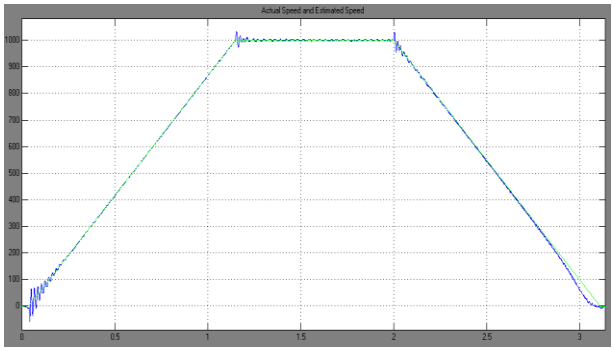

Fig. 4a actual speed and reference speed for 100 rpm

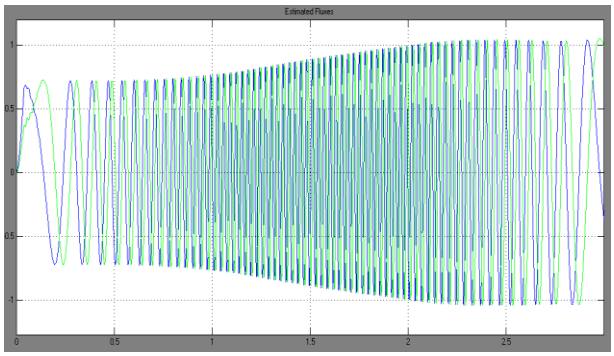

Fig. 4b Estimated fluxes at reference speed of 100rpm

IV. CONCLUSION

Controlled ac drives without mechanical sensors for speed have the attraction of lower cost and higher reliability. A variety of sensorless controlled ac drive schemes are available for practical application. In this paper, a sliding mode observer implemented in the stationary reference frame is proposed to identify the rotor speed of an induction motor. This system is simulated using MATLAB. The results proved that the proposed system can give better overall performance regarding to estimation accuracy, and has a good convergence performance and better steady identification characteristics. Also results confirm the robustness of the proposed observer to the parameter variation

REFERENCES

[1] P.Vas, Sensorless Vector and Direct Torque Control, New York: Oxford University Press, 1998.

[2] B. K. Bose, "Modern power electronics and AC drives", Prentice hall Inc, 2002.

[3] Tursini, M., and Petrella, R.: 'Adaptive Sliding-Mode Observer for Speed-Sensorless Control of Induction Motors', IEEE Trans. Ind. Appl., 2000, 36, (5)

[4] P. C. Krause, O. wasynczuk, S. D. sudhoff, "Analysis of electric machinery and drive system" IEEE press, 2002.

[5] Utkin, V., Gulder, J., and Shi, J.: 'Sliding Mode Control in Electromechanical Systems' (Taylor & Francis, 1999)

◈◈◈

Harmonic Reduction of Hybrid Active Power Filter Using Hysteresis Controller In Power System

M. Sahithullah

Er. Perumal Manimekalai College Of Engg , Hosur
E-Mail : sahithullahmahaboob@gmail.com

Abstract - The application of power electronics devices such as arc furnaces, adjustable speed drives, computer power supplies etc. are some typical non-linear characteristic loads used in most of the industrial applications and are increasing rapidly due to technical improvements of semiconductor devices, digital controller and flexibility in controlling the power usage. The use of the above power electronic devices in power distribution system gives rise to harmonics and reactive power disturbances. The harmonics and reactive power cause a number of undesirable effects like heating, equipment damage and Electromagnetic Interference effects in the power system. The conventional method to mitigate the harmonics and reactive power compensation is by using passive LC filters but this method has drawbacks like large size, resonance problem and fixed compensation behaviour etc., so this solution becomes ineffective. Subsequently, the active power filter comes in to the picture, which gives promising solution to compensate for the above adverse effects of harmonics and reactive power simultaneously by using suitable control algorithms. Different Active Power Filter topology has proposed by many authors, such as series, shunt and hybrid type and these may be based on current source or voltage source. Series Active Power Filter is used to compensate the voltage harmonics and shunt type for current harmonics. As non-linear loads are injecting current harmonics to the power system, the suitable choice to eliminate current harmonics is voltage source shunt Active Power Filter. To extract the fundamental component of source current synchronous reference frame theory is suitable because of its easy mathematical calculation compared to p-q control algorithm. Further, switching signals to drive the Voltage Source Inverter of the popular control strategies namely hysteresis current controller is used.

I. INTRODUCTION

To cancel the harmonics and compensate the reactive power APF is a suitable solution. The APF concept is to use an inverter to inject current or voltage harmonic components to cancel the load harmonic components. The more usual configuration is a shunt APF to inject current harmonics into the point of common coupling (PCC).

The APF can be installed in a low voltage power system to compensate one or more loads; thus, it avoids the propagation of current harmonics in the system. The developments of different control strategies give APF to a new location. As APF compensate the reactive power and cancel the harmonics, it is also called as active power line conditioners (APLC). The concept of shunt APLC was first introduced by Gyugyi and strycula in 1976.

The three main aspects of an active power conditioner are:

- The configuration of power converter (the scheme and the topology of converter and the electronics device used)
- The control strategy (the calculation of APLC control reference signals)
- The control method used (how the power inverter follows the control reference)

1.2 CONFIGURATION OF ACTIVE POWER FILTERS:

APF's can be classified based on converter type, topology, and the number of phases.

The converter type is mainly two types.

1) Voltage source inverter (VSI)

2) Current source inverter (CSI)

The topology of active power filter is classified in to three types.

1) Series active power filters

2) Shunt active power filters

3) Hybrid active power filters

Finally based on the phases the APF mainly two types.

1) Two-wire (single phase) system.

2) Three or four-wire three-phase system.

1. Series Active Power Filter:

Fig.3.3 shows the connection scheme of a series APLC. It is connected to the power system through coupling transformer. The compensation voltage is used to cancel the voltage harmonics of load.

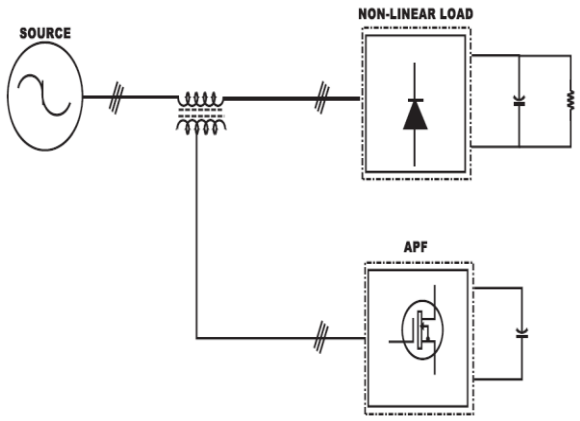

Fig.3.3 A series APLC scheme

The performance scheme of series APLC is shown in figure.3.4(a). The APLC supplies acompensating voltage as in Fig.3.4(b). These harmonic components cancel the voltage harmonicsof the load. After the compensation, the source voltage will be sinusoidal bas shown inFigure 3.4(c).

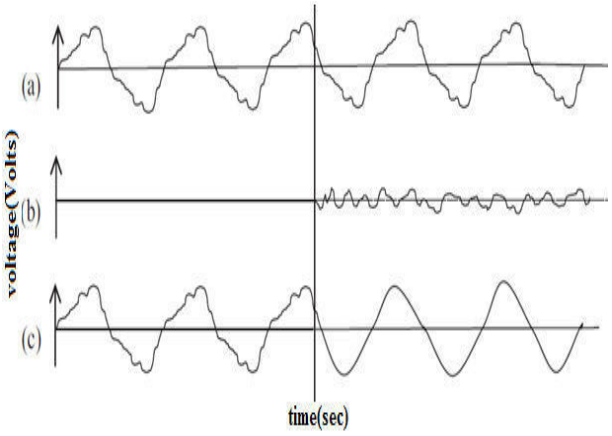

Fig.3.4 Performance schemes of series active power filter.

1.2.4 Shunt Active Power Filter:

The more usual APLC configuration is the shunt or parallel connection. Fig.4.5 shows the basic scheme of the connection, where the MOSFET switching device represents the APLC power block. The loads with current harmonics can be can be compensated by this APLC configuration.

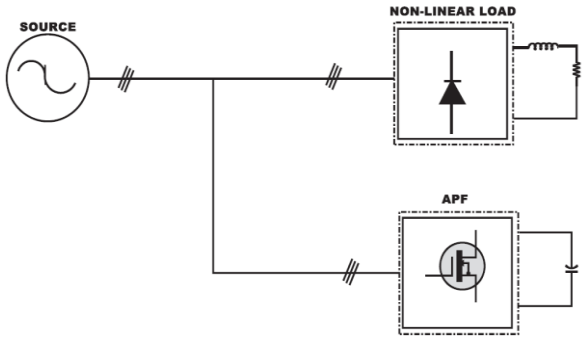

Fig.3.5 A shunt APLC scheme.

1.2.5 Hybrid Active Power Filter:

To reduce the cost of the static compensation, combination of static and passive filters is called as hybrid active power filter. The passive filters are used to cancel the most relevant harmonics of the load, and the active filter is dedicated to improving the performance of passive filters or to cancel other harmonics components. As a result, the total cost decreases without reduction of efficiency. Fig.3.6, 3.7 and 3.8 shows the more usual hybrid topologies.

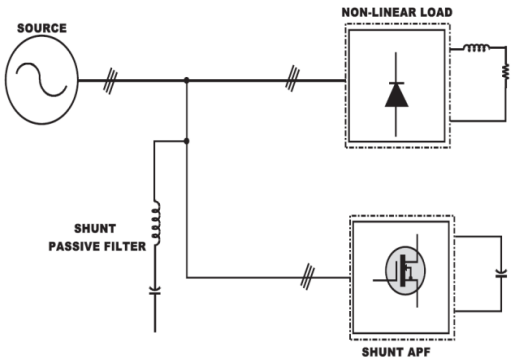

Fig.3.6 Hybrid filter with a shunt passive filter and a shunt active filter.

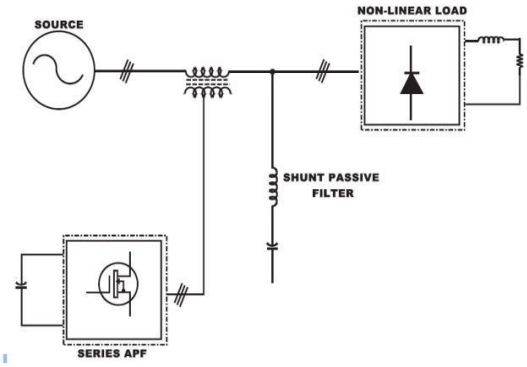

Fig.3.7 Hybrid filter with a shunt passive filter and a series active filter

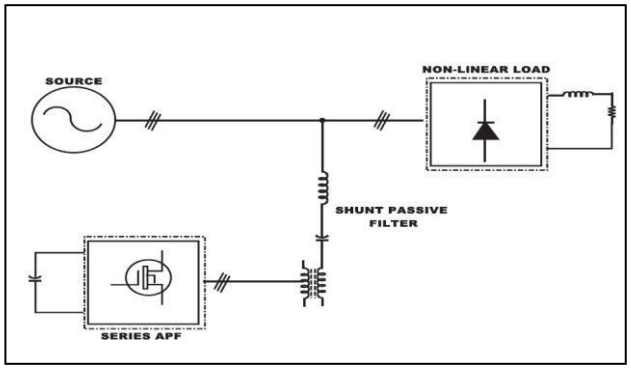

Fig.3.8 A shunts passive filter and a shunt active filter and an active filter in series with it

2.5 ADAPTIVE HYSTERESIS CURRENT CONTROLLER:

Inspite of several advantages, the basic hysteresis technique exhibits several undesirable features, such as uneven switching frequency that causes acoustic noise and difficulty in designing input filters. The hysteresis band current controller is composed of a hysteresis around the reference line current.

In equation (4.2), the reference line current of APF is referred to as iref, and measured line current of the APF is referred to as 'i'. The difference between i and iref is referred to as δ.

$\delta = i - i_{ref}$ (4.2)

The switching logic is formulated as follows:

If δ >HB upper switch is OFF (S1=0) and lower switch is ON (S4=1).

If δ <-HB upper switch is ON (S1=1) and lower switch is OFF (S4=0).

The switching logic for phase b and phase c is similar as phase a, using corresponding reference and measured currents and hysteresis bandwidth (HB).

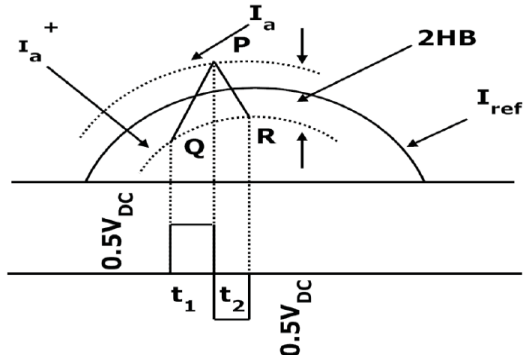

Fig.4.6 Current and voltage waveform with hysteresis band current controller

In case of Adaptive HCC, the rate of change of the line current vary the switching frequency, therefore the switching frequency does not remain constant throughout the switching, operation, but varies along with the current waveform. Furthermore, the line inductance (that interfaces inverter and PCC) value of the APF and the capacitor voltage are the main parameters for determining the rate of change of line currents. Fig.4.6 shows the PWM current and voltage waveforms for phase-a.

The currents 'ia' tends to cross the lower hysteresis band at point Q, where S1 is switched on. The linearly rising current (ia +) then touches the upper band at point P, where is S4 switched on. The following equations can be written in the respective switching intervals t1 and t2 from Fig.5.6. The MATLAB/SIMULINK model for adaptive hysteresis band is shown in fig 4.7.

$di_a^+ = \frac{1}{L}[0.5v_{DC} - v_a]$(4.3)

$di_a^- = -\frac{1}{L}[0.5v_{DC} - v_a]$(4.4)

From Fig.4.10

$\frac{di_a^+}{dt}t_1 - \frac{di_{aref}^+}{dt}t_1 = 2HB$
(4.5)

$\frac{di_a^-}{dt}t_2 - \frac{di_{aref}^-}{dt}t_2 = -2HB$
(4.6)

$t_1 + t_2 = T_C = \frac{1}{f_C}$(4.7)

where t1 and t2 are the respective switching intervals and fc is the switching frequency. Adding

equation (4.5) and (4.6) and substituting in equation (4.7), it can be written as

$\frac{di_a^+}{dt}t_1 + \frac{di_a^-}{dt}t_2 - \frac{1}{f_C}\frac{di_{aref}^+}{dt} = 0$

(4.8) $HB = \frac{0.125V_{DC}}{f_C L}[1 - \frac{4L^2}{V_{DC}^2}\left(\frac{V_a}{L} + m\right)2]$(4.9)

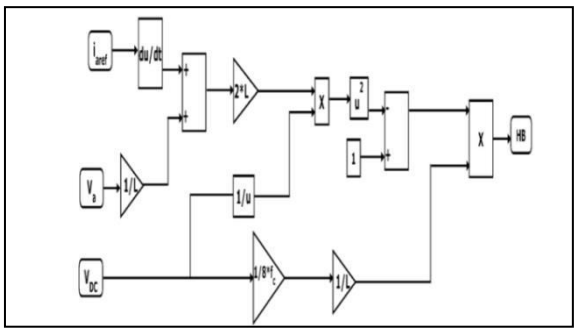

Fig. 4.7 Adaptive hysteresis bandwidth calculation block diagram.

2.6 CHAPTER SUMMARY:

In this chapter the basic compensation principle is described. That purely deepens up on the control algorithms. For extraction of reference current the superior features of SRF controller are described. The Hysteresis and adaptive hysteresis current controller algorithm are explained. The digital hysteresis current controller algorithm is also described.

3.1 SIMULATION RESULTS:

3.1.1 System Parameters:

The system parameters considered for the study of APF for both SRF controller and adaptive hysteresis current controller are given in Table 5.1. The PI controller used inside the SRF controller for maintaining the capacitor voltage constant having proportional gain (KP) and integral gain (KI) are 0.1 and 1 respectively. The gain of the PI control is chosen by iterative manner until good performance is achieved.

TABLE 5.1 APF System Parameters using SRF theory.

SYSTEM PARAMETERS	VALUE
Line Voltage	415V
Supply Frequency	50HZ
Source mpedance:(Resistance Rs, Inductance Ls)	1 Ω, 0.1 mH
Non-Linear load under steady state:(Resistance Rs, inductance Ls)	10 Ω, 100 mH
Filter Impedance:(Resistance Rs, inductance Ls)	1 Ω, 2.5 mH
Dc side capacitance	800 V
Power converter	6 OSFET/DIODE

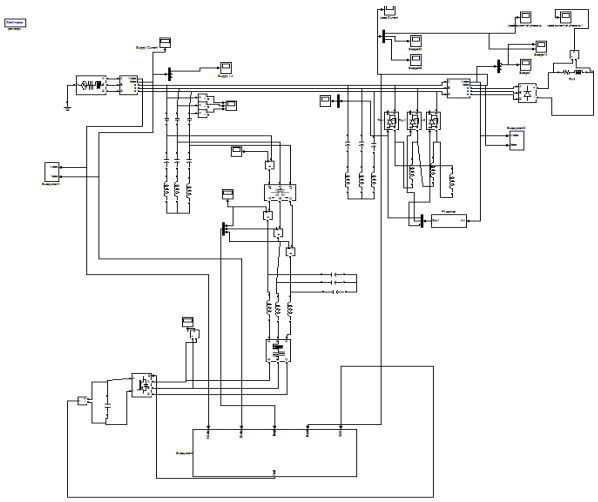

Fig. 5.1 Simulation diagram of APF.

During the period t=0 to t=0.1 sec R, L parameters of the nonlinear load are set as 10 Ω and 100 mH respectively. The corresponding load current waveform obtained are shown in the Fig. 5.2(a).

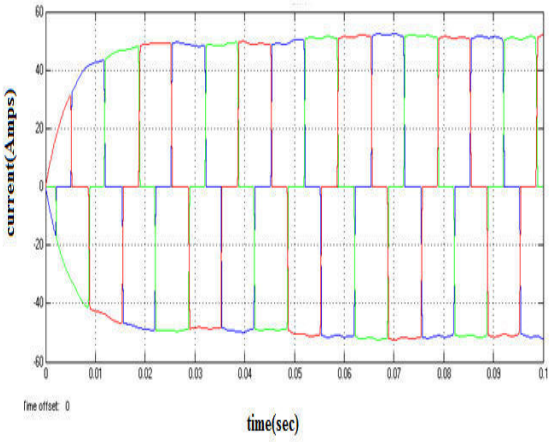

Fig. 5.2 (a) Load Current

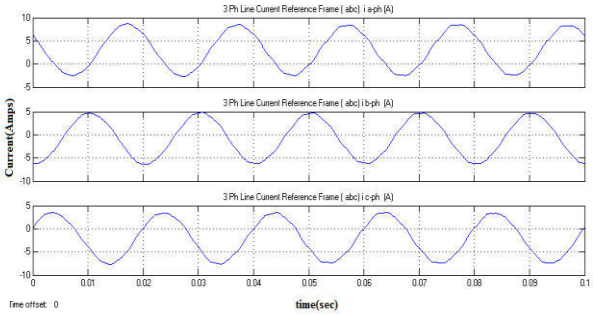

Fig. 5.2 (b) Reference Current

During the period t=0 to t=0.1 sec R, L parameters of the nonlinear load are set as 10 Ω and 100 mH respectively. The corresponding compensating current waveform obtained are shown in the Fig. 5.2(c).

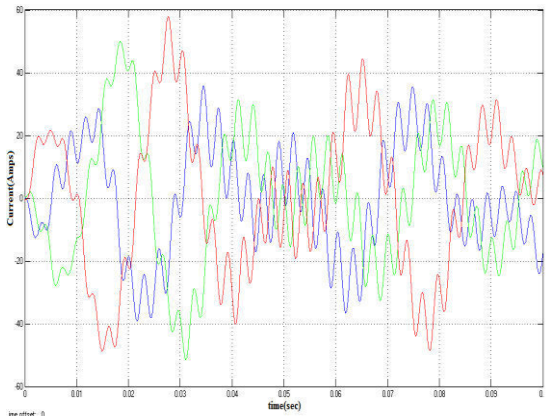

Fig. 5.2 (c) Compensating Current

During the period t=0 to t=0.1 sec R, L parameters of the nonlinear load are set as 10 Ω and 100 mH respectively. The corresponding source current waveform obtained are shown in the Fig. 5.2(d).

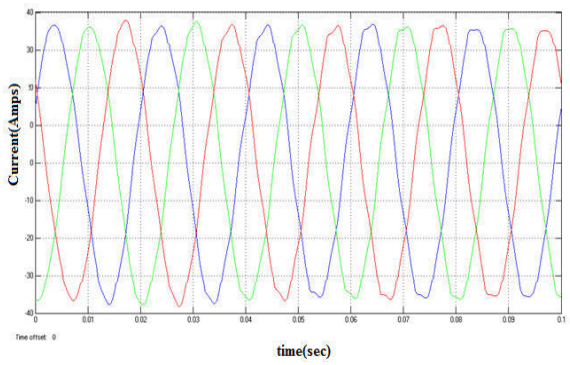

Fig. 5.2 (d) Source Current after compensation

In steady state condition the simulation time is taken as t=0 to t=0.1 sec with constant load. The load current is shown in Fig. 5.2 (a), which is highly non-linear in nature. The actual reference current for phase-a,b,c is shown in Fig. 5.1(b). This waveform is obtained from SRF controller. The APF inject the compensating current to PCC, which is shown in Fig. 5.2 (c). The compensating current containing only the harmonic current, which is introduced to the power system due to non-linear load but in opposite phase. The source current after compensation is as shown in Fig.5.2(d). It is clear from the Fig. that, the waveform is sinusoidal with some high frequency ripples.

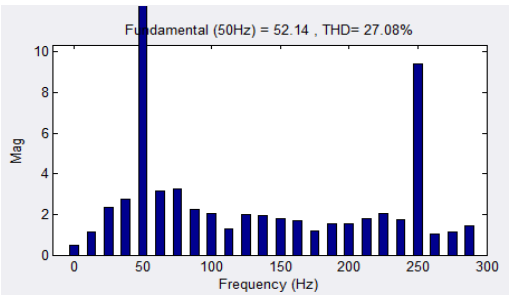

Fig. 5.2 (e) THD of load current

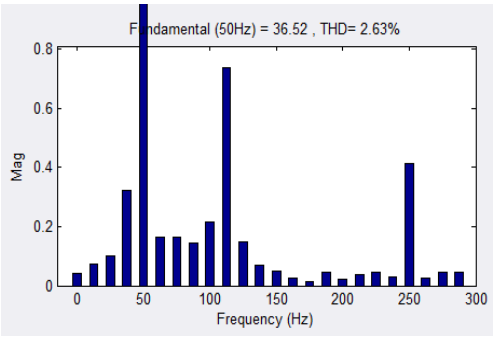

Fig. 5.2 (f) THD of source current

Fig. 5.5(f) shows the total harmonic distortion (THD) of source current by using hysteresis current controller. The results in Fig. 5.5(f) presented in the steady state conditions. Clearly source current THD indicating that, the harmonic content is reduced by using HCC. A comparison is made between load current and source current in the following table at various load conditions.

TABLE 5.2 THD Analysis

Conditions	Load current (%THD)	Source current (%THD)
Steady State	27.08	2.62

Simulations of integrated control circuit of APF are conducted with steady state. The results obtained show that the source current and load current THD has small variation in steady state. FFT analysis of the active power filter brings the THD of the source current into compliance with IEEE-519 & IEC-6000-3 standards.

4.1 CONCLUSIONS:

During this part of the project work the performance of the shunt active power filter is analyzed using HCC technique for minimizing harmonics, in the power system.

The SRF theory is used to generate reference current from the distorted load current and maintain the PWM VSI DC side capacitor nearly constant. Also it is used to extract the reference current and maintain the PWMVSI DC side voltage nearly constant. The beauty of this controller is, it can applicable to any system where mathematical models are difficult to get.

The performance of the HCC shunt active power filter are verified with the simulation results. Form the results; it clearly indicates that, the current ripple is less by using HCC. The THD of the source current after compensation is 2.62 % which is less than 5 %, the harmonic limit imposed by the IEEE-519 & IEC-6000-3 standard.

REFERENCES:

[1] Yacamini R., "Power system harmonics. II. Measurements and calculations" IEEE Power Engineering Journal, vol. 9, (1995): pp. 51-56.

[2] Amoli M. E. and Florence T., "Voltage, current harmonic content of a utility system-A summary of 1120 test measurements," IEEE Trans. Power Delivery, vol. 5, (1990):pp. 1552– 1557.

[3] Robert D Henderson, Patrick J. Rose "Harmonics: The effect on power quality and

transformer" IEEE Trans. Industry Applications, vol. 30, no.3, (1994):pp. 528-532.

[4] Singh B., Haddad K. A., and Chandra A.,"A review of active power filter for power quality improvement", IEEE Trans. Industrial Electronics, vol.46. no.5, (1999):pp. 960-971.

[5] Peng F. Z., Akagi H., Nabae A., "A new approach to harmonic compensation in power system- a combined system of shunt passive and series active filters " IEEE Trans. Industry Applications, vol. 26, (1990):pp.983-990.

[6] Chen C. and Divan D.M., "Simple topologies for single-phase AC line conditioning" IEEE Trans. Industry Applications, vol. 30, (1994):pp. 606–612.

[7] Nastran J., Cajhen R., Seliger M., and Jereb P., "Active power filter for nonlinear AC loads," IEEE Trans. Power Electron., vol. 9, (1994):pp. 92–96.

[8] Hafner J., Aredes M. and Heumann K., "A shunt active power filter applied to high voltage distribution line" IEEE Trans. Power Delivery., vol. 12, (1997): pp. 266–272.

[9] Mendalek N., Al-Haddad K., Fnaiech F and Dessaint L.A., "Nonlinear control technique to enhance dynamic performance of a shunt active power filter" IEEE Trans. Power application, vol. 150, (2003):pp. 373–379.

[10] Moran S., "A line voltage regulator/conditioner for harmonic-sensitive load isolation," in Conf. Rec. IEEE IAS Annu. Meeting, (1989):pp. 945–951.

[11] Akagi H., Kanazawa Y., and Nabae A., "Instantaneous reactive power compensators comprising switching devices without energy storage components," IEEE Trans. Ind. Applicat., vol. IA-20, (1984):pp. 625–630.

◈◈◈

Experimental Investigations Relating to the Presence of Copper Corrosion in Paper Insulation System of Power Transformers

***Faheem Ahmed Khan[$],[#]J.Sundara Rajan[†], Senior Member IEEE [**]Mohd. Z. A. Ansari[$], Member IEEE**

[$]Dept of Electrical and Electronics Engineering, Ghousia College of Engineering
Ramanagaram, Karnataka, India
†R&D Management Division, CPRI, Bangalore, India
E-mail : [*]faheem_khanb@rediffmail.com,[**]zahedansari@gmail.com,[#] sunder@cpri.in

Abstract - Corrosive sulphur in transformer oil has been a growing area of concern for the electrical power transmission industry as a whole for the past few years. There have been a number of documented cases of transformer failures, which are believed to be due to corrosive sulphur compounds contained in the transformer oils. This has led to an industry-wide investigation into the causes and possible remedies for transformer failures. For reliable operation of transformers, the condition of insulation system is very much important. In many transformers, the insulation used is oil with cellulose material like insulation papers or pressboards. When these insulating materials are adequately impregnated with oil, their insulating and mechanical properties improve. In the present work, the breakdown strength of insulation paper and its deterioration when formation of conducting copper sulphide (Cu_2S) takes place is studied in detail. The dry paper and oil impregnated paper are evaluated for breakdown when Cu_2S formation takes different shapes such as circular or irregularshapes and the results have been tabulated and discussed.

Keywords-*Surface discharge,transformer oil, copper corrosion, voltage distribution.*

I. INTRODUCTION

In the last decade, the study of formation and effects of corrosive sulfur in insulation oil has been widely carried out and it is concluded that the corrosive sulfur content in the insulating oil has been the main concern for the failure of the insulation and the transformers [1]-[5]. Conducting particles of copper sulfide is usually formed on the copper conductor (windings) and insulating materials (papers / pressboards) become partially conducting [7]. This leads to dielectric loss within the papers and also leads to thermal instability and finally thermo-electrical breakdown of insulating system occurs. The main source of sulfur in the insulation system is transformer oil, but the other potential sources are gaskets, water based glues, copper and Kraft papers [8].

In the present work, experimental investigations were carried out on formation of copper sulfide on Kraft paper in different shapeslike regular shapes namely circular and irregular shapesfor penetration of Cu_2S. The deterioration of dielectric strength and rise in leakage current for different combinations of affected paperlayers was experimentally determined. The worst form of penetration of Cu_2S is studied in the present work.

II. EXPERIMENTALMETHODOLOGY

Breakdown evaluation was conducted using a standard high voltage testing transformer set-up as shown in Figure 1. Plane-plane electrodes of 10cm diameter were used. Five layers of clean Kraft paper shown in Figure 2 were placed between the electrodes. The voltage was gradually raised in steps and the corresponding values of leakage currents were noted until occurrence of the electrical breakdown

.

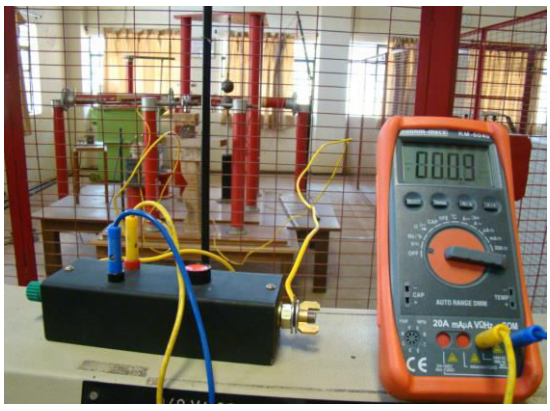

Figure 1: Experimental set-up for measurement of leakage current against the applied voltage.

1. Plain-plain electrodes 2.Standard resistor 3.Leakage current measuring device

A. Preparation of insulation paper for test and method

A set of paper samples of size 8cm x 12cm and thickness 50 µm were prepared and thickness was ascertained to be 50 ± 5 µm. These samples were dried in a hot air circulating oven at 100°C for 8 hours to remove moisture.

B. Simulation of Cu_2Smigration

Electrical grade paper was covered with Cu_2S of different concentration and breakdown strength was studied. Breakdown studies were also carried out with Cu_2S migration into different layers. Lateral migration of Cu_2S through thickness into different layers of electrical grade paper was simulated. Different layers of paper were impregnated with Cu_2S, representing its migration into first, second, third, fourth and inner most layers. Measurements made on the set of specimens prepared are leakage current and breakdown voltage. The application of copper sulphide to paper on both HV side and LV side is considered. The copper sulfide migration was simulated in the samples in two different patterns viz. circular shape and repetitive irregular shapes. The conditioning period after migration of copper sulphide was two to three days in a controlled laboratory oven, which prevents ingress of moisture but helps in permeation of some quantity of copper sulphide into volume of paper. However, no attempt was made to measure the uniformity in spread of copper sulphide to the bulk of paper.

C. Insulation Paper with different quantity of copper sulphide

In this method, Cu_2S is simulated for migration into different layers of paper insulation representingCu_2S formation and migration into first, second, third, fourth and inner most paper layers. The measurements carried out in this experiment areof breakdown voltage and leakage currentfor different layers of paper insulation placed on either high voltage (HV) or low voltage (LV) electrodes. Clean and corroded paper layers are shown in Figure 2(a) and 2(b) respectively.

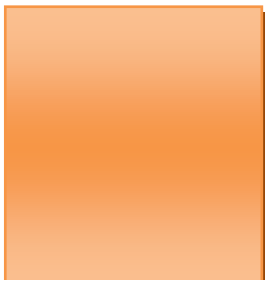

Figure 2(a): Clean Paper layer of size 9cm X 10cm and thickness 80µm

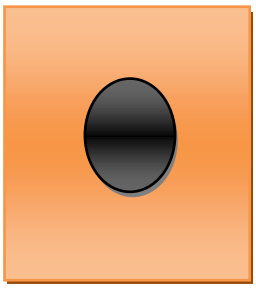

Figure 2(b):Paper layer in which Cu_2S is formed in circular shape of 2 cm

Figure 3 shows the paper in which Cu_2S formation has taken place in regularly irregular way.

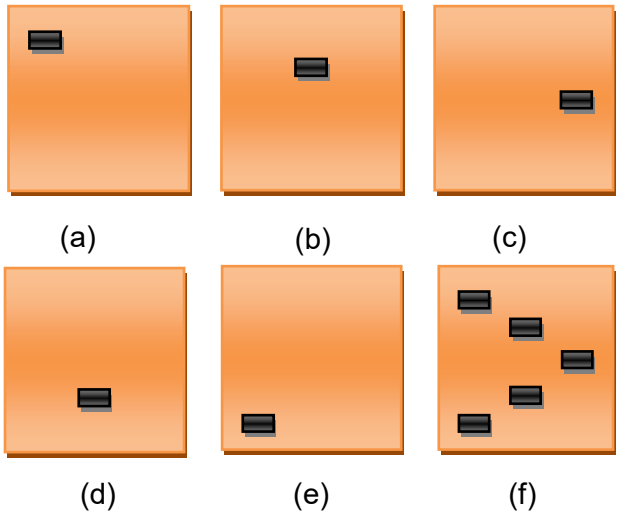

Figure 3 (a) – (e): Contamination of Paper layers in irregular form and (f) indicate equivalent contamination of all five paper layers shown in (a) – (e)

III. RESULTSANDDISCUSSIONS

The evaluation was conducted for different patterns of penetration of copper sulfide into different layers. Initially, the evaluation was carried out for dry paper (DP) samples and later for oil impregnated paper (OIP) samples for the same kind and pattern. The leakage current obtained for different combinations of clean and contaminated paper layers placed between plane-plane circular electrodes against the applied voltage is indicated in Table I.

Table I.

Applied voltage (kV)	Leakage current (mA)					
	5C + 0UC	4C + 1UC	3C + 2UC	2C + 3UC	1C+ 4UC	0C + 5UC
1	0.015	0.016	0.017	0.018	0.019	0.02
2	0.019	0.022	0.024	0.024	0.024	0.024
3	0.024	0.026	0.032	0.033	0.034	0.034
4	0.028	0.035	0.036	0.036	BD	BD
5	0.039	0.048	0.048	0.048		
6	0.048	0.05	0.055	BD		
7	0.057	0.069	BD			
8	0.062					
9	$^{\$}$BD					

Leakage current Versus Applied voltage when the Cu_2S migrates in Circular shape (DP)

As the applied voltage is increased, the leakage current rises. The insulation breaks down at about 9kV when all the paper layers were clean(C). When one out of five layers is contaminated (UC), the insulation breaks down at 7kV. As the contamination penetrates deeper into the layers, voltage at which insulation breaks down occurs shows decreasing trend. The insulation breaks down at 4 kV when all the layers are affected. While the leakage current increases linearly for lesser penetration, it raises exponentially when all the layers are affected. This trend is depicted in Figure3

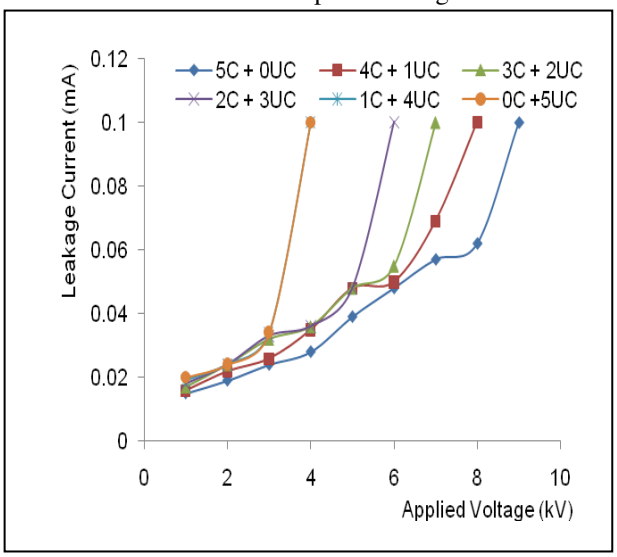

Figure 3: Leakage current versus Applied voltage for dry paper

For the oil impregnated paper, the breakdown is reduced significantly and the leakage current also rises exponentially. The leakage current is significantly higher in this case. The graph and the corresponding values are shown in Figure 4 and Table II respectively.

Table II Leakage current Versus Applied voltage when the Cu_2S migrates in Circular shape (OIP)

Applied voltage (kV)	Leakage current (mA)					
	5C + 0UC	4C + 1UC	3C + 2UC	2C + 3UC	1C+ 4UC	0C + 5UC
1	0.021	0.022	0.023	0.023	0.023	0.024
2	0.030	0.030	0.032	0.033	0.033	0.034
3	0.040	0.042	0.050	0.052	0.054	0.056
4	0.062	0.062	0.062	0.064	BD	BD
5	0.073	BD	BD	BD		
6	BD					

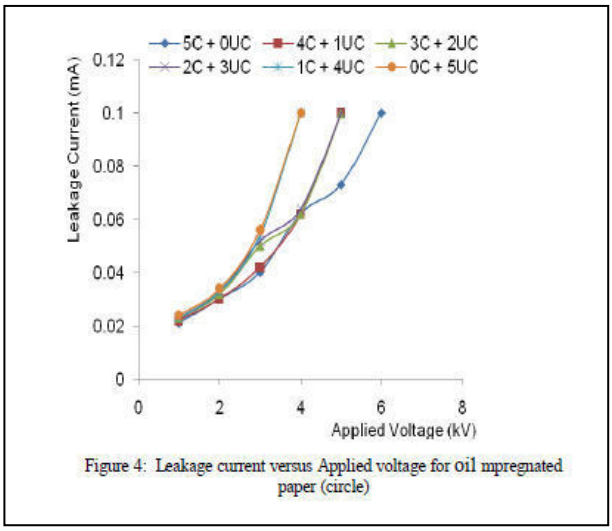

Figure 4: Leakage current versus Applied voltage for oil mpregnated paper (circle)

When the Cu_2S migrates in a irregular way, the deterioration of insulation is not as bad as the circular case. The insulation withstands up to 6 kV even when all the layers are affected. Oil impregnated paper also exhibits good withstand capacity. Table III and IVshows the leakage current for different applied voltages for dry and oil impregnated cases respectively. Corresponding graphs are shown in Figure 5and 6.

Table III

Table II Leakage current Versus Applied voltage when the Cu_2S migrates in Circular shape (OIP)

Applied voltage (kV)	Leakage current (mA)					
	5C + 0UC	4C + 1UC	3C + 2UC	2C + 3UC	1C+ 4UC	0C + 5UC
1	0.017	0.017	0.021	0.021	0.022	0.024
2	0.024	0.026	0.026	0.026	0.027	0.027
3	0.032	0.034	0.034	0.036	0.036	0.039
4	0.04	0.04	0.041	0.042	0.043	0.047
5	0.05	0.05	0.052	0.053	0.055	0.056
6	0.06	0.06	0.06	0.068	BD	BD
7	0.064	BD	BD	BD		
8	BD					

Table IV

Leakage current Versus Applied voltage when the Cu_2S is formed in irregular shape(DP)

Applied Voltage (kV)	Leakage current (mA)					
	5C + 0UC	4C + 1UC	3C + 2UC	2C + 3UC	1C+ 4UC	0C + 5UC
1	0.026	0.027	0.028	0.028	0.028	0.029

2	0.030	0.032	0.033	0.034	0.035	0.036
3	0.040	0.042	0.045	0.048	0.052	0.052
4	0.056	0.057	0.063	0.065	0.069	0.069
5	0.060	0.069	0.073	0.093	BD	BD
6	BD	BD	BD	BD		

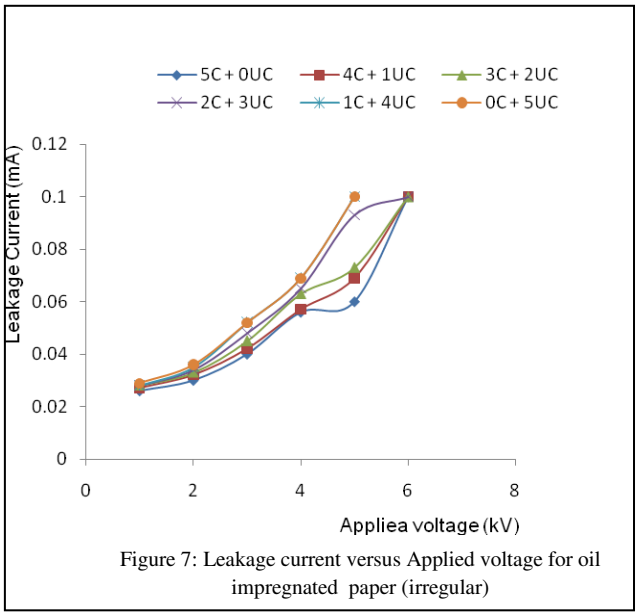

Figure 7: Leakage current versus Applied voltage for oil impregnated paper (irregular)

IV. CONCLUSIONS

Evaluation of transformer electrical grade paper samples has revealed that there is a significant reduction in breakdown voltage due to formation of Cu_2S. The minimum reduction in electric breakdown strength was observed to be 30% in the present experimental conditions. However, larger reductions are also seen under certain conditions. Some of the conclusions of the study are:

1. The reduction in breakdown strength of paper with Cu2S deposits is much larger than the reduction due to small moisture levels.
2. There is a correlation between the concentration of Cu_2S and dielectric strength/Leakage current observed in paper insulation
3. The deterioration of dielectric strength is rapid in case where Cu_2S is formed in a regular path. The reduction in dielectric strength is from 9 kV/cm to 4 kV/cm in the present case.
4. Leakage current variation is linear up to 40% of Copper sulphide contamination of paper and then increases exponentially for higher levels of contamination.
5. Formation and penetration of Cu_2S from one layer to the other in concentric rings of increasing/decreasing diameter or its penetration in irregular fashion has more effect on dielectric strength then similar penetration in an irregular fashion. (NOT CLEAR_CHECK?)
6. Penetration of Cu_2S from 1st layer to the 2nd, 2nd to the 3rd and so on in circular patches of equal diameter has significant effect on dielectric strength and hence the breakdown of insulation.

ACKNOWLEDGMENT

The authors would like to thank the authorities of Ghousia College of Engineering, Ramanagaram and Central Power Research Institute (CPRI), Bangalore for all the cooperation and encouragement in carrying out this work.

REFERENCES

[1] J. Sundara Rajan, C. Jayarama Naidu, K Dwarakanath and A.K Tripathy"Studies on the effects of sulpher in transformer oil on transformer components", XV International symposium on high voltage Engineering, Slovenia, August 2007.

[2] Copper sulphide in transformer insulation' Report from task force A2-31, ELECTRA, February 2005-6

[3] Lewand.L. "Investigating copper sulphide contamination in a failed GSU transformer" Proc. of the 72nd annual Doble Conference of Doble Clients, Boston, M.A. Insulating materials session, 2005.

[4] Claes Bengtsson, Jan Hajek, Mats Dahlund, Lars Patterson, Karin Gustafsson, Robot Leandersson, ArneHjortsberg "Oil corrosion and conducting Cu_2S deposition in power transformer windings" CIGRE 2006 session, paper A2-111.

[5] Jan Hajek, Mats Dahlund, Lars Patterson, "Quality of oil makes the difference, ABB discovers the solution to transformer breakdowns", ABB review. Nr 3-2004, pp 61-63.

[6] B.P.Singh, T.S.R. Murthy, G. Jayaraman, A. K. Adikeshalu et al. "Effect of Mercaptan sulpher on insulation performance of HVDC converter transformers" CIGRE 2006 paper A2-105.

◈◈◈

Detoxification of Dairy Waste Water By Using Compound Parabolic Concentrator (CPC) And Oxidising Agent

K. Sai Santhosh, M.Tech & A. Shaija

NIT Calicut, Mechanical Engineering Dept., Calicut, India.
Email: saisanthoshkodimala@gmail.com, shaija@nitc.ac.in

Abstract - This paper describes about 'Solar detoxification technology for the treatment of Diary wastewater contaminants'. The objectives are to develop a simple, efficient and commercially competitive solar water treatment technology based on compound parabolic collectors (CPC). For this a CPC was fabricated in the NIT Calicut and experiments were conducted using that. In this research titanium dioxide (TiO_2) and hydrogen peroxide (H_2O_2) is used as catalyst and oxidising agent respectively. Solar photocatalytic water mineralization using the interaction between ultraviolet radiation and titanium dioxide (TiO_2) has a strong potential for the destruction of toxic organics in water, as widely demonstrated in recent years. The use of additional oxidizing agent (H_2O_2) during the experimentation has improved the reaction time and increases the efficiency of the process. The experimental results were plotted with or without the addition of (H_2O_2) in wastewater.

Keywords - *Compound parabolic concentrator(CPC), catalyst(TiO_2), oxidizing agent (H_2O_2).*

I. INTRODUCTION

Photocatalysis is a rapidly expanding technology for water and air treatment. It can be defined as the acceleration of photoreaction in the presence of a catalyst. The initial interest in the heterogeneous photocatalysis was started when Fujishima and Honda discovered in 1972 the photochemical splitting of water into hydrogen and oxygen with TiO_2. Since then, date extensive work has been carried out to produce hydrogen from water by this novel oxidation reduction reaction using a variety of semiconductors. [1]

In recent years interest has been focused on the use of semiconductor materials as photocatalyst for the removal of organic and inorganic species from aqueous or gas phase. This method has been suggested in environmental protection due to its ability to oxidise the organic and inorganic substrates or no residue of the original material remains and therefore no sludge requiring disposal to landfill is produced..

In photocatalysis two or more phases are used in the photocatalytic reaction. A light source with semiconductor material is used to initiate the photoreaction. The catalysts can carry out substrate oxidations and reductions simultaneously. UV light of long wavelengths can be used, possibly even sunlight.

The catalyst itself is unchanged during the process and no consumable chemicals are required. These results in considerable savings and a simpler operation of the equipment involved. Additionally, because the contaminant is attracted strongly to the surface of the catalyst, the process will continue to work at very low concentrations allowing sub part-per-million consents to be achieved. Taken together, these advantages mean that the process results in considerable savings in the water production cost and keeping the environment clean.

II. MECHANISM

Photocatalysis is a complex sequence of reactions. The oxidation pathway is not yet fully understood. However, Pirkanniemi suggested in 2002 that the heterogeneous photocatalysis reaction follows five steps. These are: "(i) diffusion of reactants to the surface, (ii) adsorption of reactants onto the surface, (iii) reaction on the surface, (iv) desorption of products from the surface, and (v) diffusion of products from the surface".

There are two routes through which OH radicals can be formed. The reaction of the valence-band "holes" (hvb^+) with either adsorbed H_2O or with the surface OH^- groups on the TiO_2 particle. Equations (1 and 2).

$$TiO_2\ (hvb^+) + H_2Oads \rightarrow TiO_2 + HO\bullet ads + H^+ \longrightarrow (1)$$

$$TiO_2\ (hvb^+) + HO^-ads \longrightarrow TiO_2 + HO\bullet ads \longrightarrow (2)$$

In general, donor (D) molecules such as H_2O will adsorb and react with a hole in the valence-band and an acceptor (A) such as dioxide will also be adsorbed and react with the electron in the conduction band (ecb−), according to equations 3 and 4

TiO_2 (hvb+) + Dads ⟶ TiO_2 + D^+ads ⟶ (3)

TiO_2 (ecb−) + Aads ⟶ TiO_2 + A^-ads ⟶ (4)

It is generally accepted that oxygen plays an important role. Oxygen can trap conduction-band electrons to form superoxide ion (O_2• $^-$), equation (5). These superoxide ions can react with hydrogen ions (formed by splitting water), forming HO_2•

TiO_2 (ecb^-) + O_2ads + H^+ ⟶ TiO_2 + HO_2• ⟶ O_2• $^-$ + H^+ ⟶ (5)

H_2O_2 could be formed from HO2• via reactions (6)

TiO_2 (ecb^-) + HO_2• + H^+ ⟶ H_2O_2 ⟶ (6)

Cleavage of H_2O_2 by one of the reactions (7, 8, and 9) may yield an OH radical

H_2O_2 + *hv* ⟶ 2HO • ⟶ (7)

H_2O_2 + O_2• − ⟶ HO • + O_2 + HO^- ⟶ (8)

H_2O_2 + TiO_2 (ecb^-) ⟶ HO • + HO^- + TiO_2 ⟶ (9)

Photo reduction, photo oxidation and adsorption occur on or near the particle surface as shown from. The illumination of semiconductor particles such as TiO_2 generates e^-cb and h^+vb as described previously. A competition reaction occurs between water, oxygen, organic molecules and trace metals which may be present in the system. Mercury (II) will be reduced to mercury (0), oxygen molecules will also be reduced and give active species (O_2•$^-$). Cr (VI) will also be reduced to Cr (III). Cd (II) can be adsorbed to TiO_2 and water will be oxidised by the hole in the valance band to give the very active free radical •OH which can oxidize organic species.[2]

III. COMPOUND PARABOLIC CONCENTRATOR (CPC)

CPC non-imaging concentrators, extensively employed for evacuated tubes, are an interesting cross between trough concentrators and one-sun systems and are a good option for solar photochemical applications. CPCs are static collectors with a reflective surface following an involute around a cylindrical reactor tube and have been found to provide the best optics for low concentration systems; it can be designed with a CR=1 (or near one), then having the advantages of both PTCs and one sun collectors.

A CPC for absorber is one which consists of curved segments, which are two parabolas. Many improvements in the design and performance of CPC collector have been made since its invention in 1974. The CPC reflector profile for a tubular absorber is such that the reflector touches absorber at the cusp region as shown in fig 1. This results in conductive heat losses. So, a gap between the tubular absorber and the reflector has to be created to prevent this conduction heat loss from absorber to metallic reflector and also providing a glass envelope leads to loss of the incident light on the absorber, called 'gap losses'. Several modifications of the basic CPC design were suggested for the provision of the gap. Winston proposed a reflector design which preserved the ideal flux concentration on the absorber of radius r.

IV. DESIGNING OF CPC:

The following were considered for designing the CPC.

- The reflectors are sections of identical parabolas but are kept separated.
- The focus of one half of the reflector lies at the opposite edge of the absorber and similar for other half.
- The axis of symmetry of the two halves of the reflector is the optic axis of the concentrator.
- The concentrator does not produce any image of the light source, hence they are called non imaging concentrators.
- For any given direction of light source, a certain fraction of rays entering the aperture will reach the absorber directly, while the other rays will reach the absorber after one or more reflections. Therefore one can define an average number of reflections (n) for a CPC.

A. ACCEPTANCE ANGLE:

The normal values for the semi-angle of acceptance (θ_A), for photocatalytic applications, are going to be between 60 and 90 degrees. Fig. 2 shows two dimensions CPC designed with θ_A max 60. Therefore, CR($\frac{1}{sin\theta_A}$) of CPC is 1:15.This wide angle of acceptance allows the receiver to collect both direct and a large part of the diffuse light, with the additional advantage of decreasing errors of both the reflective surface and receiver tube alignment, which become important for achieving a low-cost photoreactors. [3]

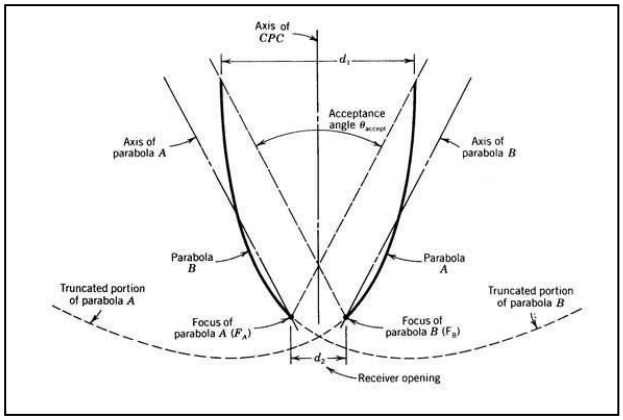

Figure 1. Reflector profile for a flat absorber

B. REFLECTOR DESIGN:

A tubular absorber (radius r) requires a cusp shaped reflector. Locate any point B on the reflector is given by its distance ρ= BC from the point C at which tangent touches the absorber, and BC is equal to the arc length AC along the absorber circumference. The reflector shape is fixed by the following requirement.[5]

- For | θ | ≤ $(\theta_A + \frac{\pi}{2})$, any ray emitted tangentially from point c of the absorber towards the onto itself reflector must be reflected back.
- For $(\theta_A + \frac{\pi}{2}) \leq$ θ $\leq (3\frac{\pi}{2} - \theta_A)$, any ray emitted tangentially from point c of the absorber towards the reflector must be reflected so as to make an angle θ_A with the y axis. The coordinates of B are represented by

  X = $r\sin\theta - \rho\cos\theta$

  Y = $-r\cos\theta - \rho\sin\theta$

  For θ ranges from A to B the value of ρ is taken as

$$\rho = r(\theta) \quad For\ \theta \leq \left(\theta_A + \frac{\pi}{2}\right) \longrightarrow \quad (1)$$

for the range of θ from C to F the value of ρ

$$\rho = \frac{r[\theta + \theta_A + \frac{\pi}{2} - \cos(\theta - \theta_A))}{1 + \sin(\theta - \theta_A)} \quad \text{For } \left(\theta_A + \frac{\pi}{2}\right) \leq \theta \leq (3\frac{\pi}{2} - \theta_A) \longrightarrow \quad (2)$$

The equation (1) is used for drawing the arc of AB and equation (2) is used for drawing the arc from B to required height.

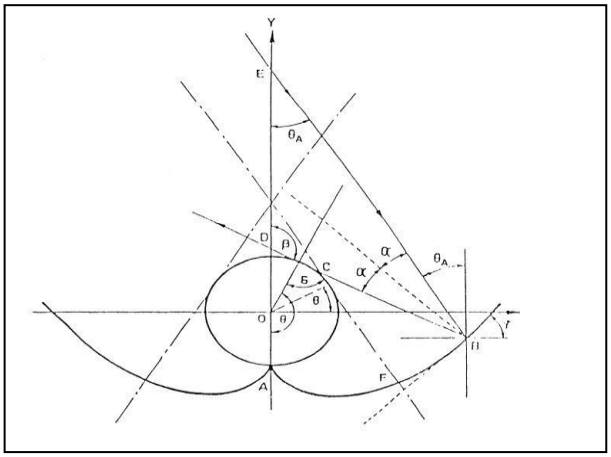

Fig 2. Reflector profile for a tubular absorber

V. DEVELOPMENT OF A SINGLE CPC PROFILE IN CATIA SOFTWARE

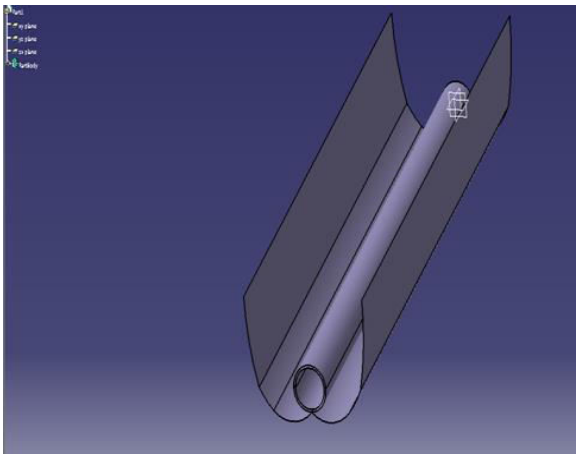

Fig 3. CPC profile using catia V5 software

VI. ENERGY ANALYSIS OF A CPC:

In order to determine the energy balance on a CPC collector all important heat fluxes must be calculated. The fluxes are then combined in heat balance equations for the absorber, aperture cover, and the transport fluid. The heat loss through the outer walls of the collector and absorber can be made very small by proper insulation. [6]

The various heat fluxes involved in CPC are described as follows:

- Direct solar radiation absorbed both directly and indirectly by the receiver after reflection from the envelope is

$$q_{b,r} = [I_{b,c}\tau_a(i)\rho_m^n\alpha_r I_{b,c}\tau_a + (i)\rho_m^n\alpha_r\rho_m^{2n}\rho_r\rho_a]\frac{A_a}{A_r}$$

$$q_{b,r} = I_{b,c}\tau_a(i)\rho_m^n\alpha_r(1+\rho_m^{2n}\rho_r\rho_a)\frac{A_a}{A_r}$$

➢ Direct solar radiation absorbed both directly and indirectly by the aperture cover after reflection from the receiver is

$$q_{b,a} = [I_{b,c}\alpha_a(i) + I_{b,c}\tau_a(i)\rho_m^{2n}\rho_r\alpha_a^*]\frac{A_a}{A_r}$$

$$q_{b,r} = I_{b,c}[\alpha_a(i) + \tau_a(i)\rho_m^{2n}\rho_r\alpha_a^*]\frac{A_a}{A_r}$$

➢ Diffuse solar radiation absorbed by the receiver is

$$q_{d,r} = I_{d,c}\tau_a^*\rho_m^n\alpha_r\frac{A_a}{A_r}$$

➢ Diffuse solar radiation absorbed by the aperture cover is

$$q_{d,a} = I_{d,c}\alpha_a^*\frac{A_a}{A_r}$$

➢ Radiative exchange between the receiver and cover is

$$q_{i,r} = \in_{eff}\sigma(T_r^4 - T_a^4)\frac{A_a}{A_r}$$

➢ Radiative exchange between the cover and environment is

$$q_{sky} = \in_{a,ir}\sigma(T_a^4 - T_{sky}^4)\frac{A_a}{A_r}$$

➢ Convective exchange between receiver and cover is

$$q_{c,r} = h_{c,r}(T_r - T_a)\frac{A_a}{A_r}$$

➢ Convective exchange between cover to the environment is

$$q_{c,e} = h_{c,e}(T_a - T_\infty)\frac{A_a}{A_r}$$

➢ Useful heat extraction by the fluid is q_u.

Where

$I_{b,c}$ = beam radiation incident on collector plane.

$I_{d,c}$ = diffuse radiation incident on collector plane.

(i)= incidence angle

T_{sky} = *effective sky temperature for radiation*

$h_{c,e}, h_{c,r}$ = *convective coefficients*

α_r, α_a = *receiver and cover absorptances*

ρ_r, ρ_a = *receiver and cover reflectance's*

α_a^* = *absorptances for diffused radiation*

τ_a^* = *transmittance for diffused radiation*

Applying energy balance equations:-

The absorber conservation of energy equation is

$$q_{b,r} + q_{d,r} = q_u + q_{c,r} + q_{i,r}$$

The cover conservation of energy equation is

$$q_{b,a} + q_{d,a} + q_{i,r} + q_{c,r} = q_{sky} + q_{c,e}$$

The transported fluid energy equation is

$$T_o - T_i = \frac{q_u \times A_r}{\dot{m}}$$

The instantaneous efficiency (η_c) is defined as the system output divided by the incident radiation

$$\eta_c = \frac{q_u A_r}{A_a(I_{b,c}+I_{d,c})}$$

VII. EXPERIMENTAL LAYOUT

A CPC was fabricated according to the solar technology for NITC ragion in NITC as shown in fig 3.

Figure 4: Experimental setup of photocatalysis in NITC

The waste water collected from the dairy industry was passed through the CPC by using a centrifugal pump and results were compared between flow rates of 0.35 kg/s and 0.4 kg/s.

Waste water was mixed with TiO_2 and was passed through the CPC and results were shown in table 1.

Waste water mixed with TiO_2 and H2O2 was passed through the CPC and results were shown in table 2.

3 mg of TiO_2 per litre of water was mixed and 3ml of H_2O_2 was mixed as oxidising agent in water for experimental purpose.

VIII. RESULTS

Time(h)	pH		TSS		TDS		COD		BOD	
	m_1	m_2	m_1	m_2	m_1	m_2	m_1	m_2	m_1	m_2
9:00	10.11	12.08	292	299	1425	1400	2471	2512	955	973
11:00	9.8	9.96	260	259	1350	1319	2019	1994	799	783
13:00	9.2	8.93	206	198	1210	1189	1609	1597	651	609
15:00	8.3	7.84	178	168	980	899	1119	1031	473	449
17:00	7.7	7.2	160	138	885	732	870	745	237	211

Table1: Experimental results when TiO_2 is used as catalyst

Time(h)	pH		TSS		TDS		COD		BOD	
	m_1	m_2	m_1	m_2	m_1	m_2	m_1	m_2	m_1	m_2
9:00	11.3	10.1	1458	1412	300	285	2508	2515	950	967
11:00	9.4	8.9	1329	1298	245	241	1993	1978	697	678
13:00	9	8	1189	1080	178	159	1496	1389	559	538
15:00	7.9	7.5	920	818	157	135	1038	998	356	339
17:00	7.1	7	789	678	122	107	699	578	178	168

Table2: Experimental results when TiO_2 & H_2O_2 is used as catalyst and Oxidizing agent

A. pH of water Vs local time

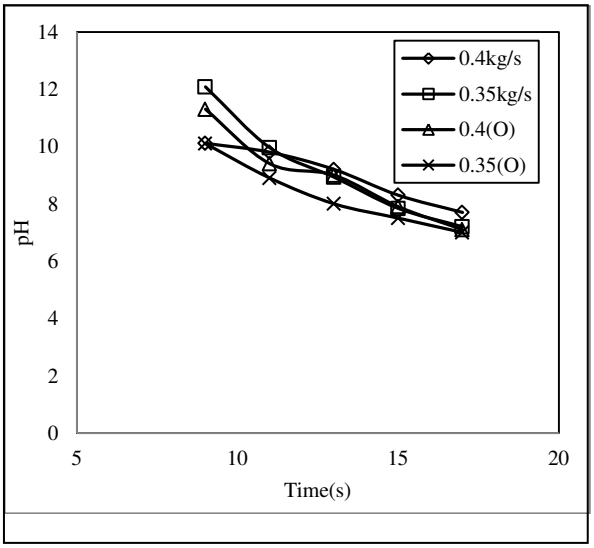

B. Total dissolved solids Vs local time

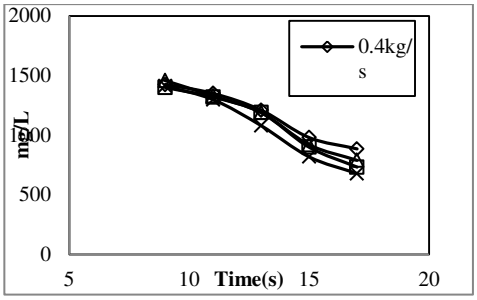

C. Total suspended solids(TSS)

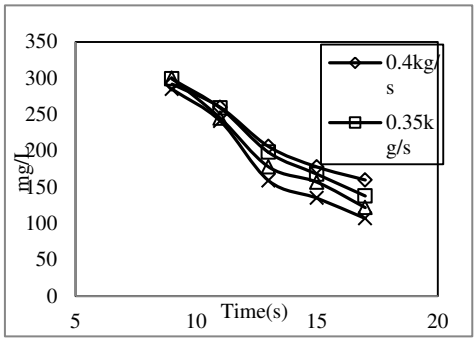

D. Chemical oxygen demand(COD)

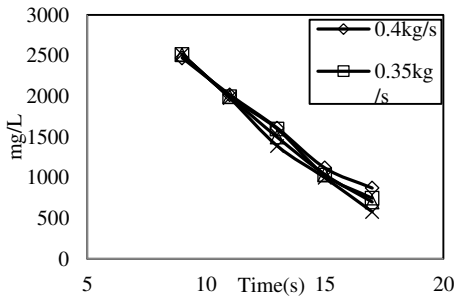

E. Biochemical oxygen demand(BOD)

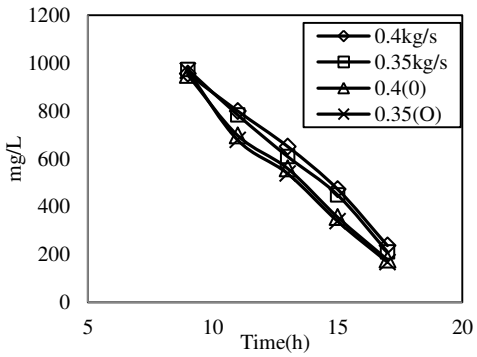

the results from A to E were plotted between time vs with respective chemical property.

IX. CONCLUSIONS:

The effect of catalyst in diary waste water is effective for the flow rate of 0.35 kg/sec from table 1.

It can be increased still by adding oxidizing agent (H_2O_2) in waste water and passing through the CPC shown in table 2.

REFERENCES:

1. P.A.S.S. Marques , M.F. Rosa, F. Mendesl, M. Collares Pereiral, J. Blanco, and S. Malato,Wastewater detoxification of organic and inorganic toxic compounds with solar collectors. Desalination 108(2004) ,213-220.
2. A Scrivani, T.El Asmar, U. Bardi, solar trough concentration for fresh water production and waste water treatment. Desalination 206 (2007), 485- 493.
3. S.p.sukhatme a text book on solar energy- tata Mc grill publications.
4. C. Sattler, L. de Oliveira, M. Tzschirner, A.E.H. Machado, Solar photocatalytic water detoxification of paper mill effluents. Energy 29(2004), 835-843.
5. Sixto Malato Rodriguez, Christoph Richter, Julian Blanco Galvez and Martin Vincent, Photocatalytic Degradation of Industrial Residual waters. Solar energy,vol.56, No5.
6. J. Blanco, S. Malato, P. Fernandez-Ibanez, D. Alarcon, W.Gernjak, M.I. Maldonado Review of feasible solar energy applications to water processes. Renewable and Sustainable Energy Reviews 13 (2009) ,1437-1445.
7. Janhavi Inamdar and S.K. Singh. Photocatalytic Detoxification Method for Zero Effluent Discharge in Dairy Industry :Effect of Operational Parameters. International Journal of Chemicaland Biological Engineering 1:4, 2008.
8. Sylwia Mozia, Maria Tomaszewska, Antoni W. Morawski - Removal of azo-dye Acid Red 18 in two hybrid membrane systems employing a photodegradation process, Desalination 198 ,(2006) ,183–190.
9. D.Yogi Goswami and Daniel M.Blake, Cleaning up with sunshine solar photocatalytic technology can be effective method of breaking up toxic chemicals and disinfecting water and air. ProQuest Science Journals pg. 56.
10. T Sakamaki, H Murata And S Kogoshi, nox removal using dbd with urea solution and plasma treated TiO_2 photo catalyst, ICESP australia 2006, paper 23.
11. S Senthilkumar, K Perumal And P S S Srinivasan, Optical and thermal performance of a three-dimensional compound parabolic concentrator for spherical absorber, Vol. 34, Part 3, June 2009.

DETECTION AND PREVENTION OF TRANSFORMER INRUSH

Johnson Abraham Mundackal & Robins Anto

Electrical and Electronics Engineering, Amaljyothi College of engineering, Kanjirappally, Kottayam, India
Email-johnsonmundackal@yahoo.com, Email-robinsanto@amaljyothi.ac.in

Abstract - Inrush current refers to the maximum, instantaneous input current drawn by an electrical device at the time of switching. When a transformer is first energized a transient current, much larger than the rated transformer current can flow for several cycles. This is caused due to the residual magnetism of the transformer and when the transformer is reenergized the incoming flux will add to the already existing flux which will cause the transformer to move into saturation and produce transient current. This transient current is termed as inrush current. There are several inrush detection techniques among which Neuro-fuzzy method and wavelet transform method are prominent. The current limiting devices like series resistor, triac and inrush current limiters are used for the prevention of inrush current. The inrush current limiter is the most commonly used inrush current prevention techniques. This paper includes the comparison of prominent inrush detection methods and prevention techniques.

Keywords- *Inrush current, Inrush current limiter, Power Transformer*

I. INTRODUCTION

Inrush current or input surge current refers to the maximum, instantaneous input current drawn by an electrical device when turned on. When a transformer is first energized a transient current, much larger than the rated transformer current can flow for several cycles. This is caused due to the residual magnetism of the transformer and when the transformer is re-energized the incoming flux will add to the already existing flux which will cause the transformer to move into saturation and produce transient current. This transient current is termed as inrush current. Transformer differential relay operation is based on the balance of the current flowing into an energizing winding with those flowing out to through-fed loads. The transformer differential relay could mistaken the inrush current as a fault current, which causes the transformer to be wrongly taken out of service by the relay. Some techniques are needed to detect and prevent the transformer inrush current.

There are several inrush detection techniques. The important transformer inrush detection techniques are neuro-fuzzy method and wavelet transform method. These methods accurately detect the inrush current in a transformer. The neuro fuzzy algorithm is based on the different behaviors of second harmonic component of inrush and fault currents. In most of fault conditions, phase angle of proportion of second harmonic to the fundamental component of differential currents is near zero, 180 or 360 degree and in various switching or inrush conditions these values are near to 90 or 270. In this method, magnitude and difference of phase angle of proportion of second harmonic to the fundamental component of differential current is calculated simultaneously. Wavelet transform and correlation factor method is another method of inrush current detection. A discreet wavelet transform has been used to identify the inrush currents of power transformers from the fault current.

There are several inrush current prevention techniques. The current limiting devices like series resistor, triac and inrush current limiters are used for the prevention of inrush current. The inrush current limiter is the most commonly used inrush current prevention techniques. An inrush current limiter is a temperature dependent resistor with a negative temperature coefficient (NTC), which means that the electrical resistance decreases with increasing temperature. Whereas NTC is frequently used as a temperature sensor measuring temperature applied from external environments an ICL uses the self-heating effect due to electrical current flow through the component. When the device is turned on, the inrush current is limited by the high resistance of the ICL in the cold state. During the initial transient sequence of switching on capacitive or inductive loads which typically take a few milliseconds depends on the ICL will heat up in the range of approximately 10 K to 30 K. Additional further warming may come from steady state current during normal operation of the device. The steepness of the R/T characteristics of ICL results in low residual resistance during operation in this mode meaning that the component has practically no effect on the application. However, industrial applications may utilize a relay,

which short-circuits the ICL path after the inrush sequence.

The paper is divided into five modules. In the first module the necessity of the inrush current detection and prevention is described. Second section describes the effects and classification of inrush current. The detection methods; neuro fuzzy method and wavelet transform method are described in module 3. The fourth module discusses about the prevention techniques. The conclusion and future aspect is listed in module five.

II. INRUSH CURRENT

The maximum, instantaneous input current drawn by an electrical device when turned on is termed as inrush current. Inrush current has a value which is 50 to 100 times greater than the rated current of transformer, which is occurred only for few cycles. When a transformer is energized a transient current, much larger than the rated transformer current can flow for several cycles. This is caused due to the residual magnetism of the transformer and when the transformer is re-energized the incoming flux will add to the already existing flux which will cause the transformer to move into saturation and produce transient current.

Inrush current is occurred in a transformer due to the abrupt increase of terminal voltage. The increase in terminal voltage is due to the effect of residual magnetism in a transformer. As shown in fig.1, when transformer flux Φ is less than saturation flux, Φs transformer core is not in saturation, here transformer magnetizing inductance is very large and transient magnetizing current is low. When Φs exceed Φ, transformer core is in saturation, here transformer magnetizing inductance is very small and transient magnetizing inrush is high. When Φs is less than Φ again, transformer core is also out of saturation. The transformer core will get in and out of saturation repeatedly; as a result the inrush current has a distinct gap in every cycle. This transient current is termed as inrush current.

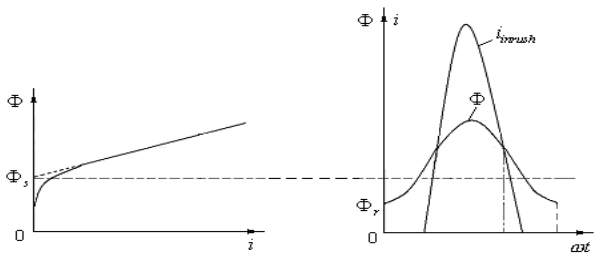

Fig.1 Inrush current and flux [7]

2.1 CLASSIFICATION

Inrush current may be of three types, energization inrush, sympathetic inrush, and recovery inrush. Energization inrush is occurred in a transformer due to the energization of a power transformer. It is occurred at the time of switching of power transformer. Inrush is due to the energization of another series or parallel connected power transformer is termed as sympathetic inrush. Inrush due to the voltage recovery after the clearing of heavy external short circuit in a power system is recovery inrush.

2.2 EFFECTS OF INRUSH CURRENT

Transformer differential relay is based on the comparison of the balance of the currents flowing into an energizing winding with those flowing out to through-fed loads. During load or through fault conditions, there is ampere turns balance, which results in differential current insufficient to cause a trip. However, unbalance currents are produced in the case of transformer inrush condition, the transformer differential relay could mistaken it as a fault current, which causes the transformer to be wrongly taken out of service by the relay. Therefore, some techniques are needed to detect transformer inrush and block differential relays. The inrush current also causes gradual damage of the circuit components. It causes damage such as welding switch contact together. The elimination of these effects is important. The measurement of inrush current is done with CLAMP ON METER

III. DETECTION METHODS OF INRUSH CURRENT

There are several methods for the detection of inrush current in a transformer. The neuro fuzzy algorithm is based on the different behaviors of second harmonic component of inrush and fault currents Wavelet transform and correlation factor method is another important method of inrush current detection. A discreet wavelet transform has been used to identify the inrush currents of power transformers from the single phase to ground faults.

3.1 NEURO FUZZY METHOD

Neuro fuzzy algorithm is also an important inrush detection method. The proposed algorithm is based on the different behaviors of second harmonic component of inrush and fault currents. In most of fault conditions, phase angle of proportion of second harmonic to the fundamental component of differential currents is near zero, 180 or 360 degree and in various switching or inrush conditions these values are near to 90 or 270. In this method, magnitude and difference of phase angle of proportion of second harmonic to the fundamental component of differential current is calculated simultaneously .

A. BASIC STRUCTURE OF DIFFERENTIAL RELAY

The block diagram of the proposed differential relay is shown in fig.8. The primary and secondary three phases current input signals were processed and magnitudes of harmonics of current were obtained by FFT algorithm, and then current have been computed [2]. These values are inputs of three differential protection units. This block diagram consists of three FNN units which each of them are specified to one phase. Also a logical unit is used to this structure to provide the correct tripping commands based on the output of three units. The inputs of these units consist of ratio and the difference phase angle of the second harmonic to the fundamental component of differential currents.

Neural networks are efficient structures able to learn from given data while fuzzy sets are designed to work with the structure knowledge in form of rules and in this system everything remains transparent and easily interpretable. They are based on human instincts and unlike neural networks cannot learn automatically.

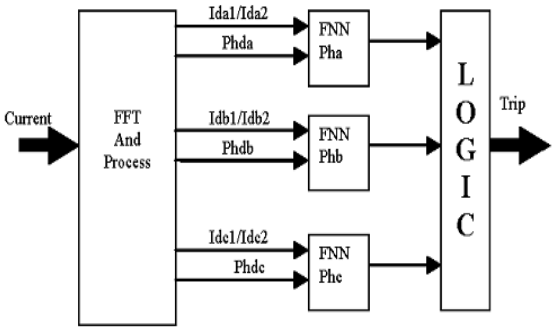

Fig.2 Block diagram of differential relay [5]

Adaptive network fuzzy is divided in three basic elements: fuzzification, fuzzy inference and difuzzification. In neural networks, the outputs behavior is determined by the weights between the input and the first hidden layer as well as the last hidden layer and output layer [5]. In a fuzzy system, these parameters are found in the fuzzification and difuzzification routines and can thus be trained. Calculated degrees of membership in the rule layers are according to IF-THEN rules. The network uses the back propagation gradient descent method to learn from the data sets. Neuro Fuzzy technologies map is shown in fig.9.

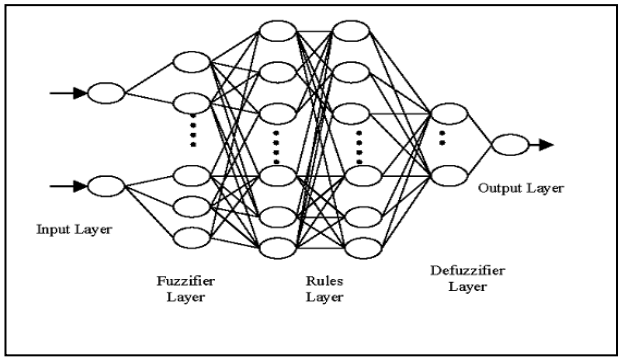

Fig.3 Neuro fuzzy technologies map [5]

B. SIMULATION RESULTS

To evaluate the performance of methods in recognition of fault current from inrush current, it is necessary to choose a suitable power system to consider the main effective factors on inrush and fault current behaviors. So the power system shown in fig.10 is modeled in PSCAD/EMTDC.

The power transformer, source and current transformer (CT) related to its differential protection are modeled in such a way that all effective factors on inrush and fault current waveforms have been considered [4]. This power system includes a 500MVA, 400/230 kV power transformer and transmission line existing on both sides of power transformer. The transformer connection is considered as star-star, here. The characteristics of inrush and fault current are shown in fig.11 and fig.12 respectively.

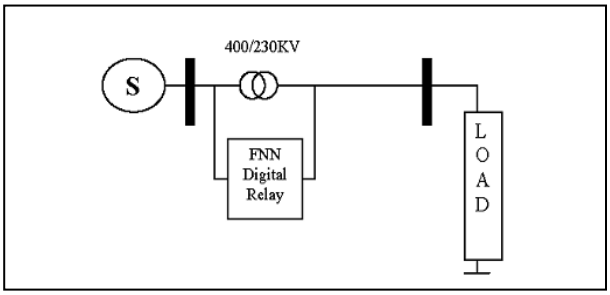

Fig.4 Simulated power system model [5]

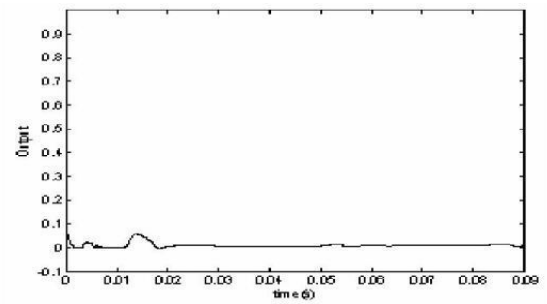

Fig.5 Characteristics of inrush current [5]

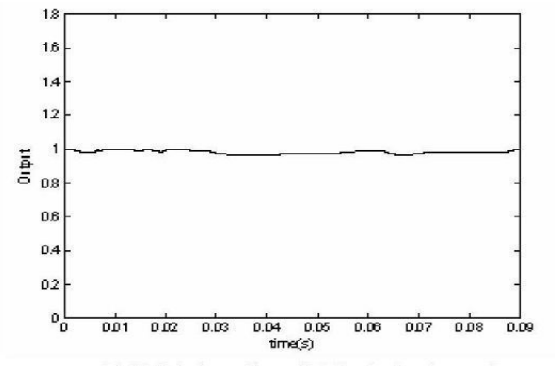

Fig.6 Characteristics of fault current [5]

In neuro fuzzy method the instantaneous detection and prevention of transformer inrush occurs simultaneously. Comparing with short window filter algorithm the neuro fuzzy method is more efficient technique.

3.2 WAVELET TRANSFORM METHOD

Wavelet transform method is a novel technique for accurate discrimination between an internal fault and a magnetizing inrush current in the power transformer. A decision making logic method for discrimination between internal faults and inrush currents in power transformers is used in this method. An algorithm for discrimination between inrush current and fault current is used based on the wavelet packet transform.

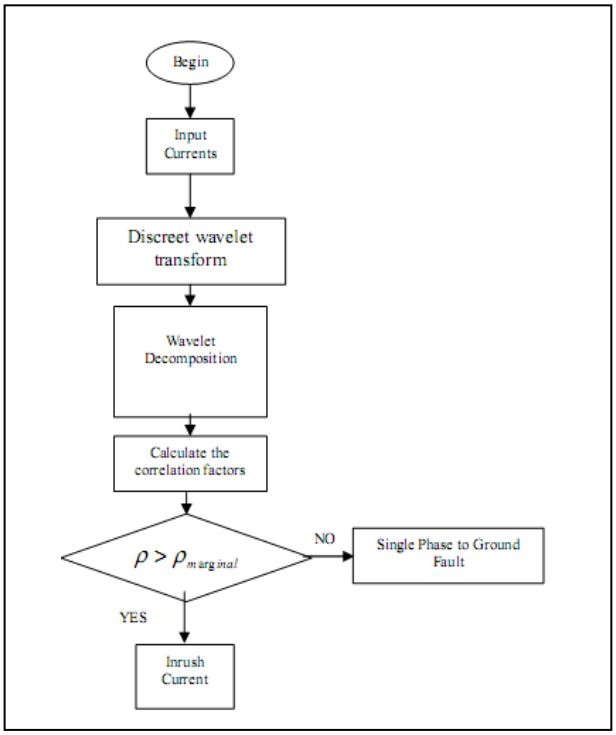

A discreet wavelet transform has been used to identify the inrush currents of power transformers from the single phase to ground faults [3]. The correlation factors values can range from -1 to +1. A complete linear correlation of two random variables can be given any value between -1 and +1 excluding 0. By calculating the correlation factor (ρ), discrimination between the inrush and fault current can be done.

The correlation factors of inrush currents are positive and that of fault currents are negative. Therefore, the sign of correlation factor can be used for discrimination of inrush currents from fault currents. Calculating the correlation factors of d3 wavelet transform, reveals that the variation range of the correlation factors of the inrush currents and the single phase to ground faults do not have any overlap. Therefore, by the use of the suggested method, the recognition of the inrush currents from the single phase to ground faults can be carried out reliably and conveniently.

$$\rho(X,Y) = \frac{\mathrm{Cov}(X,Y)}{\sqrt{\mathrm{Var}(X)\mathrm{Var}(Y)}} \qquad (1)$$

$\rho(X,Y)$ The correlation factor between X and Y

$\mathrm{Cov}(X,Y)$-The covariance of X and Y

$\mathrm{Var}(X)$ -The variance of X

$\mathrm{Var}(Y)$ - The variance of Y

A. TEST RESULTS

A power system shown in fig.14 is used in which a 150 MVA three-phase power transformer is connected to 230 kV grids by a circuit breaker. In this simulation, a saturation curve-equipped power system is used [6]. By the use of MATLAB's SIMULINK section and the FFT tools, the harmonic spectrum of the inrush currents are obtained. We got the harmonic component of inrush current and fault current as in fig.15 and 16 respectively.

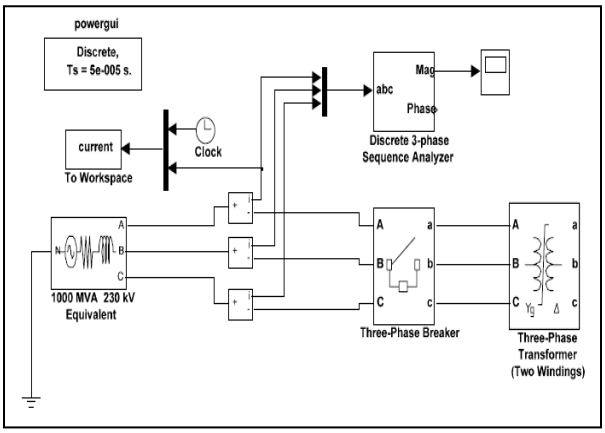

Fig.8 Power system simulated model [3]

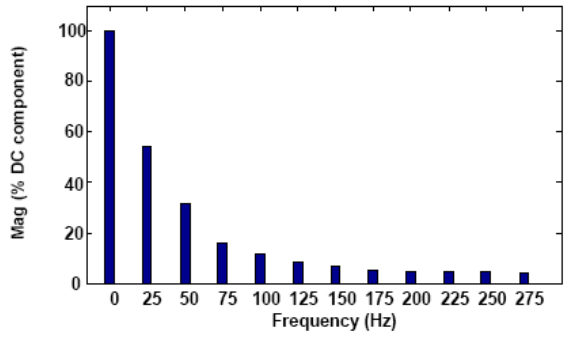

Fig.9 Harmonic component of inrush current

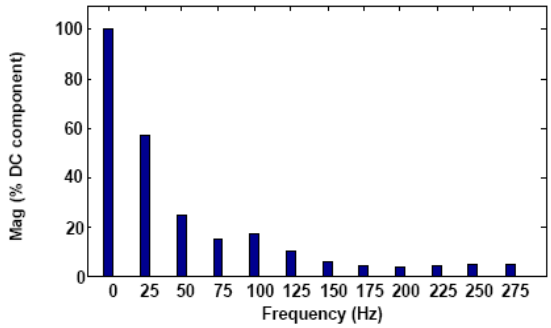

Fig.10 Harmonic component of single phase to ground fault current [3]

In wavelet transform method the detection of inrush current is done accurately by comparing the correlation factor. But the prevention of inrush current is not included in this method. Comparing the detection methods the neuro fuzzy method only gives the detection and prevention of transformer inrush simultaneously. So the neuro fuzzy method is the most efficient inrush detection technique.

IV. INRUSH PREVENTION DEVICES

There are several inrush current limiting devices like series resistor, triacs and Inrush current limiter. The ICL is the most commonly used inrush current limiter. An inrush current limiter is a temperature dependent resistor with a negative temperature coefficient (NTC), which means that the electrical resistance decreases with increasing temperature. Whereas NTCs are frequently used as a temperature sensor measuring temperature applied from external environments an ICL uses the self-heating effect due to electrical current flow through the component [8].

4.1 INRUSH CURRENT LIMITER (ICL)

Turning on electrical devices generally cause high inrush currents which can damage electronic components and cause interruption of the line voltage if measures are not taken to minimize this switch-on current. An effective way to reduce the inrush current, at low cost, is to use an Inrush Current Limiter (ICL). An ICL is a temperature dependent resistor with a negative temperature coefficient (NTC), which means that the electrical resistance decreases with increasing temperature [9]. Whereas NTCs are frequently used as a temperature sensor measuring temperature applied from external environments an ICL uses the self-heating effect due to electrical current flow through the component. When the device is turned on, the inrush current is limited by the high resistance of the ICL in the cold state (ambient temperature). During the initial transient sequence of switching on capacitive or inductive loads which typically take a few milliseconds (depends on component size and load capacity) the ICL will heat up in the range of approx. 10 K to 30 K. Additional further warming may come from steady state current during normal operation of the device. The steepness of the R/T characteristic of ICLs results in low residual resistance during operation in this mode meaning that the component has practically no effect on the application. However, industrial applications may utilize a relay, which short-circuits the ICL path after the inrush sequence. Fig.16 shows the installation of NTC in a simple circuit. The installation of NTC in a power transformer is shown in fig.17. There are several inrush current limiters. Fig.18 gives the practical inrush current limiters [8]. This device is used in a circuit for the prevention of inrush current in that circuit.

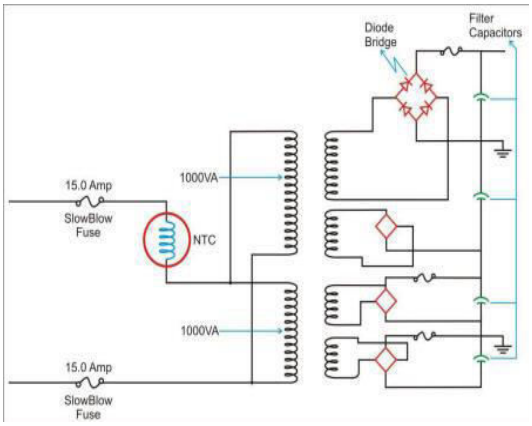

Fig.11 NTC installation in power transformer [8]

Fig.12 Practical NTCs [9]

V. CONCLUSION

The transformer differential relay could mistaken the inrush current as fault current, which causes the transformer to be wrongly taken out of service by the relay. This paper discussed the prominent detection techniques; neuro-fuzzy method, and wavelet transform method. The neuro fuzzy algorithm is based on the behaviors of second harmonic component of inrush and fault currents. In wavelet transform method a discreet wavelet transform has been used to identify the inrush currents of power transformers from the single phase to ground faults. The inrush current limiter is the preferred inrush current prevention technique. An inrush current limiter is a temperature dependent resistor with a negative temperature coefficient. When the device is turned ON, the inrush current is limited by the high resistance of the ICL. During the transient sequence of switching ON capacitive or inductive loads which typically take a few milliseconds depends on the ICL will heat up in the range of approximately 10 K to 30 K.

In neuro fuzzy method the instantaneous detection and prevention of transformer inrush occurs simultaneously. In wavelet transform method the detection of inrush current is done accurately by comparing the correlation factor. But the prevention of inrush current is not included in this method. Comparing the inrush detection techniques the neuro fuzzy method and the wavelet transform method are more advanced detection techniques. In neuro fuzzy method the detection and prevention of transformer inrush current is done simultaneously. So it is the most effective method. Comparing the prevention techniques, ICL is the efficient inrush prevention technique. But ICL is not a perfect inrush prevention device.

5.1. FUTURE WORKS

There are no perfect inrush prevention devices. To develop a perfect transformer inrush prevention technique with minimum cost is the future work.

REFERENCES

[1] G Mokryani, P Siano, A Piccolo, “Detection of inrush current using s- transform and competitive neural network”, IEEE Transaction on Optimization of Electrical and Electronic Equipment, pp.191-196, July 2010.

[2] G Mokryani, M.R.Haghifam,”Detection of inrush current based on wavelet transform and LVQ neural network”, IEEE Transaction on Transmission and Distribution, pp.1-5, June 2010.

[3] H.Kazemi Kargar, M.Jabbari, S.Golmohammad, “Inrush current identification based on wavelet transform and correlation factors”, vol-1, 6th international conference on ECTI -CONF-2009, pp.50-53, June 2009.

[4] H.Khorashadi Zadeh, “Fuzzy neuro approach to investigate transformer inrush current”, IEEE Transaction on Transmission and Distribution, pp.1302-1306, August 2006.

[5] M. Delshad, B.fani, “A new method for discrimination between internal faults and inrush current conditions in power transformers based on neuro fuzzy”, IEEE Transaction on Power Engineering, pp.731-735, November 2007.

[6] Zhang Chuanli, Huang Yizhuang, Lu Xiaoxu, “A new approach to detect transformer inrush current by applying wavelet transform”, IEEE Transaction, Power System Technology, vol.2, pp.1040-1044, August 1998.

[7] Zhengqing Han, Shuping Liu, ShibinGao, “Detection of inrush current based on short window filter algorithm”, IEEE Transaction, Power Engineering, pp.1-5, December 2008.

[8] AEMC instruments, www.aemc.com, Dec 20, 2011.

[9] Bear power products, www.bearpwr.com, Dec 15, 2011.

NOMENCLATURE

Φ	Magnetic flux
Φs	Saturation flux
ρ	Correlation factor
CT	Current transformer
FFT	Fast Fourier transforms
FNN	Fuzzy neural network
ICL	Inrush current limiter
N	Sampling rate,
KV	Kilovolt
KVA	Kilovolt ampere
NTC	Negative temperature coefficient
Var(X)	The variance of X
Var(Y)	T he variance of Y

Reactive Power Compensation and Voltage- Stabilization for Wind Power in a Weak Distribution Network

Harsha Anantwar ,Sudarshan B.S, Srinivas T. R, Vishal Singh Gurung, & Ashish Lal Chakravarthy

Department of E&EE, Dayananda Sagar College of Engineering, Bangalore
E-Mail : [1]hanantwar@yahoo.com [2]sudarshan.srinath@yahoo.in [3]srinivas.tarekere@gmail.com
[4]vishal.wer@gmail.com, [5]ashish0lal@gmail.com

Abstract **-**One of the most promising alternate sources of energy is wind energy. Energy of the wind is converted to electrical energy in wind farms and is then connected to a weak distribution network to supply local loads. Most wind farms use induction generators for electricity generation. These induction generators draw excessive reactive power for their operation and this causes shortage of reactive power in the system and leads to voltage collapse. This problem is simulated on PSCAD/EMTDC platform. For static compensation, capacitor banks are used and for dynamic compensation, Static Var Compensators (SVCs) are used.

Keywords- *Induction Generators, Wind Farms, Reactive Power Compensation, , Dynamic Compensation, SVC, Capacitor Bank, PSCAD/EMTDC.*

I. INTRODUCTION

Wind energy is the kinetic energy associated with the movement of large masses of air. Wind energy is available for longer periods and is harnessed as mechanical energy using wind turbines. The mechanical power is used as input to the induction generators to generate electricity.

Wind energy is harnessed in wind farms. Modern wind turbine generation system are employs variable speed wind generators. But over the former years fixed speed induction generator were installed. Hence still it is matter of interest to investigate fixed speed squirrel cage induction generator with power system. [1] A typical wind farm consists of many fixed speed wind turbine generation system. The mechanical input to the generator is provided using wind turbines, whose output is governed by wind turbine governors, each of these being controlled by their own control system. The ideal wind speed required for most wind turbines will be between 5 m/s and 25m/s. The wind farm is connected to distribution network using a transmission line and transformer. The most important characteristic of such an induction generator is that it draws reactive power from the grid for its operation. This is undesirable for the network, as it creates a reactive power deficit, leading to voltage dip at the generator bus. This largely affects the local loads i.e. the loads connected directly to the generator bus. The induction generator also slows down the voltage restoration process, and this might lead to voltage collapse.

Dynamic compensation device Static Var compensator (SVC), a combination of thyristor-controlled reactors can provide suitable compensation. The SVC responds faster than conventional compensators and hence is suitable for providing dynamic compensation. SVC does not contribute for short circuit currents and requires less maintenance.

In this paper, the analysis of the reactive power management of a wind farm consisting of fixed speed wind turbines is carried out. The capability of Static Var compensator (SVC) in reactive power compensation and voltage restoration in wind farms connected to weak distribution network is analyzed. A fault is simulated in the system and the system is analyzed with and without the use of compensation. The simulations are carried out on PSCAD/EMTDC platform.

II. SYSTEM UNDER CONSIDERATION

The block diagram of the system under consideration is shown in figure. The network consists of a 33kV distribution system fed from a 132kV grid. The distribution system consists of a wind farm, transmission line and step-up transformer. The 9MW wind farm is modeled as six 1.5MW wind turbines connected to fixed speed induction generators. The transmission line is a 50km line, connecting the generators to the low voltage side of the 62.5MVA,

132/33kV step-down transformer. Pitch angle control is enabled for the wind farms.

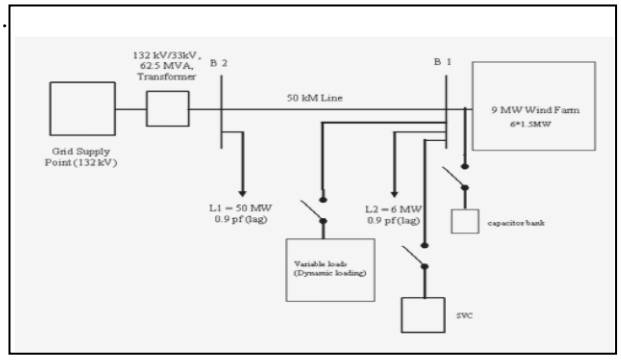

Fig-1: Single line diagram of the system

The ratings of each component are as follows:

a. Generator: 9MW (6 generators, each of 1.5MW capacity)

b. Transformer: 62.5MVA, 132/33kV (step-up)

c. Constant loads: 6MW at 0.9pf lag and 50MW at 0.9pf lag

d. Variable loads: 2MW, 1.5MW, & 0.75MW at 0.9pf lag

III. SIMULATION SET UP IN PSCAD

The test system is modeled on PSCAD/EMTDC platform in three-phase form and represented in single line display.. The simulation is carried out for 10 seconds in the following modes:

i. System with variable loads, without compensation

ii. System with variable load, with compensation

iii. Fault analysis, without compensation

iv. Fault analysis, with compensation

Capacitor bank is connected to generator terminal to compensate reactive power demand of induction generator at steady state. For Dynamic compensations are Static Var compensator (SVC), is connected to generator bus1.

SVC model can be represented with the Equations,[2]

$$V - V_{REF} + X_{SL}I = 0$$

Dynamic loading is condition is simulated using breaker switching logic, which represents the real-time local-load conditions.

In all the cases, the voltage and active and reactive powers at each bus and at the compensator is monitored, and The result of simulation are plotted on the graphs The dynamic responses are investigated for the system subject to a three phase short circuit fault starting at t = 4s and lasting for 0.04 second.

IV. SIMULATION RESULTS

4.1 *System with variable loads, without compensation*

The system has a fixed load of 4MW on bus-1 and 50MW on bus-2. The load variation effect on the dynamic performance of the SVC-compensated Induction generator is studied. The disturbance considered in a step, by addition in load demand at t=2 second, at t=4second and at t=6 second. And removing the load at t=9 second. While removing the load the instantaneous voltage swell caused by surplus reactive power in the system is observed

The load and the bus1 voltage variation are shown in the Fig 1. It is clearly seen that with addition or removal of load, the bus-1 voltage does not remain at 33kV. Fig-1 shows the variation in active power due to change in load (variable load switching) and Fig-2 shows the corresponding change in the generation bus voltage.

Fig-1: Step change in system load.

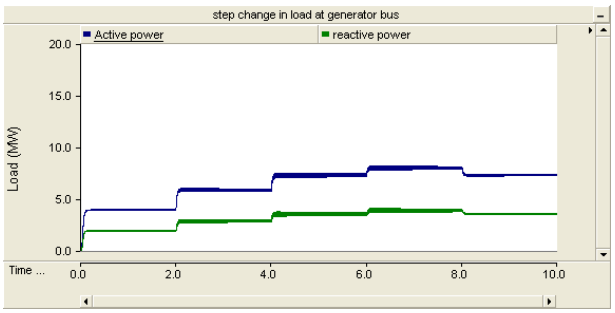

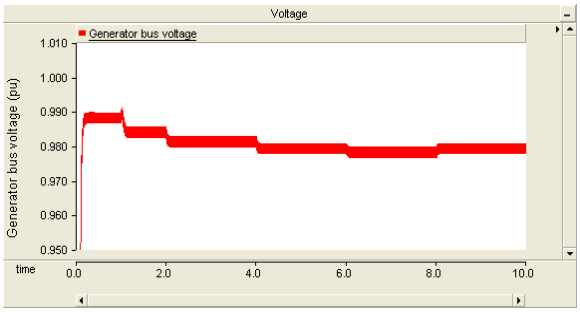

Fig-2: Variation in generator bus voltage due to step change in load (with no reactive power support)

4.2 *System with variable load, with reactive power support.*

When reactive power compensation is used in the system, it is observed that the generator bus voltage remains at 33kV even when the load on the bus has increased or decreased. The graphs of load change and

corresponding voltage at bus-1 are shown below in Fig 3 and Fig4.

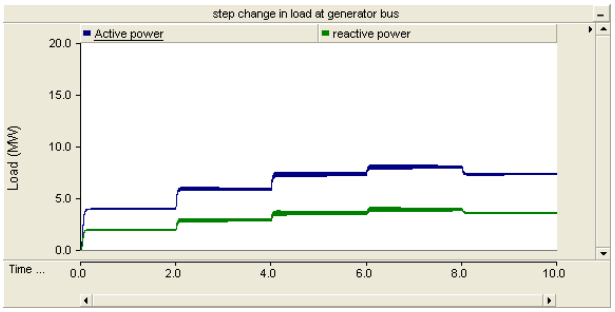

Fig-3: Step change in system load with reactive power support.

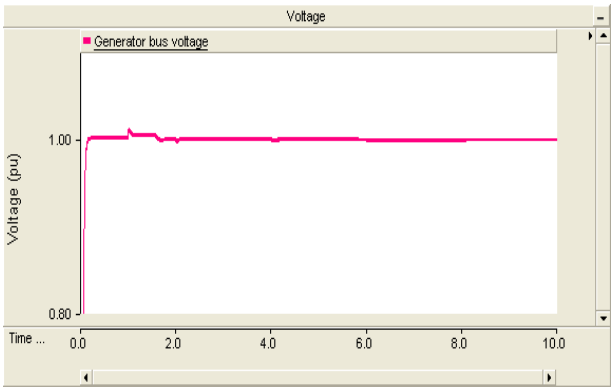

Fig-4: generator bus voltage due to change in load with reactive power support.

4.3 *Fault analysis, without compensation*

When a three phase to ground fault is simulated on the transmission line, it is observed that when the fault is cleared at 4.04 seconds, a time lag for the system to restore the bus voltage to the prefault value is observed from simulation result shown in the Fig 5. A very large dip in voltage was seen between 4 and 4.04 seconds due to the fault.

Recovery time for generator bus voltage is 0.04 seconds.

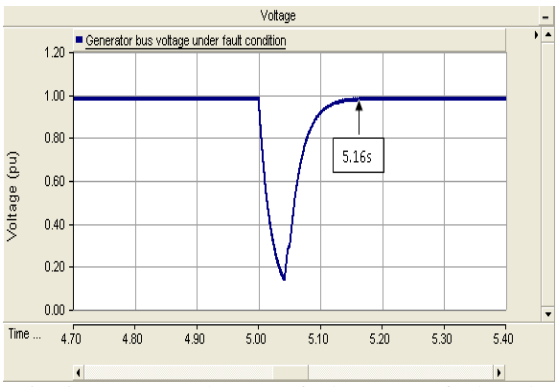

Fig-5: Generator bus pre-fault & post fault voltage with Out compensation.

4.4 *Fault analysis, with compensation*

When a SVC is connected to the bus-1 and the fault is simulated, it is observed that the time taken by the system to restore the value of the generator bus voltage to the original value is reduced. Recovery time for generator bus is 0.13 seconds

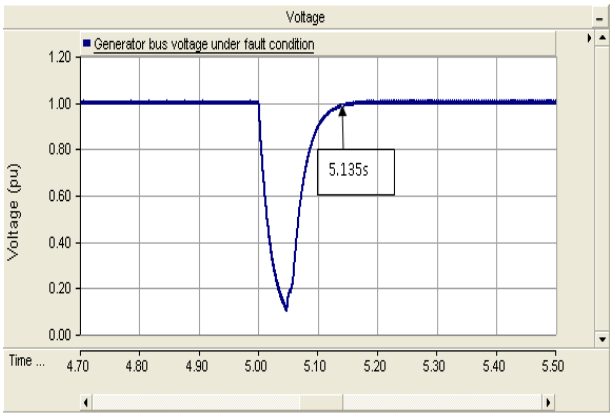

Fig-6: Generator bus pre-fault & post fault voltage with compensation

V. CONCLUSIONS

From the results obtained, the following conclusions were made:

i. When a wind farm is connected to a weak distribution network, due to the excessive reactive power drawn by the generators, the generator bus voltage dropped below the tolerance limit.

ii. When a dynamic compensator is used, the bus voltage is observed to be within the tolerance limits.

iii. The compensator supplied the reactive power deficit and hence stabilized the voltage at the bus.

iv. The time taken by the system to restore the bus voltage to the nominal value after the fault is cleared, is more without compensation, and is reduced when compensator was connected to the generator bus.

This paper presents the analysis of a wind farm connected to a weak distribution network. SVC capability to compensate the reactive power under dynamic load conditions, and fault voltage is also analyzed.

ACKNOWLEDGEMENT

This work is carried out at Dayananda Sagar College of Engineering (DSCE), Bangalore (India). The authors wish to thank Dr. K. Shanmukha Sundar, (The Head of the Department of E&EE, DSCE), and Prof. (Mrs.) Usha. P (Professor, Dept of E&EE).

REFERENCES

[1] Mohd. Hasan Ali, and Bin Wu, Fellow, IEEE 'Comparison of Stabilization Methods for Fixed-Speed Wind Generator Systems'. IEEE Trans. on Power Delivery, Vol. 25, no. 1, January 2010

[2] M. Kenan Dosoglu , Ali Ozturk 'Investigation of different load changes in wind farm by using FACTS devices' _ 2011 Elsevier Ltd

[3] A.M. Sharaf, R. Chhetri, "A Novel Dynamic Capacitor Compensator/Green Plug Scheme for 3Phase-4 Wire Utilization Loads", Electrical and Computer Engineering, Canadian Conference on, May 2006 Page(s):454 – 459

[4] E. S. Abdin andW. Xu, "Control design and Dynamic performance analysis of a wind Turbine- induction generator," IEEE trans. Energy Convers., vol. 15, no. 1, Mar.2000.

[5] PSCAD/EMTDC working group, "Static VAR Compensator",PSCAD/EMTDC User manual pp. 75 - 91.

[6] 'Overview of FACTS Devices for Wind Power Plants Directly Connected to the Transmission Network' A. Adamczyk,R. Teodorescu,R.N. Mukerjee P. Rodriguez 978-1- 4244-6392-3/10©2010 IEEE

[7] S. Kahrobaee, S. Afshania, V. Salehipoor "Reasonable Reactive Power Control for Wind Farms Using FACTS Devices", Nordic Wind Power Conference 22 – 23 May – 2006, ESPOO, Finland.

[8] F. Zhou, G. Joos, and C. Abhey, "Voltage Stability in weak connection wind farm," in IEEE PES Gen. Meeting, 2005, vol. 2, pp. 1483–1488.

◈◈◈

Effect of UPFC on System Performance under Normal and Fault Condition

Prakash D B, K.ShanmukaSundarManjunatha Babu P ShubhaKulkarni & Ramamani V

Electrical & Electronics Engineering Department,
DayanandaSagar College of Engineering, Bangalore-78
E-Mail: prakashdb.ee@gmail.com, bonniekhs@gmail.com, manjubabup@gmail.com
smk.1978@gmail.com, ramamanirao@gmail.com

Abstract - This paper deals with the effect of Unified Power Flow Controller (UPFC) on the system performance under normal and fault conditions. Simulink models are developed for 7 bus system with and without UPFC. Digital simulation using MATLAB/SIMULINK is done with these models and the results are presented. The effect of UPFC on real power, reactive power and the voltage is also presented.

Keywords*: FACTS, UPFC, Power Quality, MATLAB, SIMULINK.*

I. INTRODUCTION

One of the most important aspects of planning and operating electrical power systems is the design of protection systems. Protection systems are designed to detect and remove faults. A fault in an electrical power system is the unintentional conducting path (shortcircuit) or blockage of current (open circuit). The short-circuit fault is typically the most common and is usually implied when most people use the term fault. A fault occurs when one energized electrical component contacts another at a different voltage. This allows the impedance between the two electrical components to drop to near zero allowing current to flow along an undesired path from the one initially intended. The short-circuit fault current can be orders of magnitude larger than the normal operating current. The current from such an event can contain tremendous destructive energy , that can damage electrical equipment and pose safety concerns for both utility and non-utility personnel.

Nowadays FACTS devices can be used to control the power flow and enhance system stability. They can enable a line to carry power closer to its thermal rating. The salient features of a FACTS device are its multiple control functions, such as, power flow control, voltage control, transient stability enhancement, oscillation damping. Voltage sag compensation is necessary for secure system operation. A well designed FACTS Controller can not only increase the transmission capability but also improve the power system stability. UPFC is the most comprehensive multivariable flexible AC transmission systems controller [1-2].Investigations have been carried out to study the effectiveness of these devices in power-quality mitigation such as sag compensation, harmonics elimination, unbalance compensation, reactive power compensation, power-flow control, power factor correction and flicker reduction [5–6]. These devices have been developed for mitigating specific power-quality problemsThis paper is organized as follows. After this introduction, the principle and operation and of a UPFC connected to a network are presented. In section II, the control strategy for UPFC is introduced. Simulation results are presented in sections III. Section IV describes the conclusion.

II. UPFC CHARACTERISTICS

The basic components of the UPFC are two voltage source inverters (VSI's) sharing a common dc storage capacitor, and connected to the system through coupling transformers. One VSI is connected in shunt to the transmission system via a shunt transformer, while the other one is connected in series through a series transformer. A basic UPFC functional scheme is shown inFig.1.

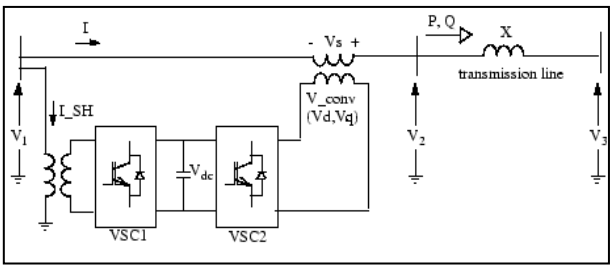

Fig. 1 UPFC functional scheme

The series inverter is controlled to inject a symmetrical three phase voltage system, Vse, of controllable magnitude and phase angle in series with the line to control active and reactive power flows on the transmission line. So, this inverter will exchange active and reactive power with the line. The reactive power is electronically provided by the series inverter, and the active power is transmitted to the dc terminals. The shunt inverter is operated in such a way as to demand this dc terminal power (positive or negative)from the line keeping the voltage across the storage capacitor Vdc constant. So, the net real power absorbed from the line by the UPFC is equal only to the losses of the two inverters and their transformers. The remaining capacity of the shunt inverter can be used to exchangereactive power with the line so to provide a voltage regulation at the connection point. If the information regarding the series converter real demand is not conveyed to the shunt converter control system, it could lead to collapse of the dc link capacitor voltage and subsequent removal of the UPFC from operation [3-4],[7].The reference input is a simple var request that is maintained by the control system regardless of busvoltage variation. The real and reactive power equations are as follows:

$$P = \frac{V_1 V_2}{X} \sin(\delta_1 - \delta_2) \qquad (1)$$

$$Q = \frac{V_2}{X}(V_1 - V_2) \qquad (2)$$

Specification of Test System:

The effectiveness of the method is carried out on 7-bus system. The 7-bus system has 3 generators nine transmission lines and six load centers with a capacity of 11 kV. The 7-bus test system, which is considered for the purpose of case study, is shown in

Fig-2.

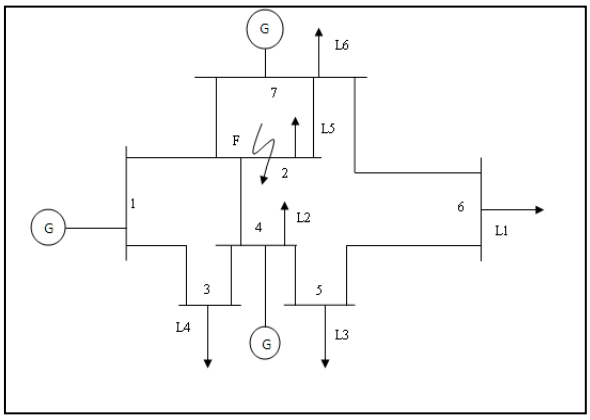

Fig-2. 7 bus test system.

Case Study and Results

The seven bus system is considered for simulation studies by using MATLAB/SIMULINK is shown in fig.3. The circuit model of seven bus system is simulated for 0.7 sec, at t=0.25 sec, a single line to ground fault is created near load 5 (L5). Due to this fault,the voltages at various load drops this simulated results are shown in fig.4. In order to over come this, UPFC is connected at various places and studied the effectiveness of the UPFC to get better performance and improved voltage profile.

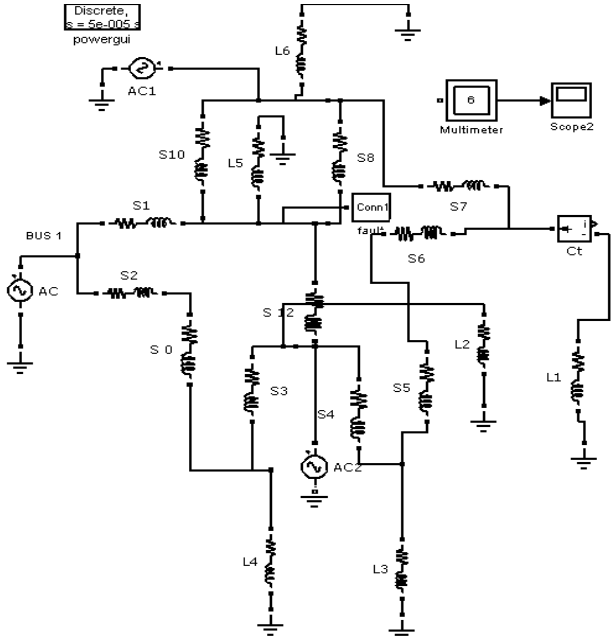

Fig-3. MATLAB/SIMULINK model of the test system without UPFC

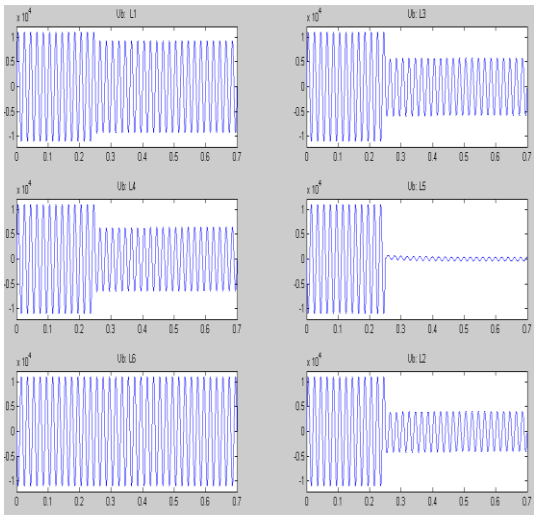

Fig-4. Voltages at various loads without UPFC

The voltage profile under fault conditions can be improved by connecting UPFC at various locations. Fig

5 shows the test system with UPFC between bus-2 and bus-4.In this paper the placement of UPFC is considered, between bus-2 and bus-4 , between bus-4 and bus-5 , between bus-6 and load 1 ,between bus-5 and bus-6 and the voltage profile respectively are shown in Fig 6, Fig 7, Fig 8 and Fig 9.

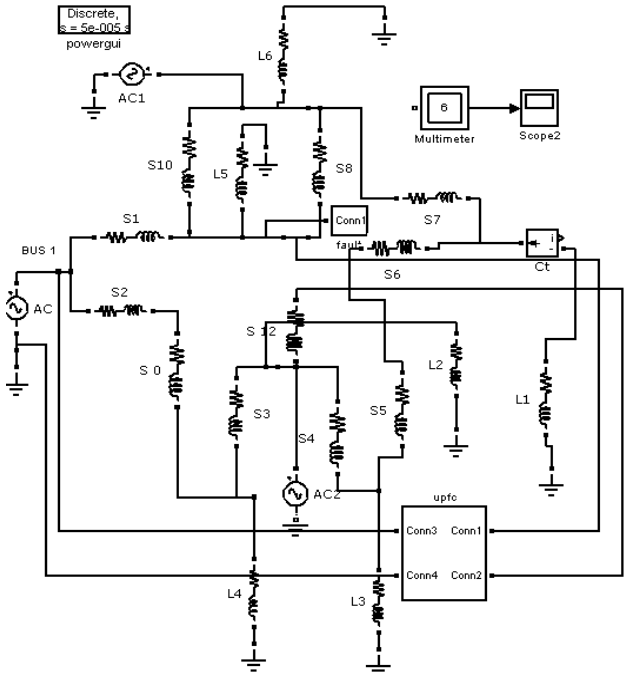

Fig-5. Test system with UPFC

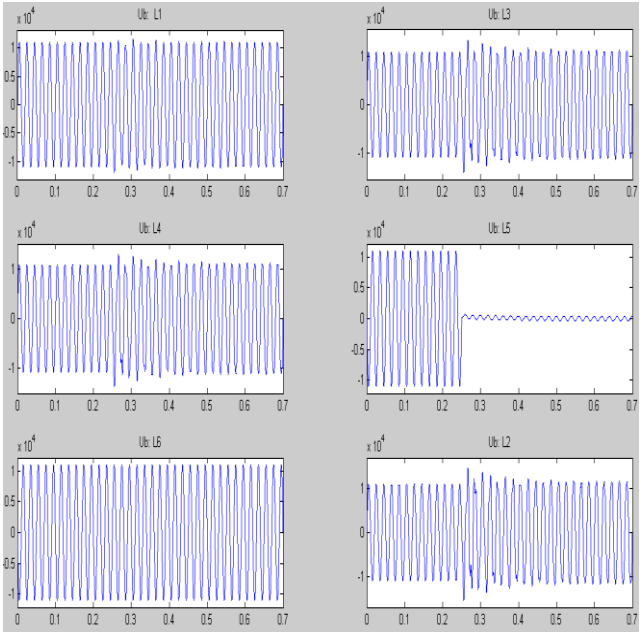

Fig-6. Voltages at various loads with UPFC connected between Bus-2 and Bus 4.

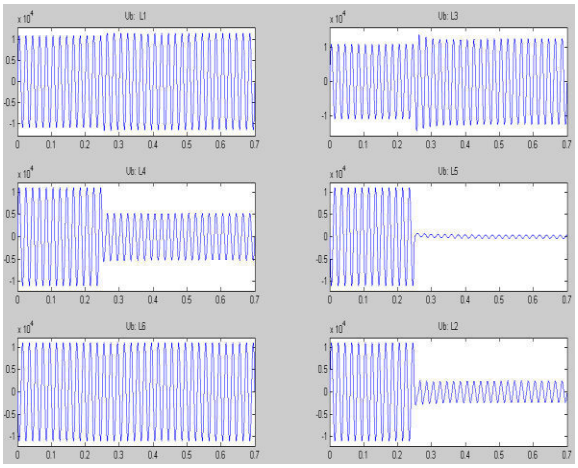

Fig-7. Voltages at various loads with UPFC connected between Bus-4 and Bus 5

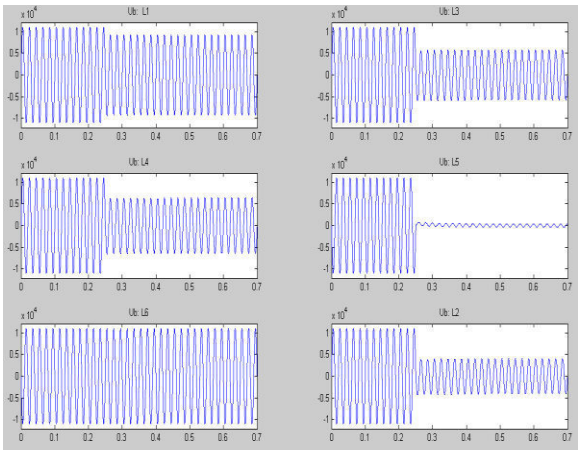

Fig-8. Voltages at various loads with UPFC connected between at Bus 6.

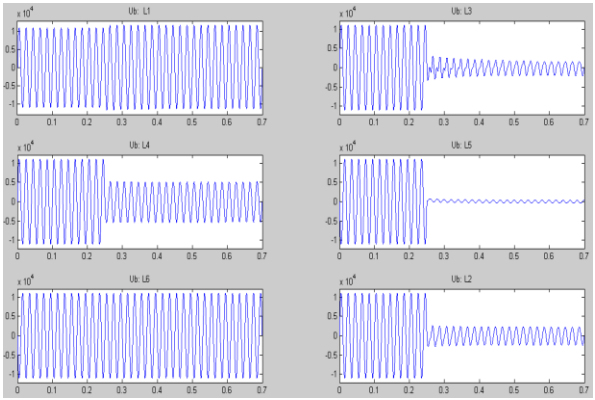

Fig-9. Voltages at various loads with UPFC connected between Bus-5 and Bus 6.

From the results it is evident that in all cases the voltage profile under fault condition has improved. The more effective results are obtained by placing UPFC between bus-2 and bus-4 as shown in Fig 6.

IV. CONCLUSION:

In the simulation study, MATLAB/SIMULINK environment is used to simulate the model of seven bus system. This paper presents the control scheme for the UPFC which is used for improvement of voltage profile at various loads during fault conditions. Simulation results confirm that by proper tuning and control of UPFC can improve the voltages at various loads therby improving the stability of the system. It is found that there is an improvement in the voltages at various loads when UPFC is introduced. The effectiveness of UPFC is obtained when it is connected between bus-2 and bus-4. The simulation results are inline with the predictions.

REFERENCES:

[1] Gyugyi, " Unified power-flow control concept for flexible AC transmission system," *Proc. Inst. elect. Eng.C*, vol. 139, no.4, pp.323-331, Jul, 1992.

[2] N.G. Hingorani and L. Gyugyi, *Understanding FACTS*. New York:IEEE Press, 2000.

[3] K.R. Padiyar and A.M. Kulkarni, "Control design and simulations of unified power flow controller", IEEE TransactionPower Delivery, Vol. 13, pp 1348-1354, Oct.1998.

[4] C.D. Schauder, L. Gyugyi, M.R. Lund, D.M. Hamai, T.R. Rietman, D.R.Torgerson and A. Edris, " Operation of the unified power flow controller (UPFC) under practical constraints", IEEE Transaction Power Delivery, Vol.13, pp. 630-636, Apr.1998.

[5] R. L. V. Arnez and L. C. Zanetta, "Unified power flow controller (UPFC): its versatility in handling power flow and interaction with the network," in Proc. IEEE/PES Asia Pacific Transmission and Distribution Conf. and Exhib., vol. 2, Oct. 2002, pp. 1338–1343.

[6] P. Pohjanheimo and E. Lakervi, "Steady state modeling of custom power components in power distribution etworks," in Proc. IEEE Power Engineering Society Winter Meeting, vol. 4, Jan. 2000, pp. 2949–2954.

[7] Nashiren.F. Mailah and Senan M. Bashi, "Single Phase Unified Power Flow Controller(UPFC): Simulation and Construction", European Journal of Scientific Research Vol.30 No.4,pp.677-684, 2009.

◈◈◈

High Frequency Boost Converter Employing Soft Switching Auxiliary Resonant Circuit

G. Naresh Goud[1], Y.Lakshmi Deepa[2], G.Dilli Babu [3] ,P.Rajasekhar [4] & N.Gangadher[5]

Abstract - A new soft-switching boost converter is proposed in this paper. The conventional boost converter generates switching losses at turn ON and OFF, and this causes a reduction in the whole system's efficiency. The proposed boost converter utilizes a soft switching method using an auxiliary circuit with a resonant inductor and capacitor, auxiliary switch, and diodes. Therefore, the proposed soft-switching boost converter reduces switching losses more than the conventional hard-switching converter. The efficiency, which is about 91% in hard switching, increases to about 97% in the proposed soft-switching converter. In this paper, the performance of the proposed soft-switching boost converter is verified through the theoretical analysis, simulation, and experimental results.

I. INTRODUCTION

RECENTLY, switch-mode power supplies have become smaller and lighter due to higher switching frequency.However, higher switching frequency causes lots of periodic losses at turn ON and turn OFF, resulting in increasing losses of the whole system. Therefore, many converters have been presented that use resonance to reduce switching losses. Many researches using resonance have presented a zero-voltage and zero-current switching (ZVZCS) converter that performs zero-voltage switching (ZVS) and zero-current switching (ZCS) simultaneously . However, the auxiliary circuit for resonance

increases the complexity of the circuit, as well as its cost. For some resonant converters with an auxiliary switch, the main switch enables soft switching, while the auxiliary switch performs hard switching. These converters cannot improve the whole system's efficiency owing to the switching losses of the auxiliary switch. Anewsoft-switching boost converter with an auxiliary switch and resonant circuit is proposed in this paper.

The resonant circuit consists of a resonant inductor, two resonant capacitors, two diodes, and an auxiliary switch. The resonant capacitor is discharged before the main switch is turned ON and the current flows through the body diode. These resonant components make a partial resonant path for the main switch to perform soft switching under the zero-voltage condition using the resonant circuit. Compared with other soft-switching converters, the proposed converter improves the whole system's efficiency by reducing switching losses better than other converters at the same frequency.

In this paper, some simulation results are presented for a 400-W, 200-kHz prototype boost converter using MOSFET. Then, experimental results are presented to verify the steady-state operational principle of the proposed circuit. Additionally, theoretical analyses are presented.

II. LOW-LOSS SOFT-SWITCHING BOOST CONVERTER

A. Configuration of the Proposed Soft-SwitchingBoost Converter

The proposed converter is shown in Fig. 1. The main switch (S1) and the auxiliary switch (S2) of the proposed circuit enable soft switching through an auxiliary switching block, consisting of an auxiliary switch, two resonant capacitors (Cr and Cr2), a resonant inductor (Lr), and two diodes (D1 and D2).

B. Operational Analysis of the Proposed Converter

The operational principle of the proposed converter can be divided into nine modes. For simple analysis of each mode of the proposed converter, the following assumptions are made. 1) All switching devices and passive elements are ideal. 2) The input voltage (Vin) is constant. 3) The output voltage (Vo) is constant. (Output capacitor Co is large enough.) 4) The recovery time of all diodes is ignored. Fig. 2 shows Equivalent circuit schemes of the operation modes in the proposed converter. And Fig. 3 shows the key waveforms of operation modes.

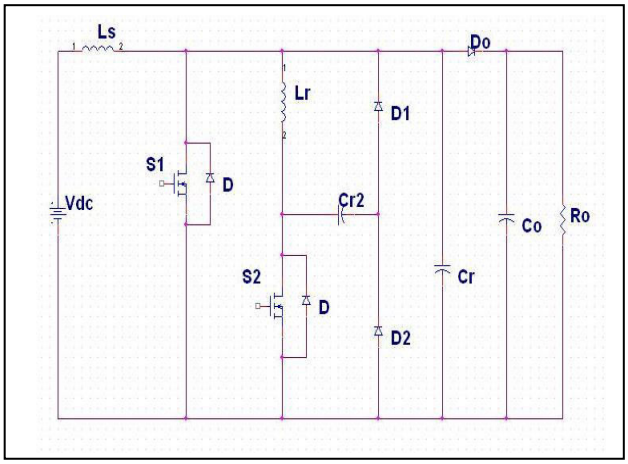

Fig1. Proposed Circuit

III. MODES OF OPERATION

Mode 1 ($t0 \le t < t1$):

All of the switches are turned OFF. The accumulated energy of the main inductor (L) transfers the load through the main diode (Do).

In this mode, the main diode (Do). In this mode, the main inductor voltage and current are represented by (1) and (2), and using these equations, the inductor current can be expressed as (3). During this time, the resonant inductor current is zero, and the resonant capacitor (Cr) has been charged to the output voltage and the resonant,

$v_L(t)=V_{in}-V_o(t)$.....(1)

$$i_L=\frac{1}{L_m}\int_{to}^{t1} v_{L(t)}dt \quad \text{.....(2)}$$

$$i_L=\frac{Vin\text{-}Vo}{L_m}[t\text{-}t_0]+I(t_0) \quad \text{.....(3)}$$

$i_{Lr}(t)=0$, $V_{Cr}(t)=Vo$, $V_{Cr2}(t)=Vo$ .....(4)

Mode 2 ($t1 \le t < t2$):

When the auxiliary switch turns ON, mode 2 begins. After turning ON the auxiliary switch, the resonant inductor current begins to increase linearly from zero. When the resonant inductor current (iLr) is equal to the main inductor current at t2 , mode 2 completes and the resonant inductor voltage equals the output voltage. Thus, the resonant inductor current is expressed by (5). The main inductor current decreases and, at the end of this mode, the main inductor current is equal to the minimum, as defined by (6).

$$i_{Lr}=\frac{1}{L_r}\int_{t1}^{t2} v_{0(t)}dt$$

$$i_{Lr}=\frac{V_0}{L_r}(t\text{-}t1) \quad \text{.....(5)}$$

$$i_L(t)=I_{min} \quad \text{.....(6)}$$

Mode 3 ($t2 \le t < t3$):

Immediately after the resonant inductor current and main inductor current have equalized, the main diode is turned OFF. The resonant capacitor Cr and the resonant inductor start their resonance, then the resonant capacitor Cr is discharged through resonant path Cr and Lr . After finishing the resonance, the resonant capacitor voltage is equal to zero. Mode 3 completes at t3 . At t2 , the resonant inductor voltage is equal to the output voltage. Thus, the time interval for the two currents to equalize after t1 is determined by (7). The resonant inductor current is the sum of the main inductor and resonant current, and is expressed by (8). The resonant capacitor Cr voltage is charged, as expressed by (9). During this mode, the resonant impedance and angular frequency are given by Zr and ωr

t1=IL/((Vo/Lr))……..(7)

$$i_{Lr(t)}=i_{min(s)}+\frac{V_0(s)\omega_r}{Z_r(S^2+\omega_r^2)}$$

……(8)

$$V_{Cr}(t)=V_0\text{Cos}(\omega_{r(t\text{-}t2)})$$

……..(9)

$$Z_r=\sqrt{\frac{L_r}{C_r}} \quad \text{.....}, \quad \omega_r=\sqrt{\frac{1}{L_r*C_r}}$$

……..(10)

Mode 4 ($t3 \le t < t4$):

As soon as the resonant capacitor (Cr) voltage has reached zero, the body diode of main switch is turned ON naturally. In this case, the main switch voltage is equal to zero and the turn-ON signal is given to the main switch under the zero-voltage condition. In this mode, the main inductor voltage is equal to the input voltage. Thus, the main inductor current is expressed by (11). After the resonance in mode 3, the resonant inductor current is constant. The resonant capacitor (Cr) voltage has been strongly discharged in mode 3. Therefore, the resonant capacitor voltage is zero

$i_L(t)=i_{min}+\frac{V_{in}}{L_m}(t-t3)$ ....(11)

$V_{Cr2}(t)=0$ ..., VCr = 0....................(12)

Mode 5 ($t4 \le t < t5$):

In mode 4, the main switch turns ON under the zero-voltage condition. When the auxiliary switch is turned OFF for the same condition, mode 5 begins. In this stage, the resonant inductor and resonant capacitor (Cr2) start the resonance. After the quarter-wave resonance of Lr and Cr2 , the current of Lr is zero. Mode 5 is complete and Cr2 has been fully charged by the resonance. In this mode, the resonant inductor current can be expressed as (13). In addition, the resonant impedance and angular frequency are given by Za and ωa

$i_{Lr}(t)=i_{Lr}(t3)Cos(\omega_a(t-t4))$
....(13)

$\omega a=1/\sqrt{LrCr2}$...... $Za=\sqrt{\frac{Lr}{Cr2}}$
............................(14)

Mode 6 ($t5 \le t < t6$):

After mode 5 completes, the current flow of the resonant inductor Lr reverses and the next stage starts. In mode 6, a reverse resonance of L and Cr2 through the main switch and D2 occurs. When the Cr2 voltage has reached zero by resonance, the resonance of Lr and Cr2 is complete and the Cr2 voltage is zero.During modes 5 and 6, the resonant capacitor voltage is charged and discharged, according to (15). Thus, the resonant capacitor voltage (vCr 2) for each point of time is expressed by (16)

$V_{Cr2}(t)=Z_a i_{Lr}(t3)Sin(\omega_a(t-t4))$ ....(15)

$V_{Cr2}(t5)=Z_a i_L$ ..... $V_{Cr2}(t6)=0$..........(16)

Mode 7 ($t6 \le t < t7$):

After theCr2 voltage has reached zero, the body diode of the auxiliary switch is turned ON. The current flows through the freewheeling path of the body diode—the resonant inductor—the main switch. By the pulsewidth modulation (PWM) algorithm, when the main switch is turned OFF, this mode is complete. In this interval, the magnitude of the resonant inductor current is equal at t3 . However, the current flow is reversed. In this mode, the main and auxiliary inductor currents are as follows:

$i_{Lr}(t)=i_{min}(t)+\frac{V_{in}}{L}(t-t3)$ ....(17)

$i_{Lr}(t)=-i_{Lr}(t3)$. ....(18)

Mode 8 ($t7 \le t < t8$):

When the main switch is turned OFF under the zero-voltage condition, mode 8 starts. The sum of the two inductor currents is the charging current of the resonant capacitor Cr in this mode. When the resonant capacitor (Cr) voltage is equal to the output voltage, this mode is completed. Because the two inductor currents charge the resonant capacitor Cr , the resonant inductor current is expressed by (19), and (20) represents the zero-voltage condition

$iLr(t) = iL(t7) - \{iL(t7) + iLr(t3)\} \cos \omega r t$
.......................(19)

$Zr\{iL(t7)+iLr(t3)\}>Vo$.........................(20)

Mode 9 ($t8 \le t < t9$):

At t8 , the resonant capacitor Cr has been charged and the main diode voltage is zero. Therefore, the main diode turns ON under the zero-voltage condition and the resonant inductor current decreases linearly toward zero. After the current has reached zero, mode9 completes and the next switching cycle starts. In this mode, the main inductor current and resonant inductor current are given by the following:

$i_L(t)=i_{min}(t7)+\frac{V_0-V_{in}}{L}*t$ ....(21)

$i_{Lr}(t)=\frac{V_0}{Lr}*t-i_{Lr}(t3)$ ....(22)

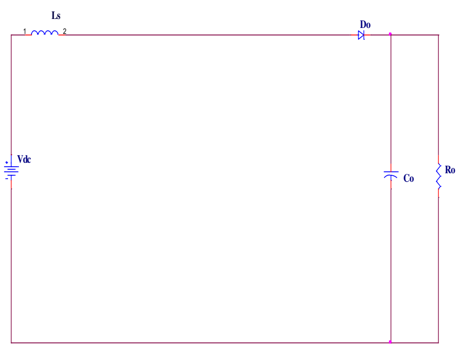

Mode:1($t0 \le t < t1$)

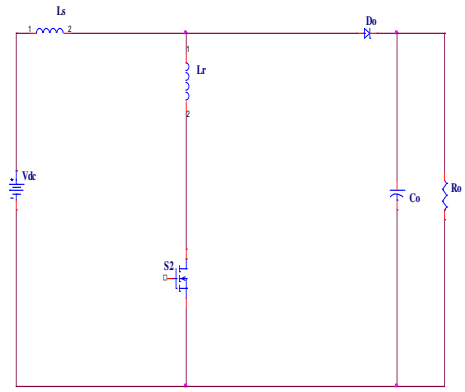

Mode: 2(t1 ≤ t < t2)

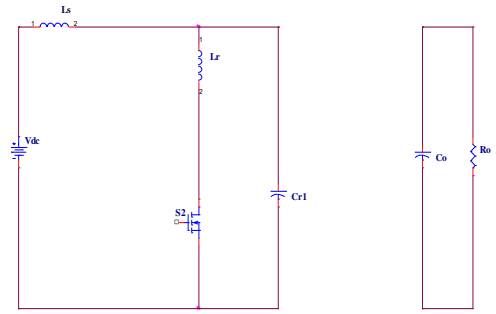

Mode: 3 (t2 ≤ t < t3)

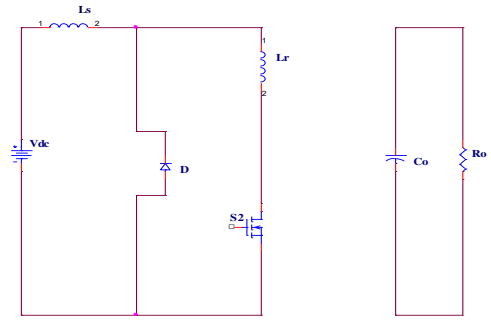

M ode: 4(t3 ≤ t < t4)

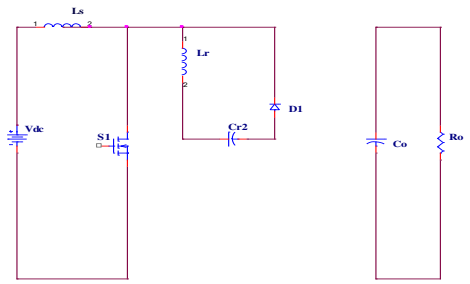

Mode: 5 (t4 ≤ t < t5)

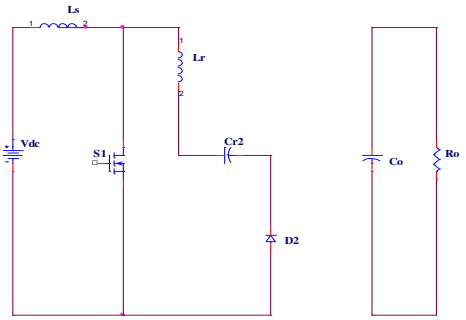

Mode: 6 (t6 ≤ t < t7)

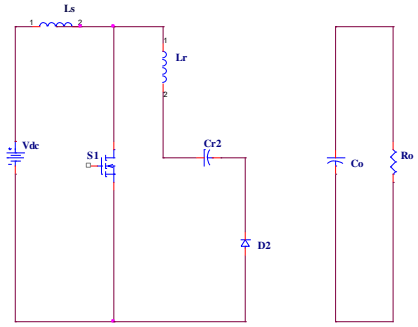

Mode: 7(t7 ≤ t < t8)

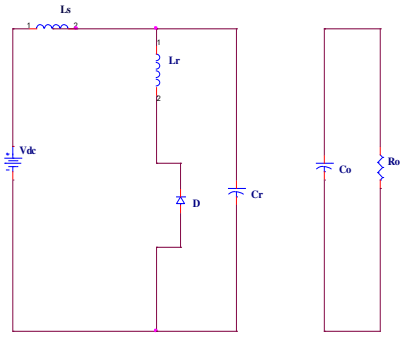

Mode: 8 (t8 ≤ t < t9)

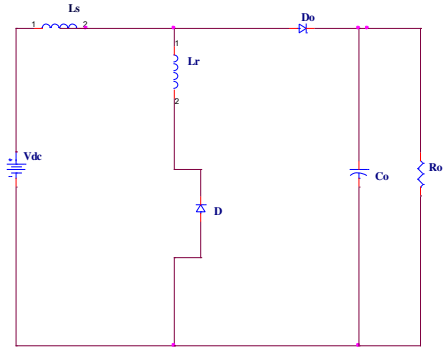

Mode: 9 (t9 ≤ t < t0)

Fig2: Modes of Operation

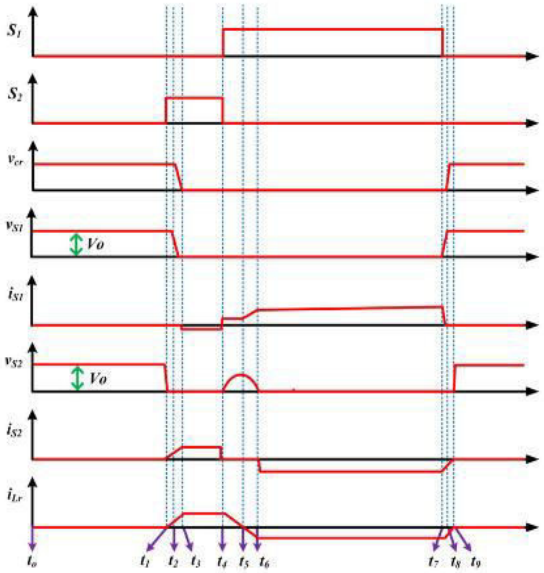

Fig3: Expected Waveforms

TABLE I

PARAMETERS OF THE PROPOSED CIRCUIT

PARAMETER	SYMBOL	VALUE
INPUT VOLTAGE	V_{DC}	50V
OUTPUT VOLTAGE	V_O	200V
SWITCHING FREQUENCY	Fr	200KHz
RESONANT INDUCTOR	Lr	16.5µH
RESONANT CAPACITOR	Cr	1nF
RESONANT CAPACITOR2	Cr2	16.5nF

IV. SIMULATION RESULTS

In this paper the proposed converter is simulated by ORCAD 16.5 software. The simulation was performed under a 200-kHz switching frequency and a 50-V input voltage. Figs. 4 and 5 show the simulation waveforms of the main gate voltage and voltage across switch S1 and current, flowing through it respectively. Before the main switch is turned ON, the body diode is turned ON. As a result, the main switch enables zero-voltage switching and the auxiliary switch performs soft switching. Fig 6 shows that output voltage Vo and output current Io.

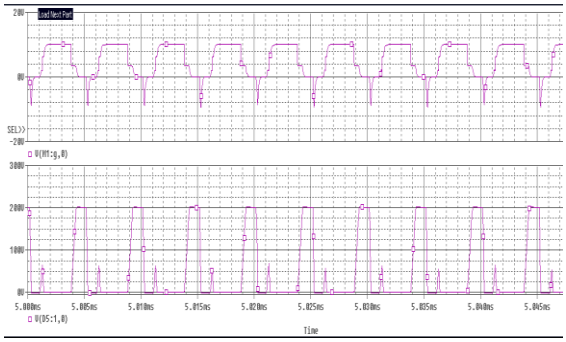

Fig4: Vgs1 and Vs1

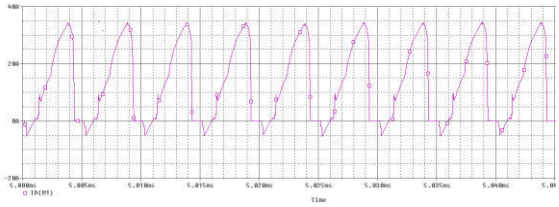

Fig5:Current across switch S1, Is1

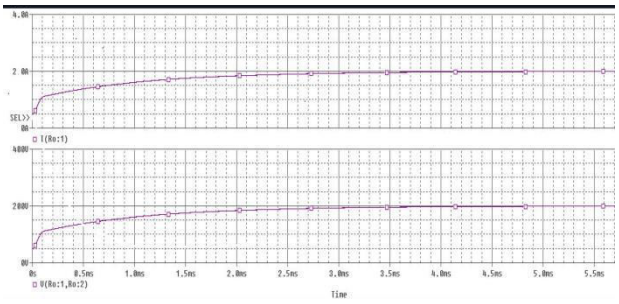

Fig6: Output current Io and Output Voltage Vo

REFERENCES

[1] G. Hua, C.-S. Leu, Y. Jiang, and F. C. Y. Lee, "Novel zero-voltagetransition PWM converters," IEEE Trans. Power Electron., vol. 9, no. 2, pp. 213–219, Mar. 1994.

[2] G. Hua, E. X. Yang, Y. Jiang, and F. C. Y. Lee, "Novel zero-currenttransition PWM converters," IEEE Trans. Power Electron., vol. 9, no. 6, pp. 601–606, Nov. 1994.

[3] H. Bodur and A. F. Bakan, "A new ZVT-ZCT-PWM DC-DC converter," IEEE Trans. Power Electron., vol. 19, no. 3, pp. 676–684, May 2004.

[4] H. Bodur and A. F. Bakan, "A new ZVT-PWM DC-DC converter," IEEE Trans. Power Electron., vol. 17, no. 1, pp. 40–47, Jan. 2002.

[5] S. S. Saha, B. Majumdar, T. Halder, and S. K. Biswas, "New fully softswitched boost-converter with reduced

conduction losses," in Proc. Power Electron. Drive Syst. 2005 Int. Conf., Jan., 2006, vol. 1, pp. 107–112.

[6] N. Jain, P. K. Jain, and G. Joos, "A zero voltage transition boost converter employing a soft switching auxiliary circuit with reduced conduction losses," IEEE Trans. Power Electron., vol. 19, no. 1, pp. 130–139, Jan. 2004.

[7] B. R. Lin and J. J. Chen, "Analysis and implementation of a soft switching converter with high-voltage conversion ration," IET Power Electron. vol. 1, no. 3, pp. 386–394, Sep. 2008.

[8] L. Jong-Jae, K. Jung-Min, K. Eung-Ho, and K. Bong-Hwan, "Dual series resonant active clamp converter," IEEE Trans. Ind. Electron., vol. 55, no. 2, pp. 699–710, Feb. 2008.

[9] X. Wu, J. Zhang, X. Ye, and Z. Qian, "Analysis and derivations for a family ZVS converter based on a new active clamp ZVS cell," IEEE Trans. Ind. Electron., vol. 55, no. 2, pp. 773–781, Feb. 2008.

[10] D. W. Erning and A. R. Hefner, Jr., "IGBT model validation for softswitching applications," IEEE Trans. Ind. Appl., vol. 37, no. 2, pp. 650– 660, Mar./Apr. 2001.

[11] S.-R. Park, S.-H. Park,C.-Y.Won, andY.-C. Jung, "Lowloss soft switching boost converter," in Proc. 13th Power Electron. Motion Control Conf 2008, Sep. 2008, pp. 181–186.

◈◈◈

Simulation of VSC based HVDC Transmission System for the Integration of Windfarm into Grid

Mahalakshmi. R & P. Usha

Department of Electrical & Electronics Engineering
Dayananda Sagar College of Engineering, Bangalore, India
E-mail : deivamaha@yahoo.co.in & pu1968@yahoo.co.in

Abstract - Wind energy has huge potential to become major source of renewable energy for the modern world. For integrating wind farms to the AC grid, HVDC transmission systems have several advantages over AC transmission systems. This paper presents the design and control of voltage source converter based HVDC system for integration of wind farms in to AC grid. The designed VSC-HVDC system performance under steady state conditions and various transient conditions are presented. The PSCAD/EMTDC software package is used for the simulation studies.

Keywords*-HVDC power transmission system,Voltage source converter, Windfarm,PSCAD/EMTDC.*

I. INTRODUCTION

Ever increasing energy demand and challenges like pollution, consumption of conventional energy sources, global climate changes etc have made renewable energy sources to penetrate into the grid. Renewable energy is sustainable as it is obtained from the sources that are inexhaustible. These energy sources include solar, wind, biomass, geothermal and hydro. Both wind and solar have tremendous potential to fulfill world's energy need. In this, wind energy connected with the utility grid is widely adopted. There are two ways to connect wind farms with the grid, with AC transmission lines or with HVDC system. For short distances up to 60km AC transmission is economical but beyond this distance HVDC transmission is more advantageous[1]. The connection of large wind farms over long distance with AC lines has technical, economical, environmental difficulties[4]. AC over head lines require large reactive power compensation and long distance cables requires large amounts of charging currents. Hence, HVDC transmission is more suitable and feasible. The HVDC link decouples the two networks which are on either side of its converters. Both the networks can operate at different voltage levels and frequencies. Apart from these, there are several advantages such as fast active power modulation, effective reactive power compensation, less voltage drop on an on shore substation etc. Moreover with HVDC link, disturbances at the grid are not transmitted to the wind farms. There are two types of HVDC topologies, line commutated HVDC system (LCC-HVDC) and voltage source converter based HVDC system (VSC-HVDC) which are used for off shore wind farms. A VSC-HVDC system needs no external voltage source for commutation and reactive power control is independent of real power control. These features make VSC-HVDC system more attractive for connection of renewable sources to grid, island networks and connection of weak AC systems [8].

Main objective of this paper is to develop a low rating VSC based HVDC transmission system for the integration of wind farm to the grid. This paper deals about the modeling of VSC based HVDC transmission system and its control.

II. VSC-HVDC SYSTEM

The block diagram of the VSC-HVDC system is shown in Fig. 1. The VSC-HVDC technology is based on voltage source converters. The converters convert AC power to DC power or DC power to AC power[2]. The converter station consists of an IGBT/GTO valve bridge operated with high frequency Pulse Width Modulation (PWM), the converter control, the phase reactor, DC capacitor, and an AC-filter as shown in Fig.2. Inductance of the transformer acts as phase reactor.The bridge, in its basic form is a two-level, three-phase topology with six valves and series connected IGBT's/GTO's in each valve. Every IGBT/GTO is provided with an anti parallel diode as in Fig. 2. Turn on/off of each single IGBT is controlled from the control equipment on ground potential.

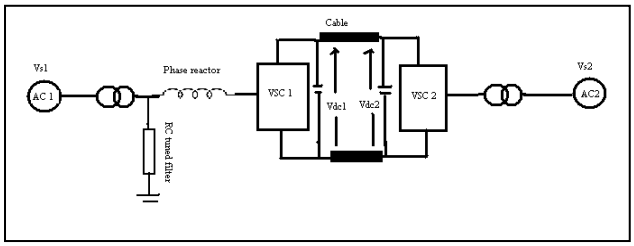

Fig. 1 Schematic diagram of VSC transmission system

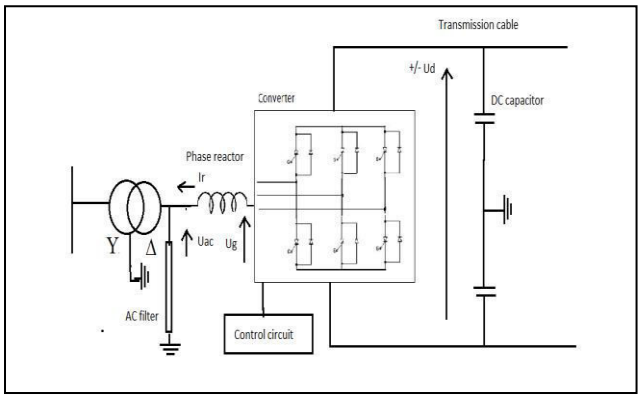

Fig. 2 Converter station

III. MODEL SYSTEM (VSC TRANSMISSION) AND CONTROL

A synchronous generator of 10MVA rating is connected to VSC1 via 13.8KV/62.5KVthree phase transformer as shown in Fig.1.VSC1, VSC2 are two six pulse converters connected through a cable of 100 Km length. Here, VSC1 is considered as rectifier and VSC2 as inverter. GTOs are used as switching devices of the converters. To reduce the harmonics at the input side, 1 MVAR- RC tuned damped filter is used and at the inverter AC bus 4MVAR filter is used. The DC voltage of the system is 120KV and current 0.18kA. Capacitors of each 500 µF is used at the rectifier and inverter end.

- Converter and inverter controls are independent with each other. The following are the control techniques which are adopted.
- Power flow can be controlled by adjusting the phase angle of ac side voltage of the sending end converter.
- DC voltage and AC voltage at the receiving end can be controlled by adjusting the phase angle of AC side voltage of the receiving end converter.
- Reactive power is held to a lower value by adjusting the magnitude of voltage at the sending end converter.

Control of DC voltage by inverter and control of power flow by rectifier is done by using PWM technique. Reference wave is compared with the carrier wave which is 33 times of fundamental frequency and generates the PWM pulses. The fundamental component of the inverter output voltage can be operated with the DC operating voltage by the following equation

$$U_{L\text{-}L} = \frac{\sqrt{3}*M*U_d}{2\sqrt{2}} \qquad (1)$$

Where,

$U_{L\text{-}L}$ Fundamental component of line to line voltage

Ud DC Voltage

M Modulation index

The modulation index (M) is the ratio of triangular wave amplitude to sinusoidal reference wave amplitude. Fig 3. shows the carrier signal and reference signal for generation of triggering pulses of VSC using Sinusoidal Pulse Width Modulation (SPWM) technique.

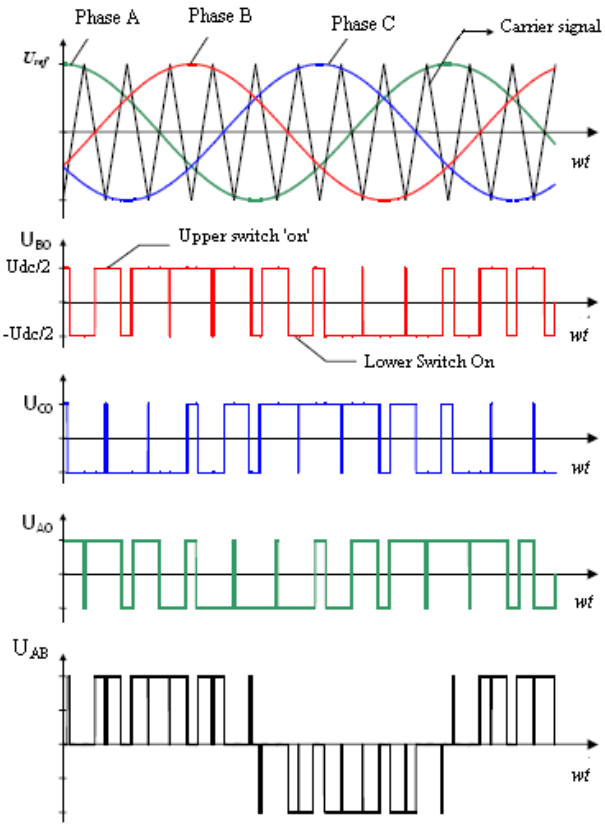

Fig. 3 AC output voltage of VSC using SPWM technique

Modulation index of the rectifier can be adjusted by comparing the system reactive power with reference reactive power. Pdc, mr ,Vrec are used as input to the sending end controller .Modulation index of the receiving end is varied by comparing the reference

voltage and receiving end AC voltage of the system. Vac, mi, Vdc are the input parameters of the receiving end controller. By means of the sending, receiving end controller, output can be stabilized.Fig:4 represents the overall control diagram at sending end. Similar type of controller is developed at the receiving end to generate ON and OFF pulses. Instead of comparing the reactive power, It compares the reference voltage with the voltage at the inverter station. System controls are activated at one second.

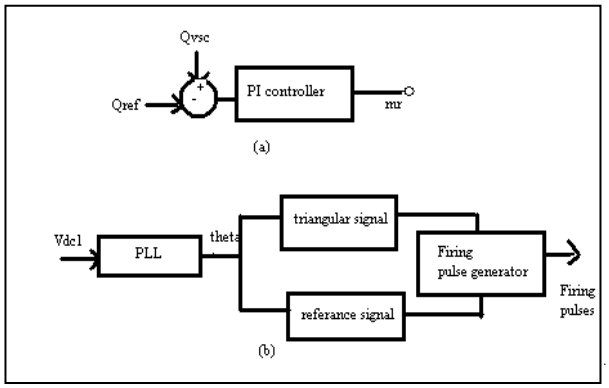

Fig.4. Control diagram at sending end-PWM Pulse generation

IV. SIMULATION RESULTS OF VSC HVDC TRANSMISSION

The performance of the controllers and HVDC system are tested for steady state condition and for various transient conditions. Fig.5 gives the AC current harmonics at the sending end converter station. Fig.6 shows the DC voltage at rectifier and inverter under steady state and Fig. 7 shows the steady state DC current. Fig. 8 and 9 show the mi, mr and PU AC voltages at rectifier/inverter under steady conditions. The simulation is run for 5 seconds. The system response is tested for the following four different transient conditions

- DC line fault near rectifier station
- Three phase to ground fault at inverter AC bus
- Single phase to ground fault at inverter AC bus
- Double line to ground fault at inverter AC bus

The above mentioned faults are simulated at 2.2seconds for a duration of 2 ½ cycles.

Fig. 10 shows the DC voltage at rectifier and inverter under DC line fault near rectifier station. Fig. 11 shows DC voltage of the system for three phase to ground fault at inverter AC bus. Similarly, Fig. 12 and Fig. 13 shows the DC voltage under single line to ground fault and double line to ground fault at inverter AC bus respectively. Single phase to ground fault is created at inverter end to test the performance of mr, mi under normal and faulted conditions and also to test the PU AC voltage at rectifier and inverter end .Fig. 14 shows mr, mi when single phase to ground occurred at receiving end and Fig.15 shows PU AC voltages at rectifier and inverter for single phase to ground fault at inverter end

Simulation results gives us the change in the value of dc voltage,mi,mr,AC voltages for different types of faults. For all types of fault, VSC based transmission system gets effected for short duration and finally it is reaching its steady state value very fastly.

V. INTEGRATION OF VSC WITH WINDFARM

Proposed VSC based HVDC system is integrated with the windfarm as shown in Fig. 16 and tested the AC voltage at the rectifier end and DC voltage at rectifier/inverter end. Windfarm consists of five synchronous machines which are rated at 2 MVA. All the machines are operated by the wind turbine individually.

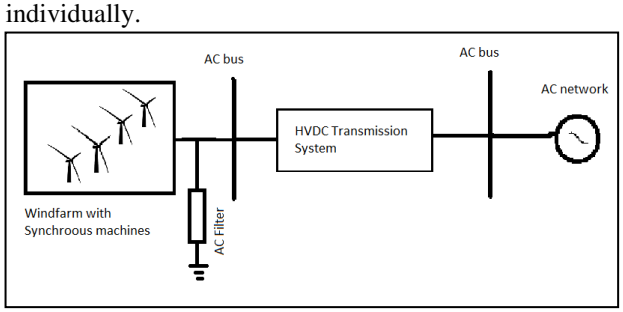

Fig.16: Integration of wind farm with the VSC based transmission system.

VI. SIMULATION RESULTS OF WINDFARM WITH VSC HVDC SYSTEM

Performance of the integrated system is tested by the simulation result of DC voltage at inverter/rectifier and AC voltage at sending end. Fig.17 and 18 show the DC voltage at rectifier and inverter.Fig.19 shows the PU AC voltage at the sending end under steady state conditions..

VII. CONCLUSION AND FUTURE WORK

Performance of the proposed VSC-HVDC system under steady state and under various transient conditions are studied. The performance of the controllers is satisfactory as the HVDC system takes very less time to reach steady state after clearing of the fault. Proposed system is integrated with the wind farm to extract the wind energy and to supply the power to the grid and system response is checked with the help of DC voltage and AC voltage. Detailed analysis of this integrated system has to done.

REFERENCES

[1] Nikolas Flourentzou, Vassilios G. Agelidis, "VSC based HVDC Power Transmission System An overview" IEEE Transactions On Power Electronics, vol. 24, no. 3, march 2009,pp-

[2] K. R. Padiyar,Nagesh Prabhu , ,Modelling, Control design and Analysis of VSC based HVDC Transmission Systems, 2004 lnternational Conference on Power System Technology - POWERCON 2004,Singapore, 21-24 November 2004

[3] Khatir Mohamed, Zidi Sid Ahmed, Hadjeri Samir, Fellah Mohammed Karim,Amiri RABIE, Performance Analysis of a Voltage Source Converter (VSC) based HVDC Transmission System under Faulted Conditions, Leonardo Journal of Sciences ISSN 1583-0233 Issue 15, July-December 2009

[4] Aishling Reidy, Rick Watson ,"Modelling and simulation of VSC based HVDC connected offshore wind farm"

[5] General Information,Deutsches Windenergie Institute,DM Energy,Wind Turbine Grid Connection and Interaction.

[6] K. H. Sobrink, P. L. Sorensen, P. Christensen, N. Sandersen, K.Eriksson, and P. Holmberg, "DC feeder for connection of a windfarm," in Proc. Cigre Symp., Malaysia, Sep. 1999.

[7] A.K. Skytt, P.Holmberg, and L. E. Juhlin, "HVDC light for connection of wind farms," in Proc. 2nd Int. Workshop Transmission Networks for Offshore Wind Farms, Sweden, Mar. 2001.

[8] Lie Xu, Liangzhong Yao, Christian Sasse," Grid Integration of Large DFIG-Based WindFarms Using VSC Transmission" IEEE Transactions On Power Systems, Vol. 22, No. 3, August 2007

◈◈◈

Transformer Fault Detection by Frequency Response Analysis

Vikash.M, Sharlinprija.K,, Ilampoornan.M.K,

Power Electronics and Drives, Loyola Institute of Technology, Chennai-600 123,India.
Professor, EEE-Dept, Loyola Institute of Technology, Chennai-600 123,India
E-mail: vikaashmanick@gmail.com, j.sharlin02@gmail.com & academicaffairslit@gmail.com

Abstract - Power transformers are one of the most vital as well as expensive equipment in an electric power system. Therefore, it is the responsibility of utilities to decrease the transformer lifecycle costs and to increase the usable service time. The damage may cause a change in the physical condition of transformer which would be reflected in the electrical parameters- resistance, inductance and capacitance. The insulation performance is influenced by thermal, electrical and mechanical stresses. The displacement of windings can occur during transportation of transformers or during a short circuit near the transformer in the power system. The Frequency Response Analysis (FRA) can detect the type of fault and the exact location of fault. The result obtained for the various fault condition is compared with the reference set and the conclusion are drawn.

Keywords- *Short circuit faults, interturn fault, failure of transformer oil and mechanical displacement.*

I. INTRODUCTION

This project proposes to detect short circuit faults between two turns in a winding of a transformer and mechanical displacement. Power transformers are the most expensive single elements of EHV transmission systems. Therefore, it is the prime duty of utilities to decrease the transformer life cycle costs and to increase the usable service life. One possibility is to extend the monitoring and diagnosis of power transformers to all possible types of faults. Special monitoring devices for the detection of different types of faults are in use.

Transformers are designed to withstand the effects of limited duration short circuit at their terminals. This ability can be affected by thermal and transient mechanical stresses, which occur during operation. Especially, power transformers having a winding displacement caused by a mechanical stress due to a short circuit which is critical. Generally such pre-damaged power transformers show a serious fault when a next short circuit event occurs. To ensure a sufficient ability to withstand short circuit, the operating personal should identify such pre-damaged power transformers. In the standard, the reactance measurement is the basic detection method to demonstrate the integrity of the windings.

II. SHORT CIRCUIT FAULT IN WINDINGS

System short circuit may occur across any two lines or if the neutral point is earthed between any one lines. The effect of system short circuit will produce over currents, magnitude of which are dependent on the system MVA, feeding the fault or the voltage, which has been short circuited and on the impedance of the circuit up to the fault.

Short circuit may cause winding movement and shorted turns. Short circuits near transformers usually cause currents of high amplitudes. This leads to extreme mechanical stress of core and coil assembly. The mechanical forces do not always cause a failure. Sometimes there is only some significant damage, which are not recognized and further service is not possible.

III. SHORT CIRCUIT FORCES

The insulation performance is influenced by thermal, dielectric and mechanical aspects. Electrical and thermal failure mechanisms and the forces resulting from the short circuits can damage the transformers. The short circuit withstand capability of a power transformer is defined as the ability to withstand the full asymmetrical short circuit currents without impairing its suitability for normal service conditions. Steady increase in unit ratings of transformers and simultaneous growth of short circuit levels of networks have made the short circuit withstand capability of the transformer one of the most important aspect of its design.

The short circuit may lead to symmetrical short circuit currents of the order of 6-7 times the rated current and peak asymmetrical current as high as 15-18 times the rated current. The basic formula for force acting on a current carrying conductor in a magnetic field at any instant is given by:

F=BIL Newton

where,

B-Flux density in Tesla

I-Current in Amperes

L-Length of the conductor in Meters

This means that resulting forces shall be tremendously high since they will increase in square of the current. These forces shall be exerted directly on all current carrying parts of the transformer in a magnetic field. Short circuit forces are of pulsating nature since short circuit current and flux are sinusoidal. Therefore, time variable stresses are applied to the affected structures. These forces are very high during the first asymmetrical peak and come down to the symmetrical rms value. The forces generated during short-circuit are transferred to all parts mechanically coupled to winding assembly. The effects of these forces are radial force due to leakage field distribution during short-circuit and axial forces will be generated due to mechanical stress of the end rings.

IV. DETECTION TECHNIQUE

If the transformer has been switched off by protective equipment, there is a need to determine whether the transformer can be safely re-energized. Visual inspections require dismantling of the transformer, removing of the transformer oil and are time consuming. Hence effective detection techniques are required.

The most commonly used techniques are:

1. Leakage reactance measurement
2. Low voltage impulse
3. Frequency response analysis

V. HISTORICAL DEVELOPMENT IN FAULT DETECTION TECHNIQUE

Before 1980, LVI tests were performed on transformers in order to obtain the information considering the transformer condition. In this method, a very steep impulse was applied to one of the HV terminals and the response signal across a 50 Ω resistor was recorded.

For mechanical faults, neither method (LVI or FRA) is used. For electrical faults, the swept frequency method gives better results because it has a finer resolution at low frequencies. The LVI method is subjected to several disadvantages and hence FRA is widely used to detect winding deformation.

VI. DISADVANTSGES OF LVI METHOD

- It is subjected to interference effects.
- It requires extensive calibration procedures.
- It also requires a specially constructed and finely trimmed instrumentation system to obtain repeatable results.
- The amount of power injected into the test object is different at different frequencies. This leads to differences in precision across the frequency range.
- It is difficult to filter out broad band noise.

The *swept frequency response analysis* (SFRA) method removes many of these difficulties while increasing the sensitivity of detecting winding deformation.

VII. FREQUENCY RESPONSE ANALYSIS

Frequency response analysis (FRA) consists of measuring the impedance of a transformer winding over a wide range of frequencies and comparing the results with a reference set. This FRA technique is gradually being introduced in the field of power transformer testing and diagnosing. Differences may indicate damage to the transformer, which can be investigated further using other techniques or by an internal examination.

VIII. REASONS FOR ADOPTING FRA

- Prediction of response of the circuit for any input.
- Sinusoidal waveforms have the elegant property that they can be combined to form other waveform which is usually non-sinusoidal. Thus frequency response allows us to understand a circuit's response to more complex inputs
- Designing of circuits with particular frequency characteristics is possible.
- Changes in the winding geometry have an effect on the characteristic frequencies. Hence winding deformation can be detected more effectively by this method.

IX. FRA METHOD

This method uses a sweep generator to apply sinusoidal voltage at different frequencies to one terminal of a transformer winding. Amplitude and phase of signals are obtained from selected terminals of the transformer are plotted directly against frequency.

An accurate measurement of the frequency response provides a finger print of the transformer. If differences are found in the measurements, then it indicates that a

mechanical change inside the transformer has occurred. The obtained frequency response can also be used in transformer modeling and in understanding resonance excitation phenomena. The measured frequency range is usually rather large and so the results are usually presented on a graph of amplitude or phase against frequency.

The phase-frequency graph does not contain as much useful information as the amplitude-frequency graph does, so it is often not plotted or analyzed. It is possible to use either a linear scale or a logarithmic scale for frequency in the graphs. A logarithmic scale has the advantage of allowing all of the information to be presented on a single graph.

X. CHARACTERISTICS OF WINDING FREQUENCY RESPONSE

The low-frequency response is typically characterized by decreasing amplitude reaching a minimum in a resonance at or below 1 kHz. This resonance is caused by the interaction of the shunt capacitance of the windings with the magnetizing inductance. If there are two flux paths in the core of different lengths, then it will be a double resonance. The first resonant frequencies can vary with the state of residual magnetization of the core. They will also be different on sister transformers, where manufacturing differences in the core joints will give different reluctances.

At medium frequency there is a group of resonances, corresponding to the interaction of the shunt capacitance and air-cored inductance of the windings. These are generally the most repeatable. Slight differences may exist between sister transformers, owing to the effect of manufacturing differences in the windings. More significant differences may be found between windings on different phases of three-phase transformers, owing to different lead configurations or different winding external clearances.

At high frequency there is a more confused group of resonances, corresponding to the interaction of the shunt and series capacitances and air-cored inductances of parts of the windings. The high-frequency response is affected by manufacturing differences, lead configuration, and winding external clearances in much the same way as is the medium-frequency response. At the highest frequencies the influence of the measurement cables can become important, especially on large transformers. Grounding of the transformer and the cable screens can also have an important influence. The upper limit of the reproducible range is likely to be at least 1MHz, probably rather more for small transformers.

XI. DIAGNOSING FAULTS

Faults, such as short-circuited turns, change the magnetizing characteristics of the transformer and, hence, the low-frequency response. Circulating currents loops, if they are sufficiently large, redirect leakage flux into the core and also change the low-frequency response. An ungrounded core changes the shunt capacitance of the winding closest to the core and also the low-frequency response.

The medium-frequency response is sensitive to faults that cause a change in the properties of the whole winding. A significant increase in the medium-frequency resonances normally indicates axial movement of a winding. A significant decrease normally indicates radial movement of the inner winding. Slight differences are often accepted as being a result of “windings settling into place.”

The high-frequency response is sensitive to faults that cause changes in the properties of parts of the winding. Localized winding damage causes seemingly random changes in the high-frequency response, often leading to the creation of new resonant frequencies. The high-frequency response may also be affected by the tank or cable grounding. Poor tank grounding is easy to spot, as it affects all windings, whereas damage is usually confined to one winding or at worst one phase. Poor cable grounds are more difficult to detect, as they may cause changes to just one winding, but are unlikely to lead to the creation of new resonant frequencies.

XII. MEASUREMENT OF WINDING DEFORMATION IN POWER TRANSFORMERS USING FRA METHOD

When a transformer is subjected to high through fault currents, the mechanical structure and windings are subjected to large mechanical stresses. These stresses may cause serious deformation of winding and precipitate a transformer failure. Winding deformation is difficult to determine by conventional measurements of ratio impedance and inductance and capacitance of the winding structure. These changes can be detected externally by FRA method.

XIII. MODELLING OF TRANSFOMER WINDING

A simplified equivalent circuit for one outside phase of the winding of the 8 MVA, 110/22 kV, wye-delta power transformer, using cascade π section is modeled for eight sections which equals to the number of winding disc in the transformer is shown in Figure 1. The model consists of eight sections. The equivalent circuit is useful in modeling and is sensitive to winding changes. Conversely, a change in response could be related to a calculated amount of winding deformation.

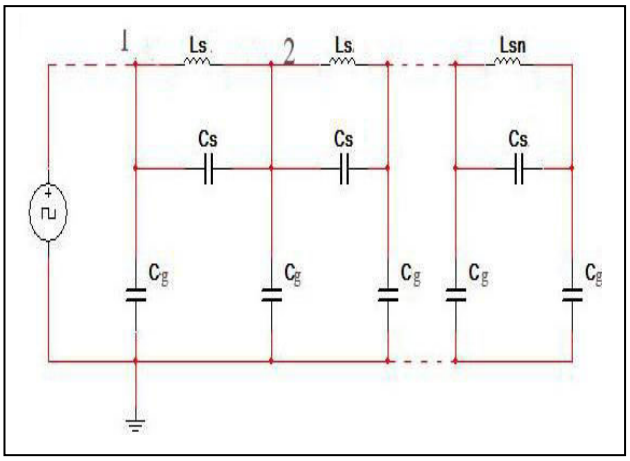

Figure 1. Equivalent circuit of 8 MVA transformers

In a winding there exists capacitance between the adjacent turns within a disc or layer, capacitance between the adjacent discs or layers, capacitance to ground and to other windings. Similarly there exists self and mutual inductances as pertaining to the individual turns, the disc/sections, one part the winding to another or one whole winding to another. Although both capacitance and inductance are of distributed nature, for practical computation purposes these have to be lumped in varying degrees according to the desired accuracy. Also, the effect of the winding resistance is not significant and can therefore be neglected.

XIV. SIMULATION OF FAULTS

Frequency response analysis can detect many type of faults includes short circuit fault, interturn fault, failure of transformer oil and mechanical displacement. These faults are thus simulated and the frequency response is obtained.

A. SHORT CIRCUIT FAULT

Short circuit faults are simulated by including a resistor between the nodes at which the fault occurrence is to be analyzed is shown in Figure 2. The circuit may be studied for various resistor values like 100 Ω, 1 kΩ and 10 kΩ.

It can be seen from the analysis that the behavior of the circuit changes from that resembling a short (R=100 Ω) to that resembling an unfaulted case (R=10 kΩ). The intermediate value (R=1 kΩ) shows the transition. For the analysis purpose, consider R=100 Ω, which resembles a short. It is further clearly observable in the Table 1 indicating the resonant frequencies of faulty condition in comparison with healthy condition and creation of new resonant frequencies.

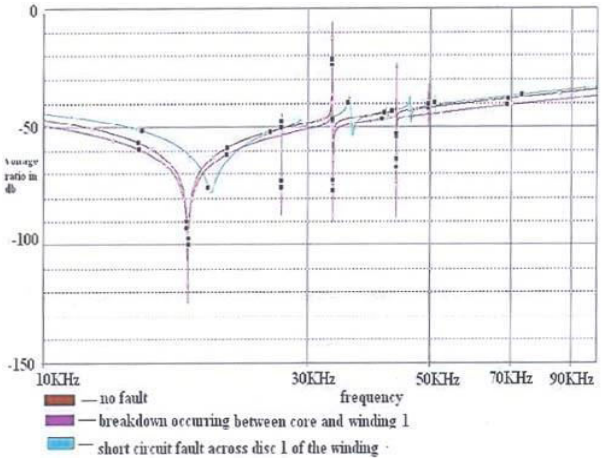

Figure 2**.** Comparison of no fault with short circuit fault across disc 1 of the winding and breakdown occurring between core and winding at resonant frequencies.

INFERENCE

For section 1, the resonant frequencies of the response for breakdown occurring between core and winding 1 occurs at a lesser frequency when compared with a response for short circuit across the disc1 of the winding.

For the remaining sections the resonant frequencies of the response for breakdown occurring between core and winding occurs at a higher frequency when compared with a response for short fault across the disc of the winding.

Table I. Comparison of no fault with short circuit fault across disc 1 of the winding and breakdown occurring between core and winding at resonant frequencies.

Poles	Resonant Frequencies of No Fault Response in khz	Resonant Frequencies of Short Circuit Fault Across Disc1 of The Winding in khz	Resonant Frequencies of Breakdown Occuring Between Core and Winding 1 in khz
1	26.903	29.141	26.884
2	33.167	35.752	33.197
3	43.391	41.476	43.311
4	49.636	45.825	49.556
5	-	49.102	-
6	-	51.015	-

B. INTERTURN FAULT

The inter-turn faults are better expressed by variation in series capacitance. The occurrence of short between the turns is indicated by including a resistor (R=100 Ω) across the series capacitance of winding. Similarly, the fault across each winding can be simulated and frequency response is obtained.

The frequency response analysis for short circuit fault across adjacent discs of the winding is shown in Figure 3 and poles occur at the respected frequencies is shown in Table II.

It is observable in Table II, indicating the resonant frequencies of short circuit fault across disc1 in comparison with short circuit fault across disc2 of the winding.

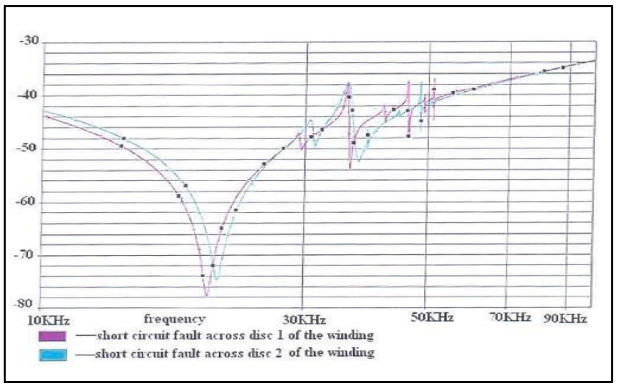

Figure 3. Comparison of short circuit fault across disc 1 and disc 2 of the winding.

INFERENCE

From the Table II, it is inferred that the frequency shift occurs. The maximum frequency shift that occurs in pole 3 is approximately 2.71 kHz whereas the frequency shift is negligible in pole 2.

Table II. Comparison of short circuit fault across disc 1 and disc 2 of the winding

Poles	Resonant Frequencies of Short Circuit Fault Across Disc 1 of the Winding in khz	Resonant Frequencies of Short Circuit Fault Across Disc 2 of the Winding in khz
1	29.141	30.669
2	35.752	35.760
3	41.476	38.905
4	45.825	44.218
5	49.102	48.350
6	51.015	50.886

C. FAILURE OF TRANSFORMER OIL

The failure of insulation or dielectric is simulated by adding a resistor across the ground capacitance. The ground capacitance denotes the distance between the core and the winding, which indicates that a fault has occurred between the winding and the core. The resistor (R=100 Ω) is included across each ground capacitor and the frequency response is obtained as shown in Figure 4.

It is further clearly observable in the Table III indicating the resonant frequencies of breakdown occurring between core and winding 1 in comparison with breakdown occurring between core and winding 2.

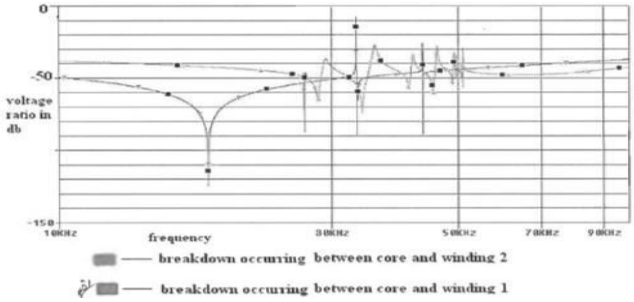

Figure 4. Comparison of breakdown occurring between core and winding 1 with breakdown occurring between core and winding 2 at resonant frequencies.

INFERENCE

From the Table III, it is inferred that the new resonant frequencies occurs between core and winding 2. The maximum frequency shift that occurs in pole 4 is approximately 3.604 kHz.

Table III. Comparison of breakdown occurring between core and winding 1 with breakdown occurring between core and winding 2 at resonant frequencies.

Poles	Resonant Frequencies of Breakdown Occuring Between Core and Winding 1 in khz	Resonant Frequencies of Breakdown Occuring Between Core and Winding 2 in khz
1	26.884	29.289
2	33.197	35.777
3	43.311	41.754
4	49.556	45.952
5	-	49.181
6	-	51.062

D. MECHANICAL DISPLACEMENT

This includes both vertical and horizontal displacement of the winding.

(i) AXIAL DISPLACEMENT:

The axial displacement of the winding is referred as vertical displacement. The vertical displacement is simulated by causing a change in the coupling value between two windings. Hence the coupling value is reduced by 0.1 and 0.2 for each section and the frequency response is obtained.

The frequency response analysis for axial displacement is shown in Figure 5 and their corresponding frequency is shown in Table IV.

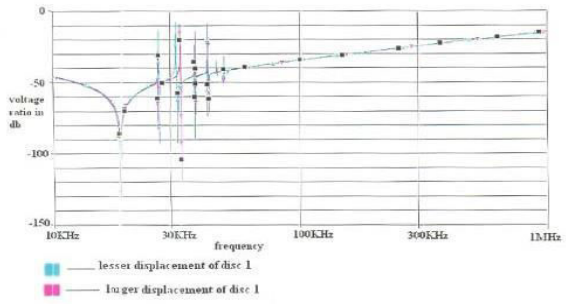

Figure 5. Comparison of axial displacement of disc 1.

INFERENCE

From Table IV, it is inferred that for disc 1, the larger displacement occurs at a frequency of 26.588 kHz and lesser displacement occurs at a frequency of 26.509 kHz.

Table IV. Comparison of axial displacement of disc 1.

Axial Displacement in Disc 1	
	FREQUENCY OF FIRST POLE IN kHz
LARGER DISPLACEMENT	26.588
LESSER DISPLACEMENT	26.509
DIFFERENCE BETWEEN THE FREQUENCIES	79

(ii) RADIAL DISPLACEMENT

The displacement of winding from the core is referred as the horizontal displacement. Horizontal displacement causes a change in the ground capacitance value. Hence the ground capacitance value is increased for each section and the frequency response is obtained.

The frequency response analysis for radial displacement is shown in Figure 6 and their corresponding frequency is shown in Table V.

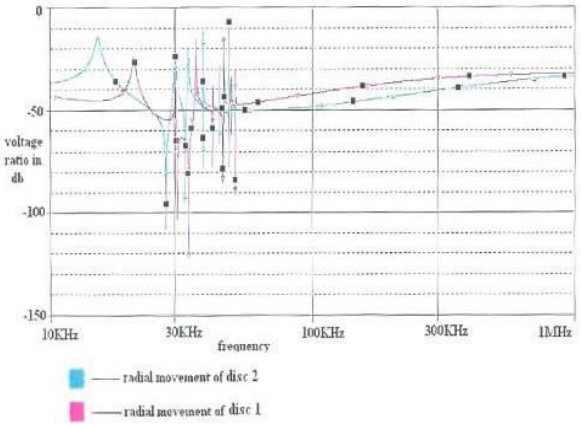

Figure 6. Comparison of radial displacements of disc 1 and disc 2.

INFERENCE

As seen in Table V, the radial displacement of disc 1 occurs at a frequency of 20.898 kHz whereas in disc 2, the radial displacement occurs at a frequency of 14.792 kHz.

Table V. Comparison of radial displacements of disc 1 and disc 2.

Radial Displacement in	**Frequency of Peak Occurrence in kHz**
DISC 1	20.898
DISC 2	14.792

XV. CONCLUSION

Every transformer winding has a unique signature that is sensitive to changes in the parameters of the winding, namely resistance, inductance, and capacitance. Frequency spectrum of a transformer is very sensitive to any deformation or displacement of the winding. Frequency response analysis is a very effective tool for diagnosing transformer condition. It is particularly useful in detecting any fault that is due to mechanical damage to the winding. The technique is also very reliable for detecting any short circuit to the winding. Results from a measurement can be analyzed through several techniques via graphical presentation. However, reference is needed for better interpretation. The reference can either be from historical data of the same transformer or from sister transformers. In many cases, historical data for transformers already in operation is difficult to get owing to shutdown requirement. Sister transformers are used in those cases as the reference measurement. The interpretation of the results is meanwhile a great help in determining further action to be taken especially for suspected transformers. FRA can be a very effective tool for condition

monitoring. It can avoid catastrophic failure in transformers and also help maintenance engineer to estimate time and cost for repairing the transformer after the fault before undertaking maintenance.

REFERENCES

[1] Ryder (2003) 'Diagnosing transformer faults using frequency response analysis'- IEEE Electrical Insulation Magazine, pp 16-22.

[2] P.T.M. Vaessen, E. Hanique (January 1992) 'A New Frequency Response Analysis Method for Power Transformers'- Transactions on power delivery, vol.7, No.1, PP 384-389.

[3] K. Feser, J. Christian, C. Neumann, U. Sundermann, T. Leibfried, A. Kachler, M. Loppacher- 'The Transfer Function Method for Detection of Winding Displacements on Power Transformers after Transport, Short Circuit or 30 Years'.

◈◈◈

Plasma Cell

T.V.Vetrivel,C.G.Ashwin Karthik & Molla Ramizur Rahman

Department of Electrical & Electronics Engineering,
Dayananda Sagar College of Engineering, Bangalore,India
E-mail: vetribox@gmail.com, mail2ashhwin6@gmail.com, ramizurscience@yahoo.com

Abstract - Plasma cell is a device which uses properties of metals for generating electricity. It works by circulating electrons in and out of the metals with the help of charge differences that can be produced with the help of the laser source having energy more than that of work function of metals. The metals used here are positively charged where the charges are always equal. Two metals are made use of, between which the electrons are allowed to circulate resulting a state where the metals are having equal amount of charges and the process of achieving this state involves flow of charges which intern produces electricity.

Keywords-*Plasma Cell; electricity; current*.

I. INTRODUCTION

Electricity is one of the important sources of energies which have the potential for being used as substitute for other sources of energy and it is also one of the important things that require increase in production for the energy hunger of the world. This Plasma Cell is a method for production of electricity that might server our power requirements.

II. CONSTRUCTION

Fig 1 shows the structure of Plasma Cell metals and Fig 2 shows the actual cross-section of Plasma Cell where it contains three metals P-Cell metal 1,P-Cell metal 2 and the Charge Neutralization metal. The P-Cell metal 1 is first subjected to removal of definite quantity of electrons. Then the P-Cell metal 2 is placed near the P-Cell metal 1. Now charge neutralization metal is connected between the two P-Cell metals. The two ends of the P-Cell metal 1 and P-Cell metal 2 are kept under low pressure for the travel of electrons. Here these electrons which travel between the metals externally are not the current which we are going to take out. The current which we are going to take out is the current due to movement of the electrons in the Charge Neutralization metal by the process of equalizing the charge between the P-Cell metal 1 and P-Cell metal 2. This whole setup is placed in the center of the Field Protection Hollow sphere. The electric field produced is opposite and equal to the intense field produced by the P-Cell metals.

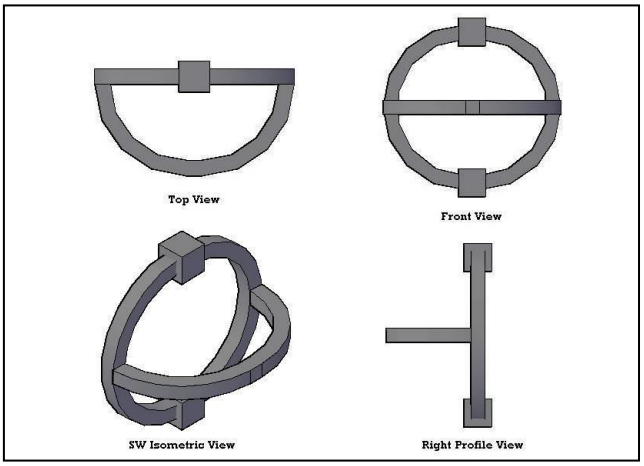

Figure1. The picture shows the whole view of the plasma cell where the dimensions will be described with reasons.

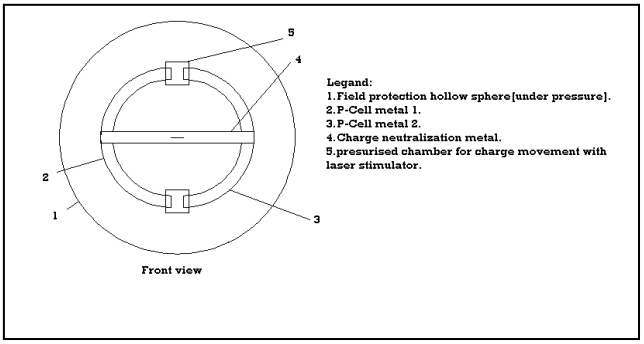

Fig. 2: The picture shows the front view of Plasma Cell with the outer shell.

The equations for the charges and the pulse time and the energy of the laser are given by.

$$Q_{per\ pulse} = k.I_L.e.A\frac{t_i}{t_{pulse}}$$

Where,

$Q_{per\ pulse}$ → Amount of charge produced per pulse of the laser.

$k = \frac{1}{h.v}$ → Inverse of the inergy of single photon.

I_L ⟶ Intensity of the pulsed laser used.

e ⟶ Charge of electron.

A ⟶ Area spread of the pulsed laser in the metal surface.

t_i ⟶ Total time where the pulsed laser device is being on.

t_{pulse} ⟶ Time interval of the pulsed laser.

$$h.v = h.v_0 - E$$

Where,

$h.v$ → Energy required for pumping out electron.

$h.v_0$ → Work function of the metal.

E ⟶ External electric field.

The important parameter we got to consider is that the charge flowing between the P-Cell metals externally must always be greater than the charge produced initially in the metals this must be followed if not there won't be electrons to travel between the junctions. Thus the output of the Plasma Cell depends upon the charge ejected during the working where a pulsed laser is incident on the P-Cell metal 2. Note that the laser used here is different from the laser used for producing positive charge in one of the P-Cell metal during the construction.

The equation for the charge in the junction is given by.

$$Q_{Junction} = Q_{per\ pulse}.\sqrt{\frac{1}{m}.\frac{d^2}{(hv - hv_0)}}$$

Where,

$Q_{Junction}$ → Charge present in the junction at any time.

$Q_{per\ pulse}$ → Charge produced per pulse by the laser.

m ⟶ mass of electron

$hv \rightarrow hv_0$ → Kinetic energy supplied for the electron by the pulsed lase

d^2 ⟶ Distance between the juction.

III. WORKING

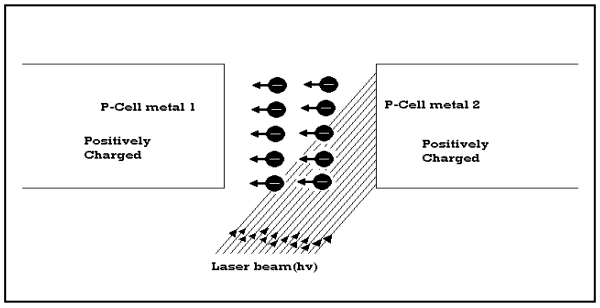

Figure 3.This is the picture of the electron transfer happening between the metals.

Here the electrons are subjected to 2 forces; force 1 is the attractive force due to the P-Cell metal 1, and force 2 is the attractive force due to the P-Cell metal 2. The metal exerts forces because those metals are positively charged. An important phenomenon happen that is the electrons ejected increases the positive charge in P-Cell metal 2. This increase in charge calls for equalization of the charges between the P-Cell metals 1 with the help of the Charge Neutralization metal. Thus the positive charge in

P-Cell 1 and P-Cell metal 2 are same thus the attractive force exerted by the P-Cell metals are same and acting in opposite in direction thus the net force acting on the electrons moving externally is zero. Now the electron move form P-Cell metal 1 to P-Cell metal 2 externally with the kinetic energy gained by the electron from the incident laser on the P-Cell metal 1. The movement of charges internally from P-Cell metal 1 to P-Cell metal 2 through the Charge Neutralization metal is the current output of the Plasma Cell.

IV. CURRENT EQUATION

The output is continuous or pulsed which depends on the time of pulse [in this context time of pulse is the pulse time of the laser used in the power production and not the laser pulse used in the construction for charge production]. That is if the time of pulse is equal to the relaxation time of electrons in the metal then the output will be like as shown in Fig 4**.**

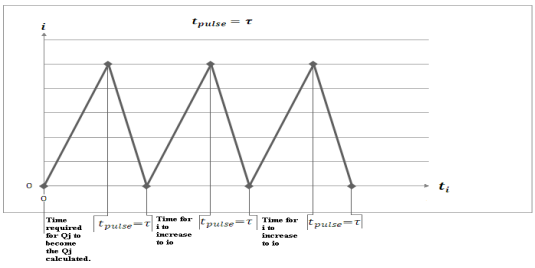

Figure4. Graph for Current vs. Time where time equal to relaxation time of the metal pulse.

For time of pulse greater than the relaxation time, the current graph will be as shown in Fig 5.

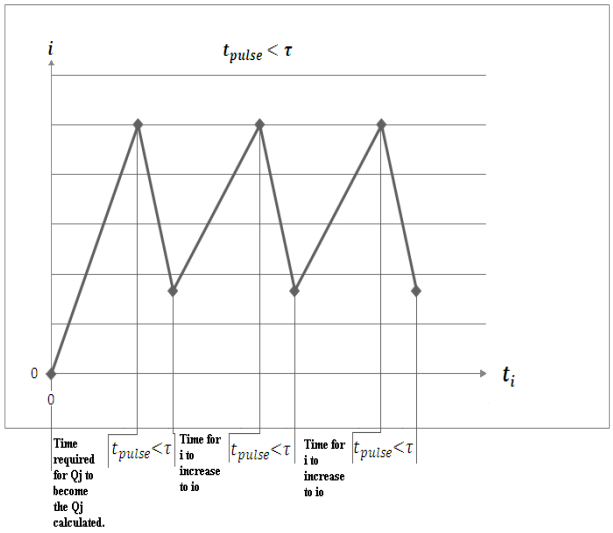

Figure5. Graph of Current vs. Time where Time of pulse is less than the relaxation time of the metal.

For current to be constant, that is not varying as above, time of pulse must be zero that is the laser must be continuous for the current to be constant. The current entirely due to the remaining free electrons in the P-Cell metals that is the difference of the number of free electrons present in a neutral metal of the same metal with the sum of the number of positive charge produced in the beginning and the charge in the junction.. The equation for the current in the metal is given by

$$i = n.e.A.v_d$$

$$i = \left(n.e.A - \left(Q_{produced} + Q_{Junction}\right)\right).v_d$$

n ⟶ **Number of free charges in the neutral metal of the same dimensons as the P-Cell metals.**

e ⟶ **Charge of electron.**

A ⟶ **Area of cross-section.**

v_d ⟶ **Drift velocity of the elctron in the metal.**

V. ADVANTAGES

The advantages of the plasma cell over the conventional power sources which we use commercially are,

- Electricity production cost is low when compared to Nuclear Power sources.
- No need of mechanical work as input to this for electricity production.
- This will give us comparatively very high current and voltage than the Fuel Cells.
- Thus it is a self sustained reaction which doesn't stop until the conditions are maintained.
- Since it produces DC output this can be set up at every places, where huge requirements are stays, which could prevent the wastage of our earth's flush.

VI. DISADVANTAGES

These are the disadvantages of the Plasma Cell when compared to the conventional power production methods.

- The electricity produced is direct current.
- Electricity production can only be near the requirements area to reduce the cost of transmission.
- These may have to be used in a stack to get the general voltage we use that is 220V and 5A.

VII. CONCLUSION

Thus we conclude that the method we have stated will give a possibility for a new way of generating electricity. This will find large applications for generating electricity and will be preferred over other sources due to its various advantages.

◈◈◈

Wearable Sensor For Activity Recognition In Healthcare Monitoring

Pushpalatha, Hema Pridarshini & Priya

D.S.C.E , Bangalore

Abstract - Alzheimer's disease (AD) is a slow progressive disease of the brain characterized by impairment of memory and eventually by disturbances in reasoning, planning, language, and perception. These disabilities are very difficult not only for the person with Alzheimer's, but also for the caregiver, family, and other loved ones as well. In order to assist the Alzheimer's patients two modules are designed. Firstly, the alert system kept at different locations of the home alert the patient by name of location. The second module is the monitoring system which gives an alert to the on duty caregivers in the form of GPRS data. This is done by tying accelerometer based mobile on patient thigh which collects data for different activities such as sleeping, sitting, walking etc., and sends the accelerometer data continuously to remote server. This helps the server to keep track of patient's usual activities and alert the system if something unusual at patient's end.

Keywords*: sensor, microcontroller, speech processor, Android based mobile, Java,*

I. INTRODUCTION

People with Alzheimer's disease have memory problems and cognitive impairment, and eventually they will not be able to care for themselves. They often experience confusion, loss of judgment, and difficulty finding words, finishing thoughts, or following directions. They also may experience personality and behavior changes. For example, they may become agitated, irritable, or very passive. Some people with Alzheimer's may wander from home and become lost.

The likelihood of having Alzheimer's disease increases substantially after the age of 70 and may affect around 50% of persons over the age of 85, in 2006 there were 26.6 million sufferers worldwide. Alzheimer's is predicted to affect 1 in 85 people globally by 2050.

Amyloidal plaques and neurofibrillary tangles are the primary hallmarks of Alzheimer's disease. Plaques are dense deposits of protein and cellular material outside and around the brain's nerve cells. Tangles are twisted fibers that build up inside the nerve cells. As the disease progresses, nerve cells in several brain areas shrink and die, including cells that normally produce critical neurotransmitters, the chemical messengers that relay brain signals from one nerve cell to another. Acetylcholine is a neurotransmitter that is deficient in people with Alzheimer's. As nerve cells continue to die, the brain itself shrinks and the wrinkles along its surface become smoother.

These disabilities are very difficult, not only for the person with Alzheimer's, but for the caregiver, family, and other loved ones as well. Caregivers need resources and reassurance to know that while the challenges are great, specific actions can reduce some of the safety concerns that accompany Alzheimer's disease.

To help the Alzheimer's disease patients and caregiver, sensors are placed in different locations of the room which remains the patient where he is exactly located when he is left alone in the home. [6]

Also, Accelerometer based mobiles monitor different activities such as walking, sleeping, sitting etc. These activities are compared with the scheduled activities in the database created at server side. If any activities of patients doesn't match with activities of database at server side it sends an alarm to caregiver.

II. HARDWARE DEVELOPMENT

2.1 BLOCK DIAGRAM:

The block diagram of the Alert system designed to keep sensors at different locations of the home is shown in Fig 1.

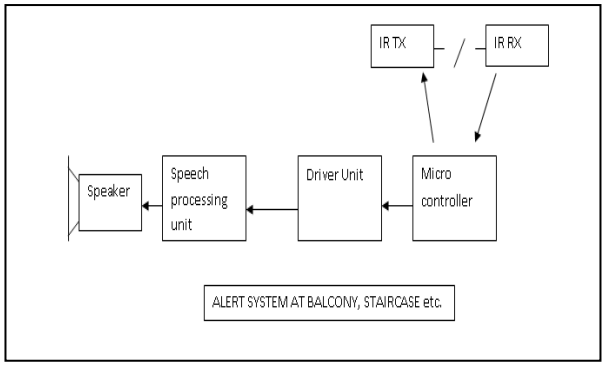

Fig 1: Block diagram of Alert system

2.2 SENSORS

A sensor is a device that measures a physical quantity and converts it into a signal which can be read by an observer or by an instrument. IR sensor is used to detect the object (Human).

2.3 MICROCONTROLLER

A PIC microcontroller is a processor with built in memory and RAM and is used to control the projects. It saves us in building a circuit that has separate external RAM, ROM and peripheral chips. PIC microcontroller can be used to re-program with the help of flash memory.PIC16F873 belongs to PIC family where analog input can be given directly to the input port. [7]

2.4 DRIVER UNIT

ULN2003 is a high voltage and high current Darlington array IC. It contains seven open collector Darlington pairs with common emitters. A Darlington pair is an arrangement of two bipolar transistors.

ULN2003 belongs to the family of ULN200X series of ICs. Different versions of this family interface to different logic families. ULN2003 is for 5V TTL, CMOS logic devices. These ICs are used when driving a wide range of loads and are used as relay drivers, display drivers, line drivers etc.

Each channel or Darlington pair in ULN2003 is rated at 500mA and can withstand peak current of 600mA. The inputs and outputs are provided opposite to each other in the pin layout. Each driver also contains a suppression diode to dissipate voltage spikes while driving inductive loads.

2.5 SPEECH PROCESSOR

The APR9600 device offers single-chip voice recording, non-volatile storage, and playback capability for 40 to 60 seconds. The device supports both random and sequential access of multiple messages.

This speech processor provides the recording of many messages and these messages can be used to inform the patient when rooms are increased. The block diagram is shown in Fig 2

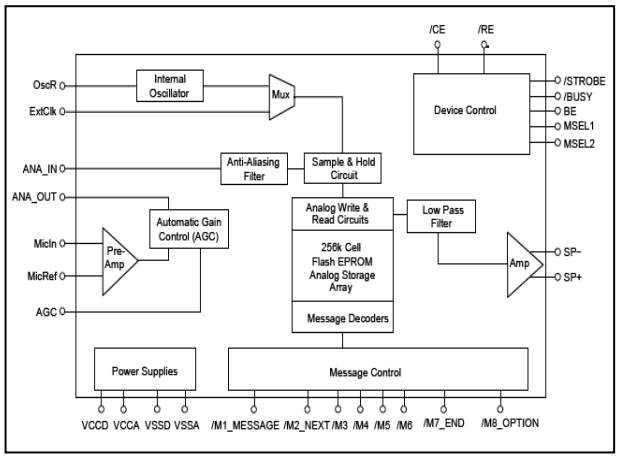

Fig 2: Block diagram of speech processor

III. SOFTWARE DEVELOPMENT

Accelerometer based mobile tied on our thigh, collect data for different activities such as sleeping, sitting, walking etc. Accelerometer is a sensor that gives an estimate of the acceleration along x, y and z axes. The real time data from the GPRS enabled mobile phone ties to the patient's thigh transmits accelerometer data continuously to the remote server.

Android based mobiles are used and java is used as a programming language.

3.1 FLOWCHART

The following GUI is created on the mobile

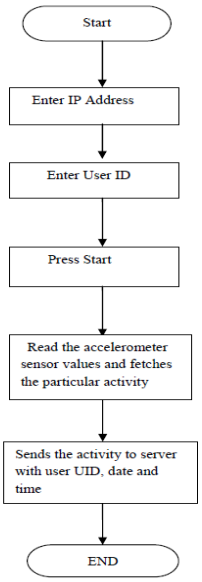

GUI is created with the use of programming language. The accelerometer sensor values are checked for Alzheimer's and non-Alzheimer patients and thresholds are set accordingly.

Threshold decides the activities of the Alzheimer's patients whether he is normal or abnormal by the database of the patient created on server side in which the activities sent from the patient mobile are compared with database at server side, anything abnormal will be informed to caregiver.

SPECIFICATION

The overall voltage required for working of entire hardware module is 5v.

IV. EXPECTED RESULTS

The alert system kept at different locations of the alert the place of location with the help of speaker.

Android based mobiles expected to display the activities of sleeping, standing and walking and the activities are sent to the server with user ID, IP address. Also, transition from one gesture to another finds difficulty to find the exact activity of the patient.

V. CONCLUSION

Real-time monitoring of human movements provides an effective means of inferring a patient's level of activity**.** This project aims at assisting living environments for people with different health issues such as Alzheimer's disease and related dementias.

This project initiates the development of a system for patient monitoring and study of their behaviors. The continuous and unobtrusive recognition of patient's dangerous movements will be a valuable tool in the hands of the caregivers, both in a short proactive care and also in long term care processes. The system can be easily extended to other monitoring applications such as continuous monitoring in hospital ICUs and baby units.

REFERENCES

[1] M. Avvenuti, C. Baker, J .Light, D. Tulpan, A. Vecchio, "Non-intrusive Patient Monitoring of Alzheimer's Disease Subjects Using Wireless Sensor Networks",2009, Pg No.161-165

[2] James Geddes and Kevin Warwick, "Cloud based global positioning system as safety Monitor for dementia patients",2009.

[3] Hao Tian, Pang Lei, Li Xingjuan, Xing Shusong, "Wearable Activity Recognition for Automatic Micro blog updates, International Conference on Advanced Intelligent Mechatronics,2009,Pg.No. 1720-23

[4] www.medicinenet.com/alzheimers-disease-causes-symptoms-stages

[5] http://www.mstracey.btinternet.co.uk/ pictutorial/progtut2.htm

[6] http://www.microcontrollerboard.com/pic-timer0-tutorial.html

[7] www.alldatasheet.com

◈◈◈

Design and Simulation of Three Phase Five Level and Seven Level Inverter Fed Induction Motor Drive with Two Cascaded H-Bridge configuration

[1]Manasa s, [2]Balaji Ramakrishna S, [3]Madhura s & Mohan H M[4]

[1,2&3]Lecturer, EEE Department , DSCE , Bangalore, India
[4]Lecturer, ECE Department, SJCIT , chickballapur, India
Email: manasa.s.athresha@gmail.com, balajikrishna.s@gmail.com,
madhu4tulip@gmail.com & mohanhm@gmail.com

Abstract - This paper deals with study of Three phase Five Level and Seven Level inverter fed induction motor drive . Both five level and seven level are realized by cascading two H- bridges. The poor quality of voltage and current of a conventional inverter fed induction machine is due to the presence of harmonics and hence there is significant level of energy losses. The Multilevel inverter is used to reduce the harmonics. The inverters with a large number of steps can generate high quality voltage waveforms. The higher levels can follow a voltage reference with accuracy and with the advantage that the generated voltage can be modulated in amplitude instead of pulse-width modulation. An active harmonic elimination method is applied to eliminate any number of specific higher order harmonics of multilevel converters with unequal dc voltages. The simulation of three phase five and seven level inverter fed induction motor model is done using Matlab/Simulink. The FFT spectrums for the outputs are analyzed to study the reduction in the harmonics.

Keywords*: Induction motor, Matlab/simulink, Multilevel inverters, voltage source inverter, Total Harmonic distortion.*

I. INTRODUCTION

Adjustable Speed Drives (ASDs) are the essential and endless demand of the industries and researchers. They are widely used in the industries to control the speed of conveyor systems, blower speeds, machine tool speeds and other applications that require adjustable speeds. In many industrial applications, traditionally, DC motors were the work horses for the Adjustable Speed Drives (ASDs) due to their excellent speed and torque response. But, they have the inherent disadvantage of commutator and mechanical brushes, which undergo wear and tear with the passage of time. In most cases, AC motors are preferred to DC motors, in particular, an induction motor due to its low cost, low maintenance, lower weight, higher efficiency, improved ruggedness and reliability. All these features make the use of induction motors a mandatory in many areas of industrial applications. The advancement in Power Electronics and semiconductor technology has triggered the development of high power and high speed semiconductor devices in order to achieve a smooth, continuous and step less variation in motor speed. Applications of solid state converters/inverters for adjustable speed induction motor drive are wide spread in electromechanical systems for a large spectrum of industrial systems.[3],[6],[10].

Voltage or current converters, as they generate discrete output waveforms, force the use of machines with special isolation, and in some applications large inductances connected in series with the respective load. Also, it is well known that distorted voltages and currents waveforms produce harmonic contamination, additional power losses, and high frequency noise that can affect not only the power load but also the associated controllers. All these unwanted operating characteristics associated with PWM converters could be overcome with multilevel converters, in addition to the fact that higher voltage levels can be achieved.

The poor quality of output current and voltage of an induction motor fed by a classical two-level inverter is due to the presence of harmonics. The presence of significant amount of harmonics makes the motor to suffer from severe torque pulsations, especially at low speed, which manifest themselves in cogging of the shaft. It will also causes undesired motor heating and Electromagnetic interference [12]. The reduction in harmonics calls for large sized filters, resulting in increased size and the cost of the system. Nowadays multilevel inverters are the promising alternative and cost effective solution for high voltage and high power applications including power quality and motor drive problems. Multilevel structure allows raising the power

handling capability of the system in a powerful and systematic way. The advancements in the field of power electronics and microelectronics made it possible to reduce the magnitude of harmonics with multilevel inverters, in which the number of levels of the inverters are increased rather than increasing the size of the filters [11]. The performance of multilevel inverters enhances as the number of levels of the inverter increases.

In this paper three phase Five Level and Seven Level inverter fed induction motor drive are designed and implemented. Both five level and seven level are realized by cascading two H- bridges with equal dc source value for five level and unequal dc source value for seven level which reduces switches for seven level. The simulation of three phase five and seven level inverter fed induction motor model is done using Matlab/Simulink. The FFT spectrums for the outputs are analyzed to study the reduction in the harmonics.

II. MULTILEVEL INVERTER

Multilevel inverters have drawn tremendous interest in the power industry. They present a new set of feature that are well suited for use in reactive power compensation. Multilevel inverters will significantly reduce the magnitude of harmonics and increases the output voltage and power without the use of step-up transformer. A multilevel inverter consists of a series of H-bridge inverter units connected to three phase induction motor. The general function of this multilevel inverter is to synthesize a desired voltage from several DC sources. The AC terminal voltages of each bridge are connected in series. Unlike the diode clamp or flying-capacitors inverter, the cascaded inverter does not require any voltage clamping diodes or voltage balancing capacitors.[1-4],[10],[13]. This configuration is useful for constant frequency applications such as active front-end rectifiers, active power filters, and reactive power compensation. Choosing appropriate conducting angles for the H bridges can eliminate a specific harmonic in the output waveform. The required conduction angles can be calculated by analyzing the output phase voltage of cascade inverter assuming that four H-bridges have been used, the output voltage Vao can be given as:

Vao = Va1 +Va2 +Va3 +Va4 +Va5…

Since the wave is symmetrical along the x-axis, both Fourier coefficient A0 and An are zero. Just the analysis of Bn is required. It is given as:

.

$$B_n = \{[4V_{dc}]/n\pi\}\left[\sum_{j=1}^{\infty} \cos(n \propto_1)\right]$$

where

j = Number of dc sources

n = odd harmonic order

Therefore, to choose the conducting angle of each H bridge precisely, it is necessary to select the harmonics with certain amplitude and order, which needs to be eliminated. [3],[4],[5] To eliminate 5th, 7th, and 11th harmonics and to provide the peak fundamental of the phase voltage equal to 80% of its maximum value, it needs to solve the following equation with modulation index M = 0.8:

$\cos(5_{\alpha 1}) + \cos(5_{\alpha 2}) + \cos(5_{\alpha 3}) + \cos(5_{\alpha 4}) = 0$

$\cos(7_{\alpha 1}) + \cos(7_{\alpha 2}) + \cos(7_{\alpha 3}) + \cos(7_{\alpha 4}) = 0$

$\cos(11_{\alpha 1}) + \cos(11_{\alpha 2}) + \cos(11_{\alpha 3}) + \cos(11_{\alpha 4}) = 0$

$\cos(\alpha_1) + \cos(\alpha_2) + \cos(\alpha_3) + \cos(\alpha_4) = 0.8*4$

III. FIVE LEVEL AND SEVEN LEVEL INVERTER CIRCUITS USING ONLY TWO CASCADED H- BRIDGES.

There are several types of multilevel inverters but the one considered in this paper is the cascaded multilevel inverter (CMI). The structure of the CMI is not only simple and modular but also requires the least number of components compared to other types of multilevel inverters. This in turn, provides the flexibility in extending the CMI to higher number of levels without increase in circuit complexity as well as facilitates packaging.

A. Single phase structure of a five level Cascaded Multilevel inverter

A single-phase structure of an m-level cascaded inverter is illustrated in Fig 1. Each separate dc source (SDCS) is connected to a single-phase full-bridge, or H-bridge, inverter. Each inverter level can generate three different voltage outputs, $+V_{dc}$, 0, and $-V_{dc}$ by connecting the dc source to the ac output by different combinations of the four switches, S11, S12, S13, and S14. To obtain $+V_{dc}$, switches S11 and S14 are turned on, whereas $-V_{dc}$ can be obtained by turning on switches S12 and S13. By turning on S11 and S12 or S13 and S14, the output voltage is 0. The ac outputs of each of the different full-bridge inverter levels are connected in series such that the synthesized voltage waveform is the sum of the inverter outputs.

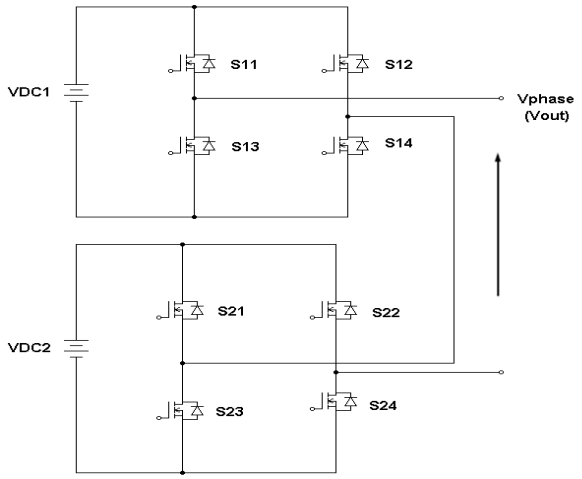

Fig. 1 Single Phase Structure of Cascaded Multilevel inverter

The structure shown in Fig.1 is used to produce Five Level Inverter output voltage by giving same DC source value and Seven Level Inverter output voltags by giving unequal DC source value. Here for Five Level output 225V is given for both upper and lower H-bridge and for Seven Level output 150V and 300V is given for upper and lower H-bridge respectively.

B. Three phase structure of Cascaded Multilevel Inverter

The Three Phase Structure of Cascaded Multilevel inverter is illustrated in Fig.2. Each dc source is connected to an inverter. Each inverter level can generate three different voltage outputs, $+V_{dc}$, 0, and $-V_{dc}$ using various combinations of the four switches. The ac outputs of the different full bridge inverter levels are connected in series such that the synthesized voltage waveform is the sum of the inverter outputs.

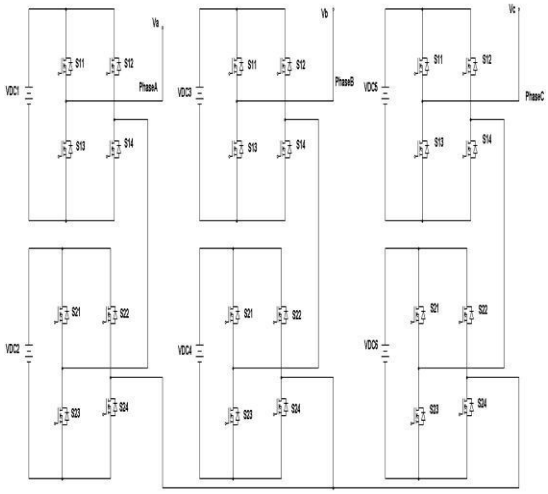

Fig. 2 Three Phase Structure of Cascaded Multilevel inverter.

IV. INDUCTION MOTOR DRIVE

Synchronous speed of Induction Motor is directly proportional to the supply frequency. Hence, by changing the frequency, the synchronous speed and the motor speed can be controlled below and above the normal full load speed. The voltage induced in the stator, E is proportional to the product of slip frequency and air gap flux. The motor terminal voltage can be considered proportional to the product of the frequency and flux, if the stator voltage is neglected. Any reduction in the supply frequency without a change in the terminal voltage causes an increase in the air gap flux. Induction motors are designed to operate at the knee point of the magnetization characteristic to make full use of the magnetic material. Therefore the increase in flux will saturate the motor. This will increase the magnetizing current, distort the line current and voltage, increase the core loss and the stator copper loss, and produce a high pitch acoustic noise. While any increase in flux beyond rated value is undesirable from the consideration of saturation effects, a decrease in flux is also avoided to retain the torque capability of the motor. Therefore, the variable frequency control below the rated frequency is generally carried out by reducing the machine phase voltage, V, along with the frequency in such a manner that the flux is maintained constant. Above the rated frequency, the motor is operated at a constant voltage because of the limitation imposed by stator insulation or by supply voltage limitations.

V. SIMULATION MODEL AND RESULTS

Multilevel inverter fed induction motor drive inverter is implemented in MATLAB SIMULINK which is shown in Fig.3. The MATLAB SIMULINK model of Single leg of five level Cascaded Multilevel inverter using two H-bridge configuration is shown in Fig.4.

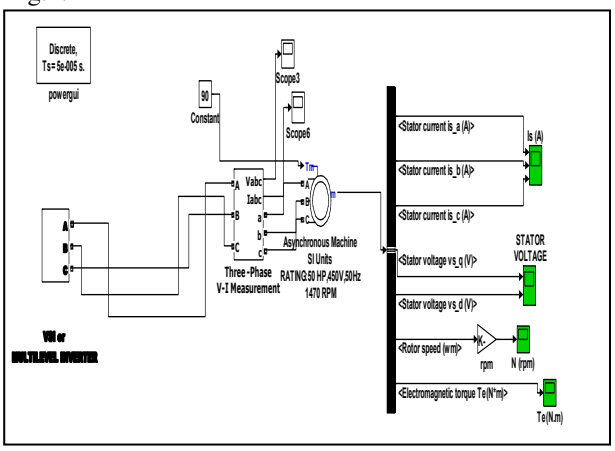

Fig. 3 Matlab/Simulink model of Multilevel Induction Motor dive.

The single phase five level inverter output is shown in Fig.5. The three phase five level inverter output phase voltage after feeding to induction motor is shown in Fig.6. The stator currents with respect to three phases are shown in Fig.7. The Variation in speed is shown in Fig.8. The speed increases and settles at 1470 rpm. The Torque is shown in Fig.9. FFT analysis is done for the voltage and current and the corresponding spectrum is shown in Fig.10 and Fig.11 respectively. It can be seen that the magnitude of fundamental voltage for five level inverter fed induction motor drive is 222.4 Volts. The total harmonic distortion is 4.95 percent and the magnitude of fundamental current is 97.93 Amperes. The total harmonic distortion is 1.57 percent.

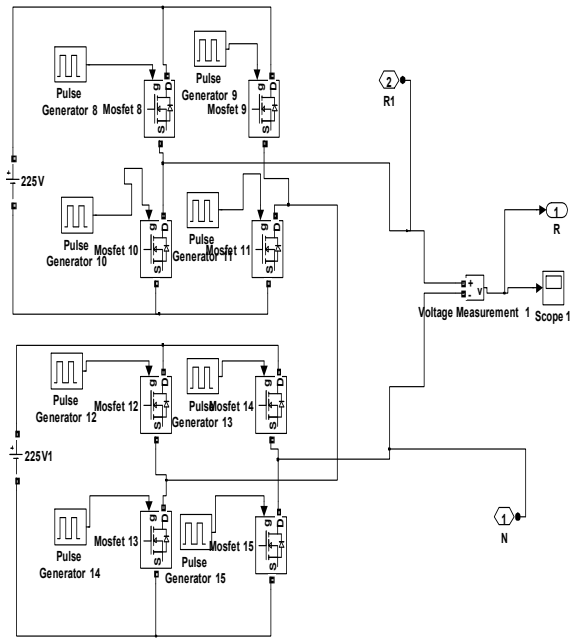

Fig. 4 Matlab/Simulink model of single leg of three phase Five level Multilevel Inverter.

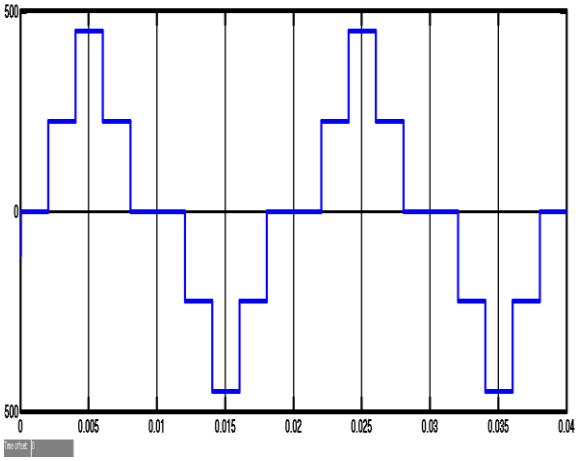

Fig. 5 Single phase five level inverter output

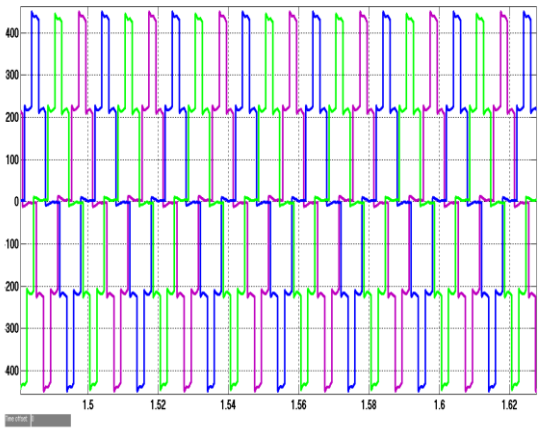

Fig. 6 Three phase five level inverter output phase voltage after feeding to induction motor

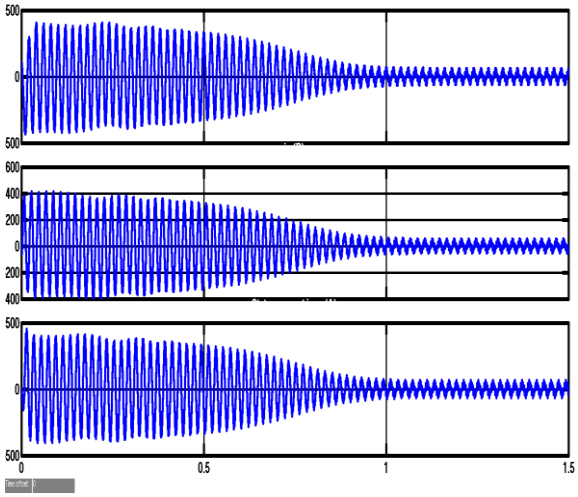

Fig. 7 Stator currents with respect to three phases

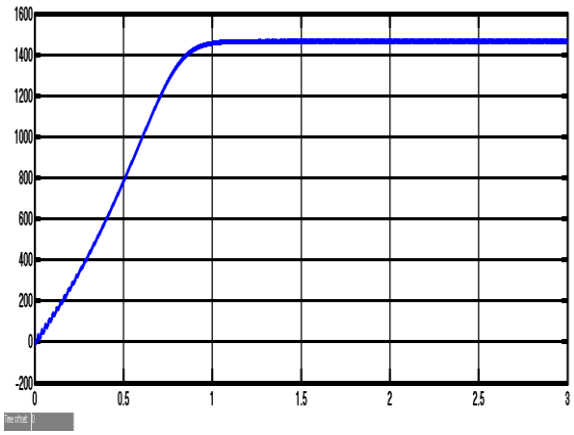

Fig. 8 Variation in speed

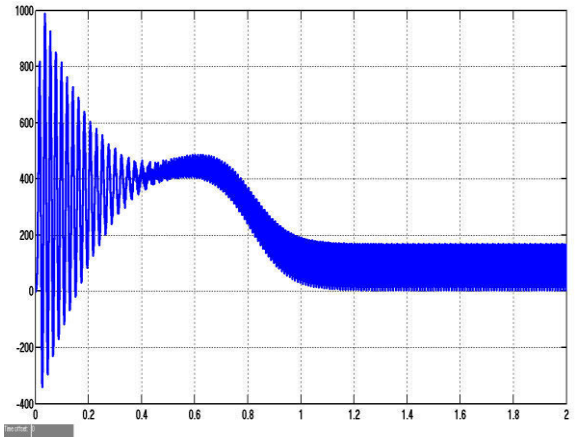

Fig. 9 Variation in Torque

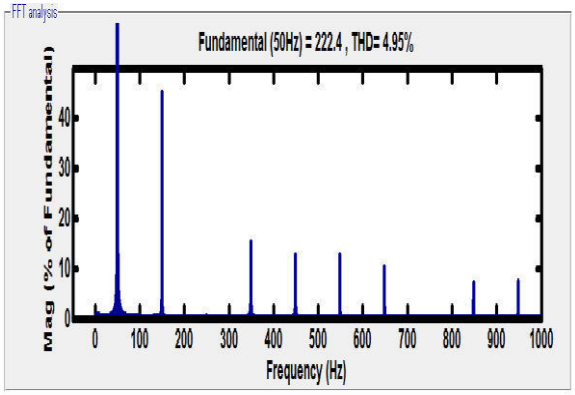

Fig. 10 FFT analysis of Voltage

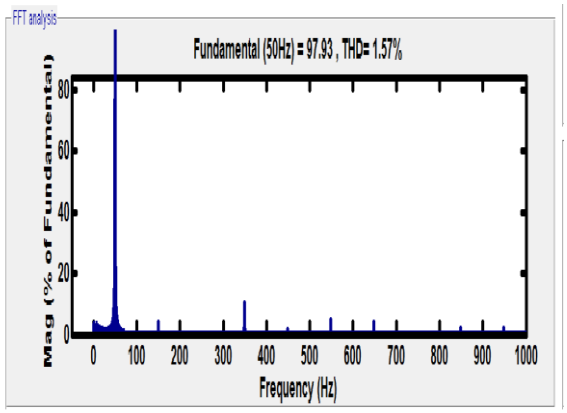

Fig. 11 FFT analysis of Current

The MATLAB SIMULINK model of Single leg of seven level Cascaded Multilevel inverter using two H-bridge configuration is shown in Fig.12

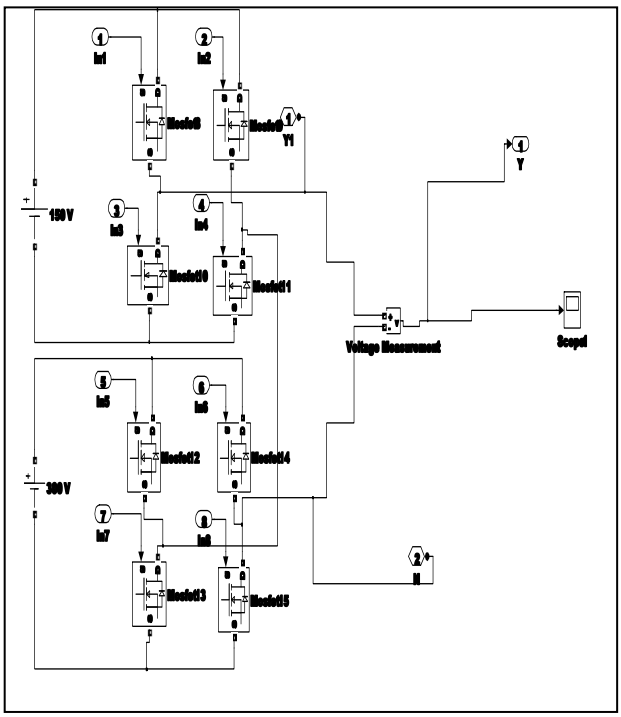

Fig. 12 Matlab/Simulink model of single leg of three phase seven level Multilevel Inverter.

The single phase seven level inverter output is shown in Fig.13. The three phase seven level inverter output phase voltage after feeding to induction motor is shown in Fig.14. The stator currents with respect to three phases are shown in Fig.15. The Variation in speed is shown in Fig.16. The speed increases and settles at 1470 rpm. The Torque is shown in Fig17. FFT analysis is done for the voltage and current and the corresponding spectrum is shown in Fig.18 and Fig.19 respectively. It can be seen that the magnitude of fundamental voltage for five level inverter fed induction motor drive is 234.4 Volts. The total harmonic distortion is 3.51 percent and the magnitude of fundamental current is 91.15 Amperes. The total harmonic distortion is 1.01 percent.

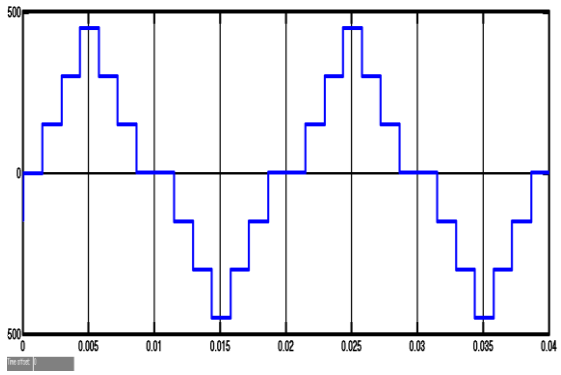

Fig. 13 Single phase seven level inverter output

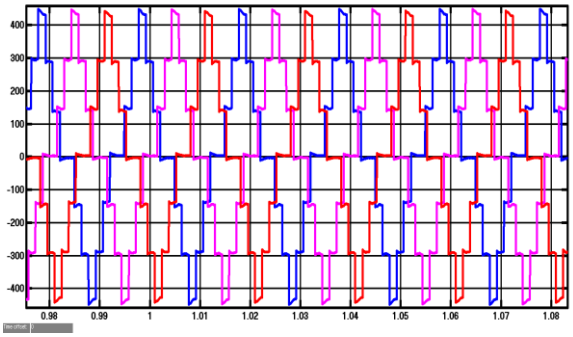

Fig. 14 Three phase seven level inverter output phase voltage after feeding to induction motor

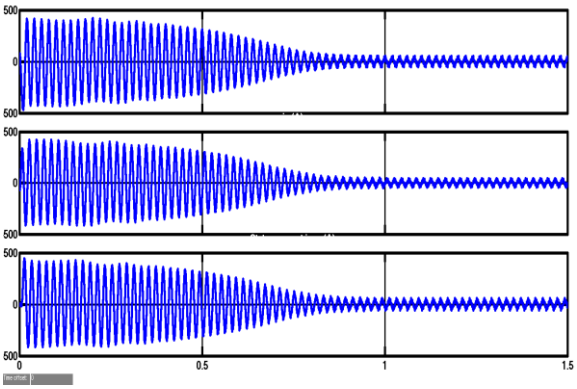

Fig. 15 Stator currents with respect to three phases

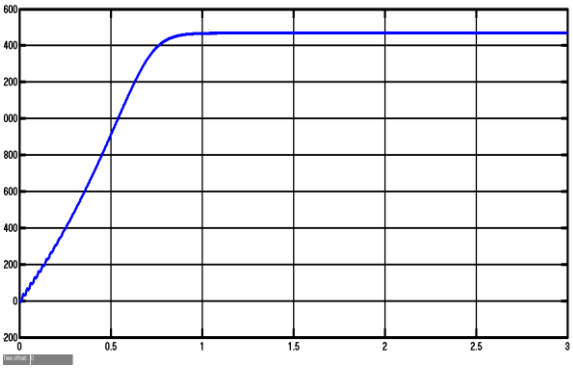

Fig. 16 Variation in speed

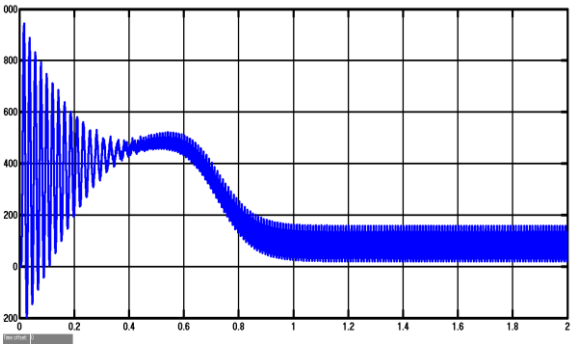

Fig. 17 Variation in Torque

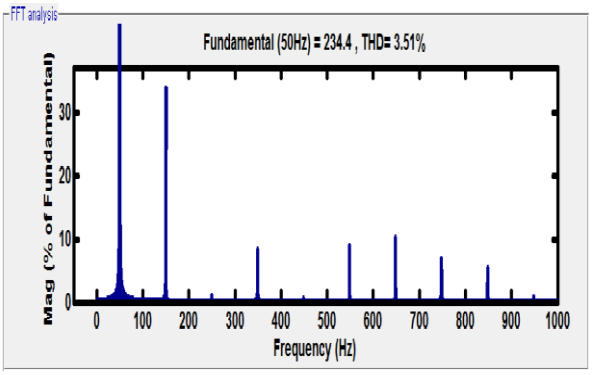

Fig. 18 FFT analysis of Voltage

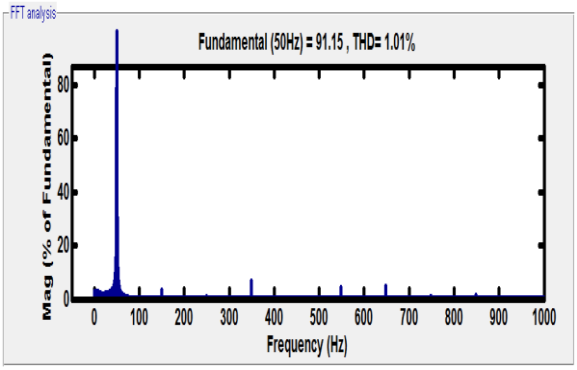

Fig. 19 FFT analysis of Current

The results are tabulated in Table I below.

TABLE I. THD ANALYSIS OF FIVE AND SEVEN LEVEL INVERTER WHEN FED TO INDUCTION MOTOR DRIVE

Parameters	**Multilevel inverter**	
	Five level Inverter	***Seven level Inverter***
Voltage Level	222.4	234.4
THD for Voltage	4.95%	3.51%
Current Level	97.93	91.95
THD for Current	1.57%	1.01%

VI. CONCLUSION

Five level and Seven level inverter fed induction motor drive are simulated using the blocks of simulink. The results of five level and seven level systems are compared. It is observed that the total harmonic distortion produced by the seven level inverter system is less than that of a five level inverter fed drive system. Therefore the heating due to seven level inverter system is less than that of a five level inverter fed drive system. The simulation results of voltage, current, speed and spectrum are presented. This drive system can be used in industries where adjustable speed drives are required

to produce output with reduced harmonic content. The scope of this work is the modeling and simulation of five level and seven level inverter fed induction motor drive systems. Experimental investigations will be done in future. Seven level inverter system is a viable alternative since it has better.

REFERENCES

[1]. J. Rodríguez, J. S. Lai, F. Z. Peng, "Multilevel inverters: A survey of topologies, controls, and applications," IEEE Transactions on Industrial Electronics, vol.49, no.4, pp. 724-738, 2002.

[2]. J. S. Lai, F. Z. Peng, "Multilevel converters-a new breed of power converters," IEEETransactions on Industry Applications, vol. 32, no.3, pp. 509-517, 1996.

[3]. L. M. Tolbert, F. Z. Peng, T. G. Habetler, "Multilevel converters for large electric drives,"IEEE Transactions on Industry Applications, vol. 35, no. 1, pp. 36–44, Jan./Feb. 1999.

[4]. J. N. Chiasson, L. M. Tolbert, K. J. McKenzie, Z. Du, "A complete solution to the harmonicelimination problem," IEEE Transactions on Power Electronics, vol. 19, no. 2, pp. 491-499,2004.

[5]. S.M Bashi, M. Mariun, N.F Mailah and S. Alhalali " Low Harmonics Single Phase Multilevel Power Converter" Asian journal of Scientific Research 1(3) 274-280 (2008) ISSN 1992-1454

[6]. Mr. G. Pandian and Dr. S. Rama Reddy" Implementation of Multilevel Inverter-Fed Induction Motor Drive" journal of industrial technology, volume 24 (2008)

[7]. Emil Levi, Senior Member, IEEE "Multiphase Electric Machines for Variable-Speed Applications" IEEE TRANSACTIONS ON INDUSTRIAL ELECTRONICS, VOL. 55, NO. 5, MAY 2008 pgs- 1893 -1909

[8]. Rahul B Nagpure, S S gokhale " Carrier Pulse width Modulation for Three Phase Multilevel Inverter to Minimise THD and enhance the Performance of Induction motor" National Conference on Innovative Paradigms in Engineering & Technology (NCIPET-2012) Proceedings published by International Journal of Computer Applications® (IJCA)

[9]. A. V. Antony Albert , V. Rajasekaran, S. Selvaperumal "comHarmonic Elimination of H-Bridge Seven Level Inverter"European Journal of Scientific ResearchISSN 1450-216X Vol.65 No.4 (2011), pp. 594-600

[10]. Neelashetty Kashappa [1] and Ramesh Reddy K. [2] "Performance Of Voltage Source Multilevel Inverter - Fed Induction Motor Drive Using Simulink " ARPN Journal of Engineering and Applied Sciences ©2006-2011 VOL. 6, NO. 6, JUNE 2011 ISSN 1819-6608

[11]. Dixon, J. and L. Moran, 2006." High-level multi-stepinverter optimization using a minimum number ofpower transistors. "IEEE Tran. Power Electron., 21(2):330-337.

[12]. Shivakumar, E.G., K. Gopukumar, S.K. Sinha andV.T. Ranganathan, 2001." Space vector PWM controlof dual inverter fedopen-end winding inductionmotor drive." IEEE APEC Conf., 1: 399-405.

[13]. R.S. Kanchan, P.N. Tekwani, M.R. Baiju, K. Gopakumar and A. Pittet "Three-level inverter configuration with common mode voltage elimination for induction motor drive.

◈◈◈

DTC and IFOC: Feasibility Analysis on Torque Control Schemes of an Induction Motor

Ramya R, Abhijith C, Shamini Raju S, Aditya M Bhat, Madhura Thilak

Department of Electrical and Electronics Engineering, Dayananda Sagar College of Engineering, Bangalore, India
E-Mail : [1]ramya2615@gmail.com, [2]abhijith.cuddapah@gmail.com, [3]24shamini@gmail.com, [4]aady_m@yahoo.com, [5]madhu4tulip@gmail.com

Abstract **-** This paper presents a detailed comparison between two control strategies for Induction machine (IM) drives: Direct Torque Control (DTC) and Indirect Field-Oriented control (IFOC). The performances of these two control schemes are evaluated and compared by simulation in terms of torque and current ripples, transient response and ease of implementation. The study is done by simulation using the Simulink Power System Blockset that allows a complete representation of the power section (inverter and IM) and the control system.

Keywords- *DTC, FOC, hysteresis, PI controller, Induction motor, PWM.*

I. INTRODUCTION

Control technology of AC motor drives has improved dramatically during the last two decades. This trend owes its progress to the new control techniques and philosophies developed by several researchers around the world. Induction machines (IM) have been widely used in industry because of their advantages: ruggedness, reliability, simple construction, low cost and minimum maintenance. However, due to their highly-coupled nonlinear structure, a high-performance control of IM is a challenging problem. Variable speed or adjustable torque control of electrical motor drives are crucial components in almost all modern industrial manufacturing processes. Traditionally variable speed electric machines were based on dc motors, but, for the last 20 years, the inverter-fed ac motor has largely taken over as the preferred solution for variable speed applications.

For low performance applications, open loop voltage/frequency control strategies are employed. Considering high-performance motion control, Field Oriented Control (FOC), or more recently Direct Torque Control (DTC) are used. Using these techniques, both the induction motor and the permanent magnet synchronous motor (PMSM) can be applied even in high performance servo applications that were once the exclusive domain of the dc machine.

The mentioned control techniques have undergone considerable research, but several problems remain: FOC is very dependent on knowledge of the rotor time constant when using an induction machine. DTC, in its traditional form, results in a non-constant inverter switching frequency, which may result in high inverter/motor losses. Techniques that fix this problem result in parameter dependent solutions. This paper provides a brief overview of the basic operating principle using DTC and IFOC. Furthermore, a comparative study of IFOC and DTC is presented. It is seen that both control approaches have their own advantages and disadvantages.

II. FIELD ORIENTED CONTROL

A. Principle

The Field Orientated Control (FOC) consists of controlling the stator currents represented by a vector. This control is based on projections which transform a three phase time and speed dependent system into a two co-ordinate (d and q co-ordinates) time invariant system. These projections lead to a structure similar to that of a DC machine control. Field orientated controlled machines need two constants as input references: the torque component (aligned with the q co-ordinate) and the flux component (aligned with d co-ordinate). As Field Orientated Control is simply based on projections the control structure handles instantaneous electrical quantities. This makes the control accurate in every working operation (steady state and transient) and independent of the limited bandwidth mathematical model.

In order to estimate the rotor flux vector is possible to use two different strategies:

` **DFOC** (Direct Field Oriented Control): rotor flux vector is either measured by means of a flux sensor mounted in the air-gap.

IFOC (Indirect Field Oriented Control): rotor flux vector is estimated using the field oriented control equations (current model) requiring a rotor speed measurement. The usual terminology *Sensor less* specifies that no position/speed feedback devices are used.

B. Block diagram

Two motor phase currents are measured. These measurements feed the Clarke transformation module. The outputs of this projection are designated iα and i_β. These two components of the current are the inputs of the Park transformation that gives the current in the d,q rotating reference frame .The i_d and i_q components are compared to the references I^*_d (the flux reference) and I^*_q (the torque reference).

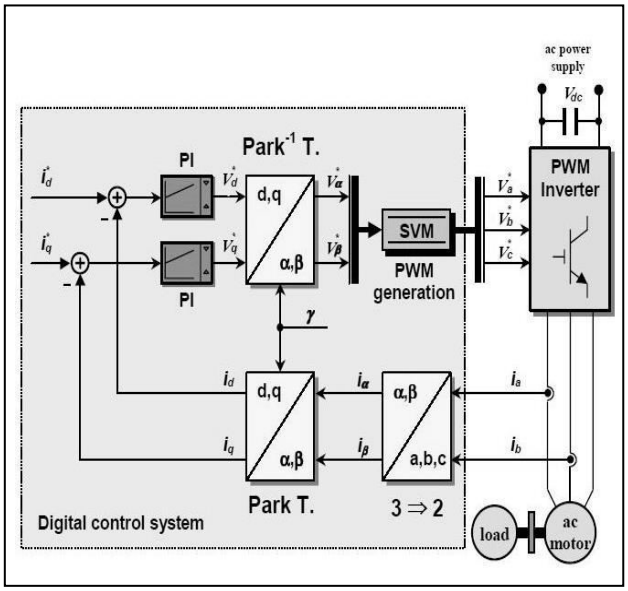

Figure 1. Block diagram of indirect field oriented control.

The outputs of the current regulators are V^*_d and V^*_q they are applied to the inverse Park transformation. The outputs of this projection are V^*_α and V^*_β which are the components of the stator vector voltage in the α, β stationary orthogonal reference frame. These are the inputs of the Space Vector PWM. The outputs of this block are the signals that drive the inverter. Note that both Park and inverse Park transformations need the rotor flux position.

C. Equations

$$\psi_r = \psi_{dr} \quad (1)$$

$$T = p\frac{M}{L_r}\psi_r i_{qs} \quad (2)$$

$$\psi_r = \frac{M}{1+T_r s} i_{ds} \quad (3)$$

$$\omega_r = \omega_s - \omega = \frac{M}{T_r}\frac{i_{qs}}{\psi_r} \quad (4)$$

$$V^*_{ds} = \sigma L_s \frac{di_{ds}}{dt} + R_s i_{ds} - \sigma L_s \omega_s i_{qs} + \frac{M}{L_r}\frac{d\psi_r}{dt} \quad (5)$$

$$V^*_{qs} = \sigma L_s \frac{di_{qs}}{dt} + R_s i_{qs} - \sigma L_s \omega_s i_{ds} + \frac{M}{L_r}\omega_s \psi_r \quad (6)$$

Where:

$$T_r = \frac{L_r}{R_r} \text{ And } \sigma = 1 - \frac{M^2}{L_r L_s}$$

III. DIRECT TORQUE CONTROL

A. Principle

The basic concept behind the DTC of AC drive, as its name implies, is to control the electromagnetic torque and flux linkage directly and independently by the use of six or eight voltage space vectors found in lookup tables. The possible eight voltage space vectors used in DTC are shown in fig.2.The basic idea of DTC for IM is to control the voltage space vectors properly, which is based on the relationship between the slip frequency and torque. The error between the estimated torque T and the reference torque T* is the input of a three level hysteresis comparator, whereas the error between the estimated stator flux magnitude ψs and the reference stator flux magnitude $\psi s*$ is the input of a two level hysteresis comparator.

The selection of the appropriate voltage vector is based on the switching table given in Table 1. The input quantities are the flux sector and the outputs of the two hysteresis comparators.

TABLE 1. VOLTAGE VECTOR SELECTION

Outputs of hysteresis comparators		Sector					
		1	2	3	4	5	6
$C_{\psi s}$ = -1	C_T =-1	$\bar{V}_2$	$\bar{V}_3$	$\bar{V}_4$	$\bar{V}_5$	$\bar{V}_6$	$\bar{V}_1$
	C_T =0	$\bar{V}_7$	$\bar{V}_0$	$\bar{V}_7$	$\bar{V}_0$	$\bar{V}_7$	$\bar{V}_0$
	C_T =+1	$\bar{V}_6$	$\bar{V}_1$	$\bar{V}_2$	$\bar{V}_3$	$\bar{V}_4$	$\bar{V}_5$
$C_{\psi s}$ = +1	C_T =-1	$\bar{V}_3$	$\bar{V}_4$	$\bar{V}_5$	$\bar{V}_6$	$\bar{V}_1$	$\bar{V}_2$
	C_T =0	$\bar{V}_0$	$\bar{V}_7$	$\bar{V}_0$	$\bar{V}_7$	$\bar{V}_0$	$\bar{V}_7$
	C_T =+1	$\bar{V}_5$	$\bar{V}_6$	$\bar{V}_1$	$\bar{V}_2$	$\bar{V}_3$	$\bar{V}_4$

Assuming the stator flux vector lying in sector 1 of the d-q plane, the voltage vectors used by DTC technique are shown in Fig.3.

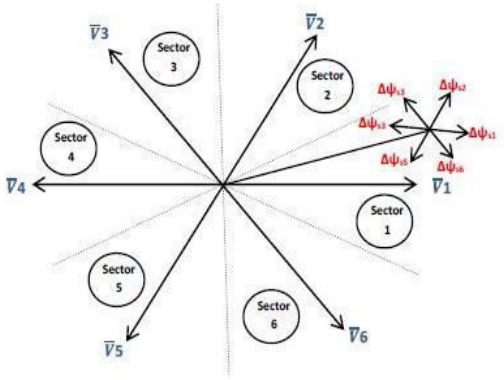

Figure 2. Voltage vectors utilized in basic scheme when stator flux is in sector 1

B. Block diagram

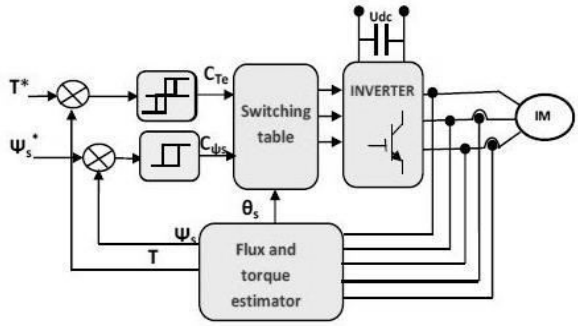

Figure 3. Block diagram of direct torque control

In most DTC control schemes, the torque is compared in a three-level hysteresis controller defining the error torque state C_{Te} in modulus and sign. The stator flux is compared to its reference value and is fed into a two-level hysteresis controller defining the error flux state $C_{\psi e}$. With this information, a voltage selector determines the stator voltage that is required to increase or decrease the variables (torque or flux) according to the demands. The affiliated look-up table and switching states are summarized in table 1. The used switching states are sector dependent and applied according to the error states C_{Te} and $C_{\psi e}$ given by the flux and torque comparators.

C. Equations

$$\psi_s = \sqrt{(\psi_{\alpha s})^2 + (\psi_{\beta s})^2}$$

$$\psi_{\alpha s} = \int_0^t (V_{\alpha s} - R_s i_{\alpha s})dt$$

$$\psi_{\beta s} = \int_0^t (V_{\beta s} - R_s i_{\beta s})dt$$

$$\theta_s = artg\left(\frac{\psi_{\beta s}}{\psi_{\alpha s}}\right) \quad (10)$$

$$T = p[\psi_{\alpha s} i_{\beta s} - \psi_{\beta s} i_{\alpha s}] \quad (11)$$

IV. SIMULATION

The simulation of the two control techniques are carried out using Simulink. The control system block diagrams shown in Fig 1 and Fig 3 and simulated for Induction Motor in the MATLAB/Simulink environment. The SimPowerSystem is used for this modelling work. The advantage of the SimPowerSystem is that it has extensive libraries for machines and power electronics circuits. The block properties are edited to suit the requirements of the load. The following parameters are used to model the induction motor.

Rotor resistance = 14.85e-3 Ω

Stator resistance = 9.295e-3 Ω

Input Voltage = 460 V

Frequency = 60 Hz

Inertia = 10 Kg m^2

Motor Rating = 200 HP

Stator self inductance = 0.3027 mH

Rotor self inductance = 0.3027 mH

Mutual inductance = 10.46 mH

Damping coefficient = 0.022 kg-m^2/s

Number of poles = 4

The Load is modeled to simulate a Fan load by using the following formula.

$$T_{mec} = K\omega_m^2 = K'N_m^2 \quad (12)$$

The Signal Selector sub-system is modeled to output the signals required to be compared. Also XY plot for the direct and quadrature axes flux is used to obtain the

plot for the rotating magnetic field. Mechanical input to the system is specified at the torque set point. It is observed that the output torque follows the input torque command applied at the set point.

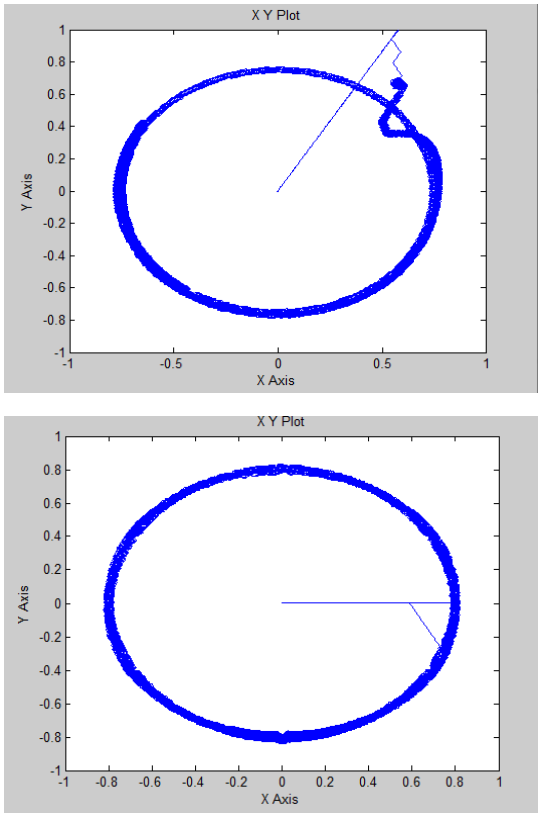

Figure 4. Comparison of XY plots of Flux of IFOC and DTC

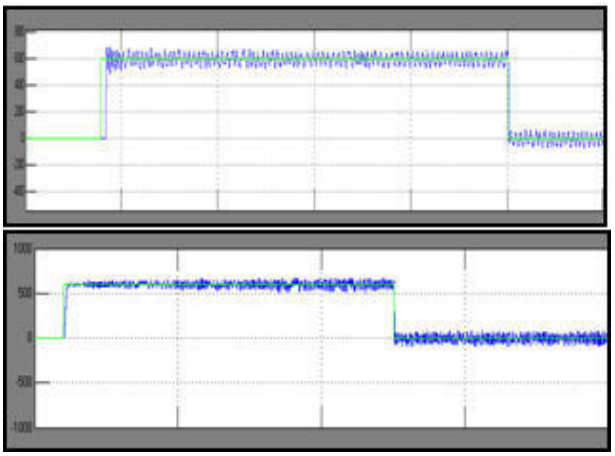

Figure 5. Comparison of Torque Ripples of IFOC and DTC Respectively

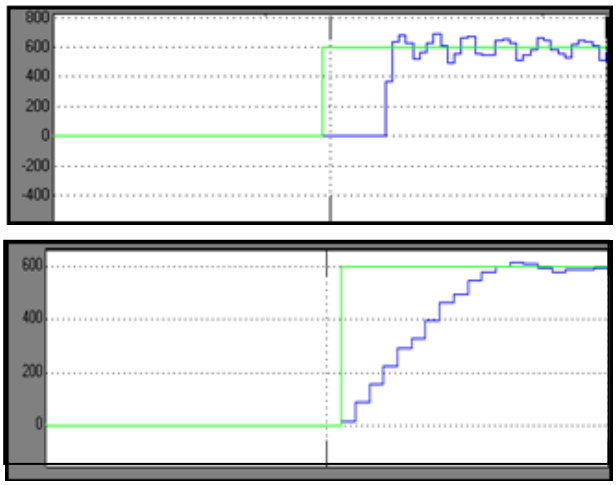

Figure 6. Comparison of Torque Response of IFOC and DTC Respectively

V. CONCLUSION

This paper has presented a comparison between two vector control methods for IM drives DTC and IFOC. The description of both control schemes and their principle of operation have been presented. The criterions for a fair comparison between DTC and IFOC have been established and the results of simulation tests have been presented to show the performance of both methods in various conditions. The simulation results are tabulated in table 2. Summarizing, it can be said that both methods provide a high performance response with quicker torque dynamics and less sensitivity to machine parameters in the case of DTC and better steady-state behaviour for IFOC. Depending on the requirements of a particular application one method can be more convenient than the other.

Parameter	IFOC	DTC
Dynamic response for torque	Slower	Quicker
Steady-state behaviour for torque, stator and currents	Low ripple and distortion	High ripple and distortion
Behaviour at Low Speed	good	Not good
Parameter sensitivity	Sensitive	Not big sensitive unsteady behaviour if stator resistance over-estimation

Requirement of rotor position	Yes	No
Current control	Yes	No
Coordinate transformation	Yes	No
Switching frequency	Constant	Variable, depending on the operating point and during transients
Audible noise	Low noise at a fixed frequency	Spread spectrum, high noise especially at low speed
Control tuning	PI gains	Hysteresis bands
Complexity and processing requirements	Higher	Lower

ACKNOWLEDGMENT

I take this opportunity to convey my gratitude to all those who have been kind enough to offer their advice and provide assistance when needed which has led to the successful completion of the Paper. I would like to express my immense gratitude to our principal Dr.Netaji S Ganesan and our head of the department Dr.Shanmukha Sundar and Internal Guide Mrs. Madhura Thilak for their constant support and motivation that has encouraged us to come up with this paper.

Finally we are also thankful to all the staff members of Electrical and Electronics Department, DSCE who have rendered their whole hearted support at all the time for successful completion of the seminar

REFERENCES

1. P.C.Krause, O.Wasynczuk,S.D .Sudhoff, "Analysis of electric machinery and drive systems" John Wiley & sons publication.
2. B.K.Bose,"Modern Power Electronics and AC drive" Prentice Hall publication, New Delhi.
3. Hamid Chaikhy ,Mohamed Khafallah, Abdallah Saad ," Evaluation of Two Control Strategies for Induction Machine" International Journal of Computer Applications (0975 – 8887) Volume 35– No.5, December 2011.
4. Domenico Casadei, Francesco Profumo, Giovanni Serra, Angelo Tani," FOC and DTC: Two Viable Schemes for Induction Motors Torque Control"IEEE TRANSACTIONS ON POWER ELECTRONICS, VOL. 17, NO. 5, SEPTEMBER 2002.
5. M.Depenbrock,"Direct Self Control(DSC) of Inverter Fed Induction Machine"IEEE Motors" IEEE Trans.,8 (1984-85) pp. 15-26.
6. M. S. Merzoug, and F. Naceri," Comparison of Field-Oriented Control and Direct Torque Control for Permanent Magnet Synchronous Motor (PMSM)" World Academy of Science, Engineering and Technology 45 2008.
7. F. Khoucha, K. Marouani, K. Aliouane, and A. Kheloui «Experimental performance analysis of adaptive flux and speed observers for direct torque control of sensorless induction motor drives », IEEE Trans. Power Electronics Germany, pp. 2678- 2683, 2004.
8. X. Xu, R. DeDoncker, and D. W. Novotny, "A stator flux oriented induction machine drive," in *Conf. Rec. PESC*, 1988, pp. 870–876

❑❑❑

Loss Allocation of Transmission line and Minimization of loss for 5 bus,14 bus &30 bus systems

[1]Sunil Kumar A.V., [2]Kumudeesh K.C, [3]Rekha C.M, [4]Dr.ShivasharanappaG.C

[1&2]Electrical & Electronics dept., ACIT, Bangalore, Karnataka
[3]Electrical & Electronics dept., IMPACT, Bangalore, Karnataka
Electrical & Electronics dept., DBIT, Bangalore, Karnataka
E-Mail : [1]avsgowda@gmail.com, [2]kumudeesh@acharya.ac.in
[3] cmrekhaiyer@gmail.com, [4]shivsharanapa@gmail.com

Abstract- The paper focuses on the issue of transmission loss allocation and transmission loss minimization by incorporating UPFC injection model using load flow analysis. To investigate the effect of the UPFC on the steady state condition of the system and load flow, different models can be used. These models are usually based on modification of traditional load flow methods. In this project, a mathematical model for UPFC referred as UPFC injection model is used. Since accurate power tracing is very difficult, allocation of losses for a particular transaction (in power business it is buying and selling system) may not be effectively realized. However loss allocation is an important aspect in determining the cost of transmission. Thus a methodology to find the losses accurately is vital. It is imperative to make sure that all users of the transmission network are charged proportionate to their usage and this aspect is all the more important because of the common infrastructure they use. The Z-bus loss allocation method is used to achieve the required objective. This method will promote more efficient network operations when implemented in deregulated electric industries. The Unified Power Flow Controller (UPFC) injection model is incorporated in Load Flow Model by the method of Newton Raphson Algorithm to study its effects for power flow control and losses minimization in the power system. In this project optimal placement of UPFC is conducted based on active power loss Sensitivity factors. Based on these sensitivity factors the UPFC is optimally placed in the required transmission line to investigate the impact of UPFC in the system. The changes in the system are studied to see the impact of the UPFC. The impact of UPFC are analyzed by using 5-Bus, IEEE 14-bus, and IEEE 30-bus Test systems. The analysis is achieved through developing of software program using MATLAB.

I. INTRODUCTION

1. UNIFIED POWER FLOW CONTROLLER (UPFC)

Fast progress of power electronics has made Flexible AC Transmission Systems (FACTS) as a promising concept. Researches on FACTS technologies are being performed very actively. Along with advanced control techniques on FACTS devices, power flow among transmission networks is more and more controllable. Among a variety of FACTS controllers, the Unified Power Controller(UPFC) is a new device in FACTS family, which has been introduced by Gyugiy(1991)[13]. It can be used in power systems for several purposes, such as shunt compensation, series compensation, phase shifting, power flow control and voltage control. With the adoption of UPFCs in power systems, the traditional power flow analysis will face new challenges in modeling and solution techniques.

The UPFC consists of two voltage source converters, which are connected back to back through a DC link. The series voltage converter is connected to the transmission line by means of a series transformer and the shunt voltage converter by means of shunt transformer. The series voltage converter injects an AC voltage into the transmission line with controllable magnitude and phase angle. The shunt converter can exchange active and reactive powers with the system, which enables the system to do shunt compensation independently. To investigate the effect of the UPFC on the steady state condition of the system and load flow, different models have been introduced. These models are usually based on modification of traditional load flow methods. The UPFC injection model is easily incorporated in Newton Raphson power flow model to study its effect for power flow control and losses minimization in the power system. The program is written using MATLAB software.

1.1 Basic circuit arrangement of UPFC:

Basically, the unified power flow controller (UPFC) consists of two switching converters. These converters are operated from a common DC link provided by a DC storage capacitor as shown in the Figure 2.

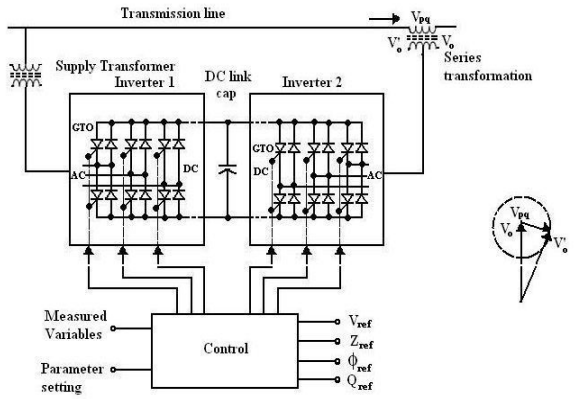

Fig.2. Basic circuit arrangement of UPFC

Converter 2 provides the main function of the UPFC by injecting an AC voltage with controllable magnitude and phase angle in series with the transmission line via a series transformer. The basic function of converter 1 is to supply or absorb the real power demand by converter 2 at the common DC link. It can also generate or absorb controllable reactive power and provide independent shunt reactive compensation for the line. Converter 2 supplies or absorbs locally the required reactive power and exchanges the active power as a result of the series injection voltage.

1.2 UPFC MODEL:

The schematic representation of the UPFC is shown in Fig.3. It consists of two voltage source converters and a dc circuit represented by the capacitor. Converter 1 is primarily used to provide the real power demand of converter 2 at the common dc link terminal from the ac power system. Converter 1 can also generate or absorb reactive power at its ac terminal, which is independent of the active power transfer to (or from) the dc terminal. Therefore, with proper control, it can also fulfil the function of an independent advanced static VAR compensator providing reactive power compensation for the transmission line and thus executing indirect voltage regulation at the input terminal of the Converter 2 is used to generate a voltage source at the fundamental frequency with variable amplitude $(0 \le V_T \le V_{TMAX})$ and phase angle $(0 \le \phi_T \le 2\pi)$, which is added to the ac transmission line by the series-connected boosting transformer.

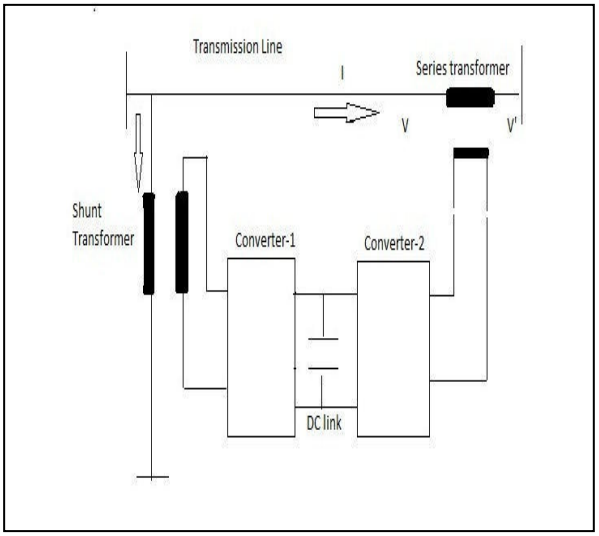

Fig.3. Schematic diagram of UPFC.

The inverter output voltage injected in series with line can be used for direct voltage control, series compensation, phase shifter, and their combinations. This voltage source can internally generate or absorb all the reactive power required by the different type of controls applied and transfers active power at its dc terminal.

1.3 UPFC injection model for power flow studies.

In this study, a model for UPFC, which will be referred as UPFC injection model [1] is derived. This model is helpful in understanding the impact of the UPFC on the power system in the steady state. Furthermore, the UPFC injection model can easily be incorporated in the steady state power flow model. Since the series voltage source converter does the main function of the UPFC, first derive the modelling of a series voltage source converter.

Series connected voltage source converter model:

Suppose a series connected voltage source is located between nodes i and j in a power system. The series voltage source converter can be modeled with an ideal series voltage Vs in series with a reactance Xs as shown in fig below,

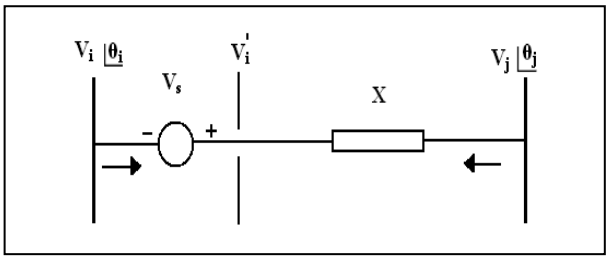

Fig.4. Representation of a series connected VSC

$$V_i^1 = V_s + V_i \quad \textbf{(1)}$$

where V_i^1 = fictitious voltage behind the series reactance.

V_s = series source voltage.

V_i = voltage at i'th node.

The series voltage source V_s is controllable in magnitude and phase, i.e,

$$V_s = rV_i e^{i\gamma} \quad \textbf{(2)}$$

where r = series voltage source co-efficient. $(0 < r < r_{\max})$

γ = series voltage source angle. $(0 < \gamma < 2\pi)$

The injection model is obtained by replacing the equivalent circuit of series connected voltage source as Norton's equivalent circuit as shown in fig.5 .The current source,

$$I_s = -jb_s V_s \quad \textbf{(3)}$$

where $b_s = 1/X_s$

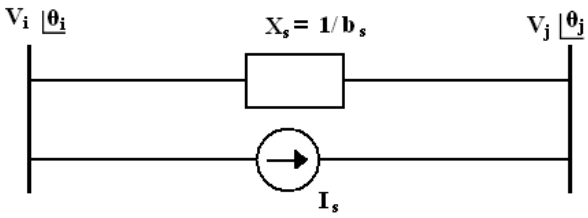

Fig.5. Equivalent Norton's circuit of a series connected VSC.

The power injected into the i[th] bus

$$\overline{S_{is}} = \overline{V_i}(-\overline{I_s})^*$$

$$S_{is} = V_i[jb_s r\overline{V_i}e^{j\gamma}]^*$$

$$S_{is} = -b_s r V_i^2 \sin(\gamma) - jb_s r V_i^2 \cos(\gamma)$$

(4)

The power injected into the j[th] bus

$$\overline{S_{js}} = \overline{V_j}(-\overline{I_s})^*$$

$$S_{js} = V_j[-jb_s r\overline{V_i}e^{j\gamma}]^*$$

$$S_{js} = b_s r V_i\, V_j \sin(\theta_{ij} + \gamma) + jb_s r V_i\, V_j \cos(\theta_{ij} + \gamma)$$

(5)

Where $\theta_{ij} = \theta_i - \theta_j$

From above equations, the injection model of series connected voltage source can be sent as two dependent loads as shown in fig.6.

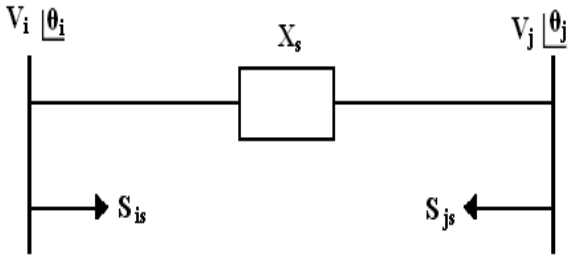

Fig.6 .Injection model for a series connected VSC.

Shunt connected voltage source converter model:

In UPFC, the shunt connected voltage source (converter1) is used mainly to provide the active power, which is injected to the network via the series connected voltage source. When the losses are neglected

$$P_{conv1} = P_{conv2}$$

The apparent power supplied by the series voltage source converter is

$$S_{conv2} = \overline{V_s}\,\overline{I_{ij}}^* = re^{j\gamma}\overline{V_i}[\frac{\overline{V_{i1}} - \overline{V_j}}{jX_s}]^*$$

(6)

After simplification, the active and reactive power supplied by converter 2 is

$$P_{conv2} = rb_s V_i V_j \sin(\theta_i - \theta_j + \gamma) - rb_s V_i^2 \sin(\gamma)$$

$$Q_{conv2} = -rb_s V_i V_j \cos(\theta_i - \theta_j + \gamma) + rb_s V_i^2 \cos(\gamma) + r^2 b_s V_i^2$$

(7)

The reactive power delivered or absorbed by converter 1 is independently controllable by UPFC and can be modelled as a separate controllable shunt reactive source. In view of above, it is assumed that $Q_{conv1} = 0$. The UPFC injection model is constructed from the series connected voltage source model with the addition of a power equivalent to $P_{conv1} + j0$ to node i.

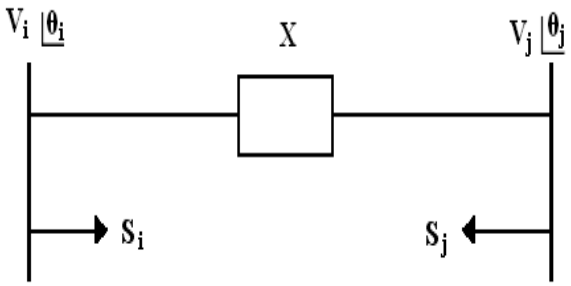

Fig.7 . Complete UPFC model.

Thus, the complete UPFC injection model is shown in fig.7.

$$Q_{si} = rb_s V_i^2 \cos(\gamma) + Q_{shunt}$$

$$Q_{sj} = -rb_s V_i V_j \cos(\theta_{ij} + \gamma)$$

$$P_{si} = rb_s V_i V_j \sin(\theta_{ij} + \gamma)$$

$$P_{sj} = -rb_s V_i V_j \sin(\theta_{ij} + \gamma)$$

(8)

1.4 Modification of Jacobian matrix:

The UPFC injection model can easily be incorporated in a load flow program. If a UPFC is located between node i and node j in a power system, the Jacobian matrix is modified by addition of appropriate injection powers. The linearized load flow model is

$$\begin{bmatrix} \Delta P \\ \Delta Q \end{bmatrix} = \begin{bmatrix} H.....N \\ J.....L \end{bmatrix} \begin{bmatrix} \Delta\theta \\ \Delta V / V \end{bmatrix}$$

(9)

The Jacobian matrix which is modified is given below, the superscript '0' denotes the Jacobian elements without UPFC.

2. METHODOLOGY

The main objective of the project is to study the effects of Unified Power Flow Controller on loss minimization and loss allocations. To achieve the main objective of the project the UPFC injection model is incorporated in the Newton Raphson algorithm. Thus, in this chapter a detail explanation about UPFC incorporation in load flow is shown. Optimal placement of the UPFC is achieved from active power loss sensitivity factors with respect to the UPFC control parameters. A brief explanation is also given about sensitivity analysis. From the solved load flow model, losses are obtained and these losses are allocated at each bus by the Z-Bus loss allocation method, which is also explained in detail further.

2.1 Incorporation of UPFC in Newton Raphson Power Flow Algorithm:

2.1.1 Newton Raphson Power Flow Algorithm:

From the mathematical modelling point of view, the set of nonlinear, algebraic equations that describe the electrical power network under the steady state conditions are solved for the power flow solutions. Over the years, several approaches have been put forward to solve for the power flow equations. Early approaches were based on the loop equations and methods using Gauss-type solutions. This method was laborious because the network loops has to be specified by hand by the systems engineer. The drawback of these algorithms is that they exhibit poor convergence characteristics when applied to the solution of the networks. To overcome such limitations, the Newton-Raphson method and derived formulations were developed in the early 1970s and since then it became firmly established throughout the power system industry. In the project a Newton Raphson power flow algorithm [2] is used to solve for the power flow problem in a transmission line with UPFC [1]

- **Steps to Incorporate UPFC in Newton-Raphson Algorithm:**

  - Step 1: Read the system input data; line data, bus data, generator and load data.
  - Step 2: Formation of admittance matrix 'Y' bus of the transmission line between the bus i and j.

Step 3: Combining the UPFC power equations with network equation, the conventional power flow equation is given as:

$$P_i + jQ_i = \sum_{j=1}^{n} V_i V_j Y_{ij} \angle(\theta_{ij} - \delta_i + \delta_j) + P_i^1 + jQ_i^1$$

- Step 4: The conventional jacobian matrix are formed due to the inclusion of UPFC. The inclusion of these variables increases the dimensions of the jacobian matrix.
- Step 5: In this step, the jacobian matrix is modified and power equations are mismatched.
- Step 6: The Bus bar voltages are updated at each iteration and convergence is checked. If convergence is not achieved in the next step the algorithm goes back to the step 5 and the jacobian matrix is modified and the power equations are mismatched until convergence is attained.
- Step 7: If the convergence achieved in Step 6, the output load flow is calculated for PQ bus that includes the Bus bar voltages, generation, transmission line flow and losses.

Sensitivity analysis of total active power loss

- A method based on the sensitivity of the total system active power loss with respect to the control variables of the FACTS device i.e, UPFC is considered.
- For UPFC placed between buses i and bus j, the considered control parameter is the injected series voltage, of controllable magnitude and its phase angle. The active power loss sensitivity factor with respect to these control variables may be given as, loss sensitivity with respect to control parameter of UPFC placed between buses i and bus j.

$$a_{ij} = \frac{\partial P_L}{\partial V_{ij}}$$

- And this can be deduced from the above equation as,

$$\frac{\partial P_L}{\partial V_{ij}} = 2V_i V_j \cos(\delta_i - \delta_j) + 2V_i V_j \sin(\delta_i - \delta_j)$$

- Thus from the above equation the sensitivity factors with respect to active power loss are obtained.

Z-Bus loss allocation method:

- The goal of the Z-bus loss allocation method, is to take a solved power flow and systematically distribute the system transmission losses, among the network buses according to,

$$P_{loss} = \sum_{k=1}^{n} L_k$$

- The loss component, L_k is the fraction of the system losses allocated to the net real power injection at bus K.
- This is assigned to each individual bus- K, the responsibility of paying for L_k at the market marginal price, λ the extra cost due to loss allocation must then be subtracted from the revenue of the generators and added to the load payments so that the pool remains revenue-neutral.

Z-BUS LOSS ALLOCATION ALGORITHM:

Step 1: Solve load flow; get bus voltage vector V and total power loss.

Step 2: Obtain bus current vector I from V and complex power injection.

$$S = (P_i + jQ_i)$$

Step 3: Obtain the vector RI.

$$RI = Re\{Z\} I.$$

$$RI = Re\{Z [Re (I)]\} + Re\{Z [Im (I)]\}.$$

Step 4: Calculate the component of total loss due to current injection I_k at the j^{th} bus.

$$L_k = \Re\left[I_k^* \left(\sum_{j=1}^{nb} R_{kj} . I_j \right) \right]$$

Step 5: Compute L_k for all buses. L_k is the loss allocated to bus K calculated using the Z-Bus loss allocation method.

Simulation results:

[5-Bus system]:

- The simulation study is done initially for without UPFC device in the 5-Bus test system.

Voltage profile without UPFC.

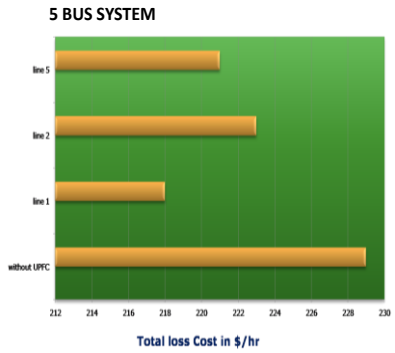

14 BUS SYSTEM

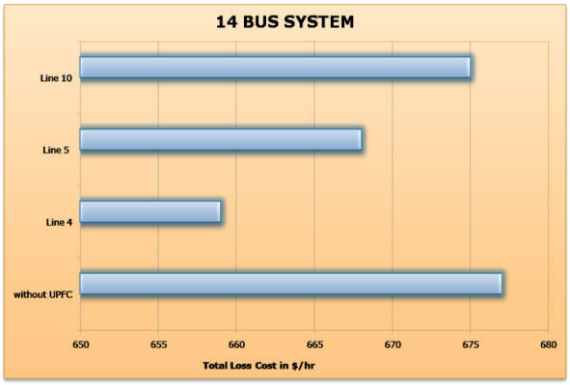

30 BUS SYSTEM

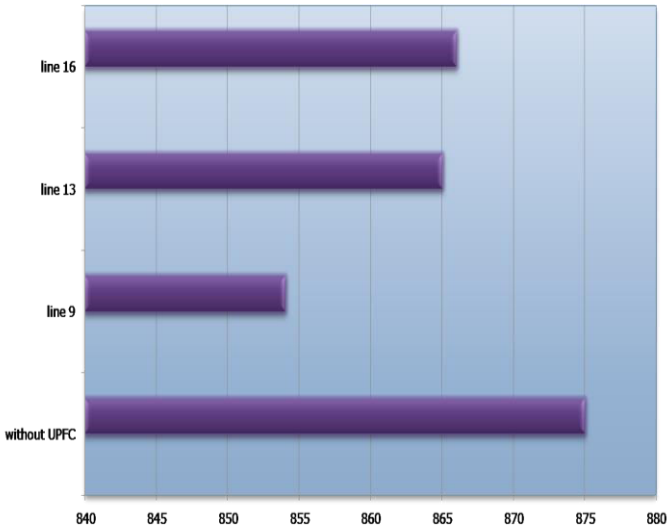

CONCLUSION:

FACTS devices are conventionally used in the power system for voltage profile improvement, helps real and reactive power flow, enhanced transmission capability. Unified power flow controller is used in this project. In this project, steady state UPFC injection model is incorporated in the load flow model. UPFC is optimally placed using active power loss sensitivity factors which were calculated after performing the load flow analysis. UPFC's role in loss minimization and its influence for loss allocation is verified. Z-Bus loss allocation methodology is used in the project for loss allocation. The impact of UPFC device is tested for 5-bus system, IEEE 14 bus system and IEEE 30 bus system. The results with and without UPFC for the test systems are tabulated and compared. It is found that generally the system loss would decrease after incorporating UPFC. Thus the loss allocation to each participant would be comparatively lower. MATLAB program was used to cross verify the theoretical results.

SCOPE FOR FUTURE WORK

In the project, UPFC's effectiveness for loss minimization is verified. Similarly other FACTS device's role in loss minimization can be checked. In the current project, standard test systems were used. UPFC working in practical systems can be further be evaluated. The loss allocation results using Z-Bus loss allocation can be compared with allocation using alternate methods such as incremental transmission loss allocation, pro-rata and proportional sharing methodologies. A dynamic model of UPFC can be realized for usage in the Optimal Power Flow.

REFERENCES:

[1] Loss minimization by incorporation of UPFC in load flow studies, s.v. ravi kumar and s. Siva nagaraju. International journal of electrical and power engineering 1(3):321-327.

[2] Power Flow Control with UPFC in Power Transmission System, Samina Elyas Mubeen, R. K. Nema, and Gayatri Agnihotri, World Academy of Science, Engineering and Technology 47 2008.

[3] Load Flow Management in the Interconnected Power Systems Using UPFC Devices C. Bulac Member IEEE, M. Eremia Senior Member IEEE, R. Balaurescu, and V. Ştefănescu.

[4] Steady State Analysis of Unified Power Flow Controller: Mathematical Modeling and Simulation Studies A.M. Vural, Student Member, IEEE, and M. Tumay.

[5] Analysis and Modeling of UNIFIED POWER FLOW CONTROLLER: Modification of NEWTON-RAPHSON Algorithm and user-defined modeling approach for POWER FLOW STUDIES, M. Tumay and A. M. Vural, October

2004 The Arabian Journal for Science and Engineering, Volume 29, Number 2B.

[6] A Novel Method of UPFC Location Based on Sensitivity Factors, Anshul Chaudhary, Manish Jain, P.S.Venkataramu, T.Ananthapadmanabha. Proceedings of the 7th WSEAS International Conference on Power Systems, Beijing, China, September 15-17, 2007.

[7] The modeling of UPFC based on circuit elements in an exact transmission line model, Ali akbar Motiebirjandi Faculty of Electrical Engineering / assistant professor, Kauomars Sabzawari Faculty of Electrical Engineering / M.Sc ,Shahid Rajaee University/ Tehran, 67616, Iran.

[8] Study and Effects of UPFC and its Control System for Power Flow Control and Voltage Injection in a Power System, Vibhor Gupta / International Journal of Engineering Science and Technology Vol. 2(7), 2010, 2558-2566.

[9] Control Setting of UNIFIED POWER FLOW CONTROLLER through Load Flow Calculation. C.H Chengaiah, G. V. Marutheswar and R. V. S. Satyanarayana, ARPN Journal of Engineering and Applied Sciences.

[10] "Estimation of UPFC value using Sensitivity Analysis" by Seungwon An,Thomas W. Gedra.

[11] "A unified power flow controller concept for flexible AC transmission systems," in Proc. 5th Int. Conf. AC DC Transmission, London, U.K., Sep. 17–20, 1991, pp. 19–26.

[12] N. G. Hingorani, "Flexible AC transmission," IEEE Spectr., vol. 30, no. 4, pp. 40–45, Apr. 1993.

[13] L.Gyugyi, "A unified power flow control concept for flexible AC transmission systems," Proc. Inst. Elect. Eng., pt. C, vol. 39, no. 4, pp. 323–331, Jul. 1992.

[14] Clodomiro Unsihay and Osvaldo R.Saavedra,"Transmission Loss Unbundling and Allocation Under Pool Electricity Markets"IEEE Trans Power Syst,vol 21,o1,feb 2006.

[15] A.J Conejo et al,"Z Bus Loss Allocation," IEEE Trans. Power Syst., vol 16 no.1,pp.105-110, feb,2001.

[16] F.D Galiana et al,"Incremental Transmission loss allocation under pool dispatch,"IEEE Trans Power Syst,vol 17.no1,pp 26-33,feb 2002.

[17] A.M Leite da silva and J.G.C Costa,"Transmission loss allocation:part 1-single energy market"IEEE Trans Syst.,vol 18,no4,pp 1389-1394,Nov 2003.

[18] J-H Teng,"Power flow and loss allocation for deregulated transmission systems,"Int.J.Elect .Power Energy Syst.,vol 27,no 4,327-333,may 2005.

[19] Optimal location of unified power flow controller (UPFC) in Nigerian Grid System, Mark Ndubuka Nwohu, International journal of electrical and Power Engineering, medwell journals,2010.

◈◈◈

Effect of Static Var Compensator on Voltage Stability under Network Contingencies

K. Shanmuka Sundar, Manjunatha Babu P & Prakash D.B

Department of Electrical & Electronics Engineering
Dayananda Sagar College of Engineering, Bengaluru

Abstract - This paper focuses on enhancement of system performance under network contingencies through an optimal placement and optimal setting of static var compensator (SVC). The goal of the methodology developed is to identify the weakest bus using an index called Line Flow Index (LFI) and to maintain the voltages at all load buses within their specified limits through an optimal placement and optimal setting of SVC under contingency Condition. This premise is attested on 6-bus and 30 bus systems and the simulation results are presented to show the effectiveness of the method.

Keywords—*Line Flow Index (LFI), Flexible AC Transmission Systems (FACTS), static var compensator (SVC).*

I. INTRODUCTION

In the present day scenario private power producers are increasing rapidly to meet the increase in demand due to heavily loaded customers. Consequently the transmission system becomes more stressed, which in turn makes the system more vulnerable to stability and security problems [1-4]. In this above process, the voltages at load buses may violate their limits and lead to voltage collapse. So based on the above, maintaining voltages at all load busses within the specified limits and maintaining voltage stability, through proper reactive power allocation is a critical problem in power system operation. Identification of the weakest bus in a transmission system that is prone to voltage collapse is of grate important in voltage stability studies [2].There are several indices / methods proposed in literature for placement of FACTS devices from voltage stability / small signal stability view points [2]-[5]. Among the FACTS controllers, SVC provides fast acting dynamic reactive compensation for voltage support. The main objective of installing SVC's in electrical power system is to provide rapid and smooth control of voltages at weak load buses in electric power systems. The application of SVC is to keep the bus voltage within the permissible values under varying load conditions, and improve the voltage stability. The location of SVC's are considered for improving the voltage profile and improving the overall power system stability [7-10].In order to maintain the steady state voltage stability, the transmission system operators have to take special measures to identify the critical lines and buses of power system network [1-2]. In this paper the voltage stability enhancement is achieved by placing SVC at appropriate location with optimal setting. Further, all line and voltage limits are respected during the assessment of voltage stability. The optimal location of SVC is identified by using line flow indices (LFI) [1]. The power flow studies are carried out using matpower package [6]. The LFI values and the optimal setting of SVC are obtained through a programming code written in MATLAB. The method proposed in the study has been carried out on 6-bus systems and the simulation results are presented.

The contingency analyses are based on a model of the power system and are used to study outages and notify the operators of any potential overloads or out-of-limit voltage. Contingencies such as unexpected line outages often contribute to voltage collapse blackouts. These contingencies generally reduce or even eliminate the voltage stability margin [11-12]. Contingency analysis techniques are used to predict the effect of outages. The analysis procedures model single failure events (i.e., one-line outage) one after another in sequence until "all credible outages" have been studied. However, here in this paper we analyzed the LFI of a power system and in the process rank branch contingencies only for single failure events.

Many power systems are now experiencing voltage problems more frequently and voltage studies have gained increasing attention from operating and planning point of views [13]. To know the impact of every contingency – single failure-on the voltage profile, it is desirable to study the impact of contingency on the line outages. By ranking the contingencies, we are able to substantially reduce the number of contingencies out of all possible contingencies that need to be considered for voltage stability analysis. A contingency is the loss or failure of a small part of the power system (e.g. a

transmission line), or the loss/failure of individual equipment.

This paper provides initially finding the critical line outage for each line and latter ranking the most critical line outage. In this study, the critical buses under contingency condition are identified by using an index called line flow indices (LFI) from the voltage stability view point.

The method which is introduced in this paper identifies the critical segments further from which we rank the critical bus and SVC is installed at critical bus to enhance the voltage stability of a power system network. The singular value decomposition (SVD) method is used to check whether the system stability is maintained or not.

The study in this paper focuses on enhancement of steady state voltage stability of a power system through an optimal utilization of static var compensator (SVC). The method proposed consists of identifying the weakest bus of the system by using an index called Line Flow Indices (LFI) and next placing SVC at appropriate location, the voltage stability enhancement is achieved with all limits respected under steady state condition. Further, the steady state voltage stability under three cases is assessed through the computation of the Minimum Singular Value (MSV). In case-1, the MSV is computed without SVC. In case-2, the voltage magnitude at SVC installed bus is maintained at 1 p.u and in case-3, the voltage magnitude at SVC installed bus is maintained at maximum voltage. The power flow studies are carried out using matpower package [8]. The MSV, optimal location and optimal setting of SVC is obtained through a programming code written in MATLAB. The method proposed in this paper is carried out on 6-bus, and 30-bus system and the simulation results are presented to authenticate the proposed method.

II. SVC MODEL

An SVC is a shunt connected static var generator or absorber whose output is adjusted to exchange capacitive or inductive reactive current so as to maintain or control specific parameters of the power system i.e. typically bus voltages. The static var compensator is a parallel combination of capacitor and inductor; the latter is under phase angle control called as Thyristor Controlled Reactor (TCR). That is, the form of SVC selected in this paper is fixed capacitor (FC) with TCR, shown in Fig. 1. This combination provides a fast variable source of reactive power.

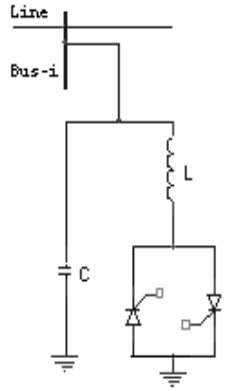

The model of SVC in this paper interprets the FACTS as a shunt element with varying susceptance B [11]. The active and reactive power value of an SVC from the injected power equations [11] is:

$$P_i = 0 \quad (1)$$

$$Q_i = V_i^2 B_t \quad (2)$$

where Pi and Q_i are injected real and reactive power to a bus respectively.

V_i is the voltage at bus-i, at which an SVC is shunted

The total susceptance with SVC shunted at bus-i is:

$$B_t = B_i + B_{svc} \quad (3)$$

The net reactive power generated by SVC is

$$Q_{svc} = Q_C - Q_L \quad (4)$$

In case, the bus voltage that falls below the specified lower limits, the SVC will supply reactive power by working as a capacitor. On the other hand if the bus voltage exceeds the specified upper limits, then the SVC will absorb reactive power by working as an inductor. The rating of SVC at bus-i is obtained by using (2).

III. PROBLEM FORMULATION

The LFI values are computed for all line segments connected between the node-i and node i+1. The LFI method identifies the critical line segments and from this the critical buses are identified under contingency condition. The line segment having the highest positive index value is the critical line segment from the voltage stability point of view. The four line flow indices [2] which are called as line stability factors and are given by:

$$LFISP = 4\frac{r_i}{V_i^2}\left(\frac{P_r + r_i Q_i^2}{V_i^2}\right) \quad (5)$$

$$LFISQ = 4\frac{X_i}{V_i^2}\left(\frac{Q_r + X_i P_i^2}{V_i^2}\right) \quad (6)$$

$$LFIRP = 4\frac{r_i}{V_{i+1}^2}\left(\frac{-P_i + r_i Q_r^2}{V_{i+1}^2}\right) \quad (7)$$

$$LFIRQ = 4\frac{X_i}{V_{i+1}^2}\left(\frac{-Q_i + X_i P_r^2}{V_{i+1}^2}\right) \quad (8)$$

The above four LFI's are calculated for all the lines in the system and the lines with highest index is considered as critical line and the receiving end bus of the critical line is identified as the weakest bus from the voltage stability point of view.

Specification of Test System:

The effectiveness of the method is carried out on 6-bus system and 9 Bus system. The six-bus system has got eleven transmission lines and nine-bus system has got nine transmission lines with a capacity of 230 kV. The 6-bus test system, which is considered for the purpose of case study, is shown in Fig-2. In the first step the candidate buses for allocation of SVC are to be found assuming that they all have the same installation cost coefficients. The overload limit of the transmission lines is due to thermal considerations. The buses with largest value of LFI's index are considered as the critical buses for allocation of SVC at bus i. The power flow solutions in each case are computed by *matpower* software package [6]. Optimal location and optimal setting of SVC were computed using software code written in *MATLAB.* Simulation studies using MATLAB programming code, on a 6-bus network are presented to illustrate the methodology and to demonstrate the benefits of the proposed method.

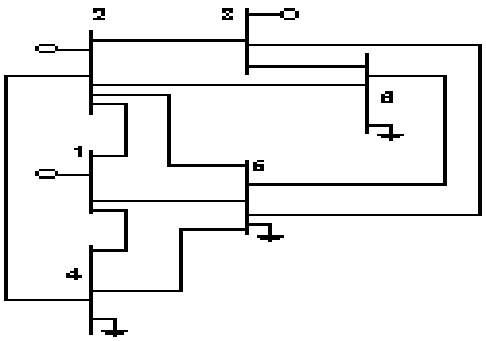

Fig .2. Six-bus test system.

A. Case Study and Results

This paper presents a methodology for ranking transmission line outages according to severity of their efforts on line flows. The contingencies ranking accomplished by ordering these normalized sensitivities from greatest to the least. As such, the method does not explicitly indicate whether a contingency is going to give bus voltage or circuit over load problem. The identified critical segments/buses have to be taken care first by the Transmission System Operator (TSO) in order to avoid voltage collapse /system blackout. In the study, the critical segments and/or buses under contingency conditions are identified by using an index called Line Flow Index (LFI). The LFI identifies the critical segments / buses with computation of the jacobian matrix. The various LFI values for all test systems are estimated using equations (5) to (8) for all possible contingencies.

(i) Branch outage for 6 bus system

The LFI indices calculated for branch outages are listed in Table 1. In this illustrated example, it is evident that the line outage 2-4 has the highest (LFIRQ) index value and therefore the line segment is 5-6 which is critical line segment (rank-1) and the receiving end bus-5 is most critical from voltage stability viewpoint. The ranking column has been formed by considering only load buses and therefore bus 5 is ranked as 1 since it is not a generator bus. The next most critical segment is 3-5 (rank 2) and the associated index is LFIRQ, hence bus-5 is critical bus and so on.

Table: 1

Ranking of critical contingencies for 6-Bus system

Line Outage	Index	Value	Line segment	Bus No	Rank
1-2	LFIRQ	0.1268	5 – 6	5	6
1-4	LFIRQ	0.1407	5 – 6	5	5
1-5	LFIRQ	0.1687	5 - 6	5	4
2-3	LFIRQ	0.1158	5 - 6	5	8
2-4	LFIRQ	0.2697	5 - 6	5	1
2-5	LFIRQ	0.1692	5 - 6	5	3
2-6	LFIRQ	0.0984	5 - 6	5	9
3-5	LFIRQ	0.1847	5 - 6	5	2
3-6	LFIRQ	0.0697	2 - 3	2	---
4-5	LFIRQ	0.1232	5 - 6	5	7
5-6	LFIRQ	0.0565	4 – 5	4	10

From the table 1 it is clear that bus-5 should be taken care first to avoid voltage collapse. The voltage stability assessment is carried out by installing the first available SVC at bus-5 (rank 1). The three different cases are studied and the results are presented. In case-1, the MSV is computed without SVC, case-2 refers to the voltage magnitude at SVC installed bus is maintained at 1 p.u and case-3 refers to the voltage magnitude at SVC installed bus is maintained at maximum voltage. The

MSV and the optimal setting of SVC for all the cases are tabulated in Table 2.

Table:2
MSV of 6-bus system for 2-4 line outage

	Case-1	Case-2	Case-3
Voltage (p.u)	0.970	1.001	1.038
MSV	1.8116	1.8452	1.8847
Optimal setting of SVC (Mvar)	----	42	90

It is clear that for 2-4 line outage the minimum singular value (MSV) is improved from 1.8116 (case 1) to 1.8452 (case2). Further MSV value is improved from 1.8116 (case 1) to 1.8847 (case3) i.e the MSV of the load flow jacobian is maximized with the increase in the injected Mvar due to SVC, which indicates that the steady state voltage stability is improved. This voltage stability enhancement is achieved by installing SVC at bus-5 with an optimal setting of 42 Mvar (case 2) and 90 Mvar (case 3). Furthermore placing SVC at bus-5 with an optimal setting not only improves the voltage at the weakest bus, but also improves the voltage profile of the remaining buses. Furthermore placing SVC at bus-5 with an optimal setting not only improves the voltage at the weakest bus, but also improves the voltage profile of the remaining buses as shown in table 3.

Table:3
Voltage Profile for 6-bus system

Line Outage	Case-1	Case-2	Case-3
3-5	0.954	0.999	1.049
2-5	0.963	1.000	1.049
1-5	0.959	1.000	1.049
2-4	0.970	1.001	1.049
1-4	0.980	1.000	1.049
1-2	0.986	1.000	1.049
4-5	0.982	1.001	1.049
2-3	0.985	1.000	1.050
2-6	0.981	1.001	1.050
5-6	0.988	1.000	1.050

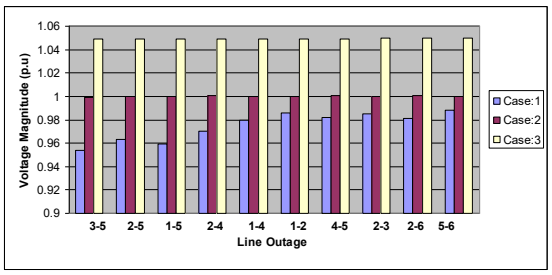

Fig. 3 Voltage profile for 6-bus system

(ii) Branch outage for 30 bus system

The LFI indices calculated for branch outages are listed in Table 4. In this illustrated example, it is evident that the line outage 1-3 has the highest (LFIRQ) index value and therefore the line segment is 2-6 which is critical line segment (rank-1) and the receiving end end bus-6 is most critical from voltage stability viewpoint. The ranking column has been formed by considering only load buses and therefore bus 6 is ranked as 1 since it is not a generator bus. The next most critical segment is 2-6 (rank 2) and the associated index is LFIRQ, hence bus-6 is critical bus and so on.

Table: 4
Ranking of critical contingencies for 30-Bus system

Line Outage	Index	Value	Line segment	Bus No	Rank
1-3	LFISQ	0.167062	2-6	6	3
3-4	LFISQ	0.163269	2-6	6	4
2-5	LFISQ	0.217842	2-6	6	1
4-6	LFISQ	0.207600	2-6	6	2
6-9	LFISQ	0.145992	6-10	10	6
9-10	LFISQ	0.102072	6-9	9	7
4-12	LFISQ	0.159249	6-10	10	5

From the table 4 it is clear that bus-6 should be taken care first to avoid voltage collapse. The voltage stability assessment is carried out by installing the first available SVC at bus-6 (rank 1). The three different cases are studied and the results are presented. In case-1, the MSV is computed without SVC, case-2 refers to the voltage magnitude at SVC installed bus is maintained at 1 p.u and case-3 refers to the voltage magnitude at SVC installed bus is maintained at maximum voltage. The MSV and the optimal setting of SVC for all the cases are tabulated in Table 5.

Table:5
MSV of IEEE 30-bus system for 2-5 line outage

	Case-1	Case-2	Case-3
Voltage (p.u)	1.005	1.001	1.024
MSV	0.2117	0.2106	0.2146
Optimal Setting of SVC(Mvar)	----	-21	90

From the table 5, it is clear that the minimum singular value (MSV) has reduced from 0.2117 (case 1) to 0.2106 (case2), as voltage is already beyond its maximum limits. Further MSV value is improved from

0.2117 (case1) to 0.2146 (case3), which indicates that the steady state voltage stability is improved. This voltage stability enhancement is achieved by installing SVC at bus-6 with an optimal setting of -21 Mvar (case 2) and 90 Mvar (case 3). Here the negative sign indicates that there is absorption of the reactive power. Furthermore placing SVC at bus-6 with an optimal setting not only improves the voltage at the weakest bus, but also improves the voltage profile of the remaining buses as shown in table 6.

Table 6
Voltage profile for IEEE 30 bus system

Line Outage	Case-1	Case-2	Case-3
2-5	1.005	1.001	1.024
4-6	1.009	1.001	1.031
1-3	1.006	1.001	1.025
3-4	1.006	1.001	1.025
4-12	1.045	1.000	1.055
6-9	1.044	1.000	1.06
9-10	1.049	1.001	1.06

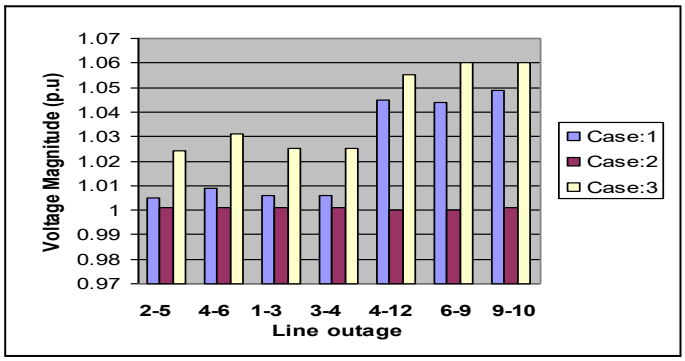

Fig .4 Voltage profile for IEEE 30-bus system

IV. CONCLUSION

In this paper a methodology is demonstrated to improve the voltage stability of a power system network using LFI. Simulation studies using MATLAB programming code, on 6-bus & IEEE 30 bus system are presented to illustrate the methodology and to demonstrate the benefits of the proposed method. From the above result and discussion, placing SVC at appropriate location with an optimal setting can improve the system performance and system stability under contingency condition.

REFERENCES:

[1] Nikhlesh Kumar Sharma, Arindam Ghosh, "A Novel placement Strategy for FACTS Controllers" IEEE Trans, on power delivery, Vol 18, No, 3, July 2003.

[2] A. Mohamed and G.B.Jasmon , "determining the weak segment of power system with voltage stability considerations ., Elect. Mach. Power Syst., vol 24 .pp 555-568, 1996.

[3] "Voltage Stability Improvement using SVC in Power System" Department of Electrical/computer science, federal University of Technology, Minna, Niger State, nigeria

[4] Hingorani N.G "Flexible AC Transmission Systems", IEEE spectrum, vol.30, No.4, pp. 40-45, April 1993.

[5] Hingorani N.G., Gyugyi, L., "Understanding FACTS, Concepts and Technology of Flexible AC Transmission Systems", IEEE Press, 2000.

[6] MATPOWER 3.0: R.Zimmerman , D.Gan. "Matpower-A Matlab power system simulation package". www.pserc.cornell.edu/matpower/

[7] B.H.Lee and K.Y.Lee . "Dynamic and static voltage stability enhancement power system," IEEE Trans. Power Syst., vol .8, pp .231-238, Feb. 1993.

[8] P.Kessel and H. Glavitch, " Estimating the voltage stabity of power system ," IEEE Trans. Power Deliverly, vol .1,pp.346-354, july 1986.

[9] R.A .Schlueter, I . Hu, M.W.Chang and A.Costi, "Method for determining proximity to voltage collapse, " IEEE Trans. Power syst., vol. 6, pp. 285-291, Feb . 1991.

[10] H.Ambriz-Perez, E.Acha, C.R.Fuerte-Esquivel, "Advanced SVC models for Newton –Raphson Load Flow and Newton Optimal Power Flow Studies", IEEE Trans. on Power Systems,2000.

[11 "Optimal location of SVC based on system loadability and contingency analysis", jurado, F.Rodriguez, J.A. department of electrical engg , University of Jaen, 23700EUP linares, (Spain).

[12] H.D Chiang, C S Wang, A J Flueck, " Look ahead voltage and load margin contingency selection function for large scale power systems", IEEE Tran. Power systems, vol. 12. no.1, Feb 1997, pp.173-180.

[13]. G C Ejebe, G D Irisarri, S Mokhtari, O Obadina, P Ristanovic, J Tong "Methods for contingency screening and ranking for voltage stability analysis of power systems", Power Systems IEEE Transactions on (1996) Volume: 11, Issue: 1, Pages: 350-356

◈◈◈

Economic Dispatch - A Comparative Study

Apoorva H., Garima Sinha, Punam Dam, Amrita Pradhan & Rrajender Reddy K.

Department of Electrical & Electronics, Dayananda Sagar College of Engineering,Bangalore, India.
E-mail : garima.sinha111@gmail.com, raju.jyothi.siri@gmail.com

Abstract - In this paper we are comparing the widely used Heuristic Method and Genetic Algorithm with a faster and effective non-iterative "λ-Logic Based" algorithm for ED (Economic Dispatch) of Thermal Units. The non-iterative method uses pre-prepared data to obtain the solution for a specified power demand. Genetic Algorithm performs directed random searches through a given set of alternative with the aim of finding the best alternative with respect to the given criteria of goodness. In this paper ED problem is solved using iterative method by Heuristic method , Non-iterative approach by "λ- logic Based" technique and genetic Algorithm approach (GA) .The proposed algorithms are tested on 3 and 38 bus system using MATLAB software and the results reported in the paper.

Keywords:

ED = Economic Dispatch, P_D = Power demand on a plant, PPD= Pre- prepared power demand data
dF_i/dP_{i-} = Incremental fuel cost of i^{th} unit

I. INTRODUCTION

Economic dispatch(ED) is the scheduling of generators to minimize the total operating cost depending on equality and inequality constraints. Many techniques have been applied to ED to obtain better solutions [1] to [19]. These include the λ-iteration method, the base point and participation factors method, gradient method, λ-Logic based method and genetic algorithm (GA) method[16]. The λ-Logic based method[19] and GA based method employ pre-prepared data to obtain the solution very fast for a specified power demand (=P_D). The actual support for such fast solution is the pre-prepared data in both λ-Logic based method and GA method. This paper mainly constitutes and compares the three methods and the effectiveness and the best possible method is discussed.

II. PROBLEM FORMULATION

Suppose that we wish to determine the economic operating point for this 3 units when delivered a total of 800 MW before this problem can be solved, the fuel cost of each unit must be specified. Consider the following 3 units

$F1\ (P_1) = 510 + 7.20\ P_1 + 0.00142\ P_1^2$

$F2\ (P_2) = 310 + 7.85\ P_2 + 0.00194\ P_2^2$

$F3\ (P_3) = 78 + 7.97\ P_3 + 0.00482\ P_3^2$

$dF1/dP_1 = 7.2 + 0.00284\ P_1 = \alpha_1 + \beta_1.$

$(150 \leq P_1 \leq 600\ MW)$

$dF2/dP_2 = 7.2 + 0.00388\ P_2 = \alpha_2 + \beta_2.$

$(100 \leq P_2 \leq 400\ MW)$

$dF3/dP_3 = 7.2 + 0.00964\ P_3 = \alpha_3 + \beta_3.$

$(50 \leq P_3 \leq 200\ MW)$

and $P_1 + P_2 + P_3 = 800MW$

solving for λ, obtains λ=8.66781

And then solving for P_1, P_2 and P_3

$P_1 = 516.834MW$

$P_2 = 210.775MW$

$P_3 = 72.3873MW$

We observe that all constraints are met; i.e., each unit is within its high and low limits and the total output when summed over all three units meets the desired 800MW total.

Method I:

In this method, the problem is solved using the iterative Heuristic Method [11]. Here, the initial value of λ is assumed.

Method II:

In this method, the problem is solved using the Genetic Algorithm[16]. The Genetic principles "Natural

Selection" and "Evolution Theory" are main guiding principles. Here, the initial value of λ is assumed and a search space is specified. The three most important aspects of Genetic Algorithm are:

1. Definition of Objective function
2. Definition and implementation of Genetic Representation
3. Definition and implementation of Genetic Operators

ALGORITHM

STEP 1.a) Read no. of units (K), Power Demand (P_d), a_i, b_i, c_i, P_{imin}, $P_{imax}$where i=1 to K, itermax, String length (SL), population size (NC), Crossover probability, Elitism probability, Mutation probability.

b) Initialize the guess value λ_{imin} and λ_{imax}.

STEP 2. Generate the initial population of chromosomes of binary bits with random number generation technique.

STEP 3. Set iteration count i=1.

STEP 4. Set the chromosome count j=1.

STEP 5. Decode binary bits of this of population

(λ*) and calculated the λ_{act} from λ*.

$$\lambda^* = \sum_{i=1}^{SL} \{d_i * 2^{-i}\} \qquad (1)$$

$$\lambda_{act} = \lambda_{min} + \lambda^* (\lambda_{max} - \lambda_{min})$$

STEP 6. Calculated powers of all the units using this value of λ_{act}.

STEP 7. Check power limits of all units

If $P_i > P_{imax}$ then set $P_i = P_{imax}$

If $P_i \geq P_{imin}$ then set $P_i = P_{imin}$

STEP 8. Calculate

$$Err[i] = \left| \sum_{i=1}^{k} P_i - P_d \right| \qquad (2)$$

$$Fit[i] = 1/\{1+Err[i]) / P_d\}$$

STEP 9. Increment the iteration count i, if i<NC go to step 5.

STEP 10. Sort the chromosomes and all their related data in the descending order according to their fitness.

STEP 11. Checks Err [0] < $(0.0001*P_d)$

STEP 12. If the step 11 is satisfied then print the result of P_i, λ_{act}, Total Fuel Cost.

STEP 13. Check if Fit [0] =Fit [NC]

STEP 14. If the step 13 is satisfied then print "All chromosomes have identical data, problem converged".

STEP 15. Perform the crossover on the two selected parents and generate new child Chromosomes.

STEP 16.Repeat step 15, for required number of times.

STEP 17. Now, copy the P_e % of chromosomes of old population to new population starting from the top.

STEP 18. Add all the generated child chromosomes.

STEP 19. Perform mutation on all the chromosomes.

STEP 20. Now replace old population with new Population.

STEP 21. Increment iteration count.

STEP 22. If i<itermax, go to step 4.

STEP 23. If iterations count is greater than maximum number of iterations initialized, then say that Maximum number of iterations is reached, problem not converged".

STEP 24. STOP

Method III

ALGORITHM

STEP 1 a) Read no. of units k, a_i, b_i, P_{min}, P_{max} for i =1 to k.

b) Calculate $\alpha_i = b_i$ and $\beta_i = 2* c_i$ for i= 1 to k.

STEP 2. Calculate $\lambda_{min} = \alpha_i + \beta_i * P_i$ at $P_i = P_{imin}$ and $\lambda_{imax} = \alpha_i + \beta_i * Pi$ at $Pi = P_{imax}$.

STEP 3. Arrange all λ values in ascending order.

STEP 4. j =1 i.e. λ_j is the least value.

STEP 5. Calculate P_i For i=1 to K and check

a. If $\lambda j \leq \lambda_{imin}$ then set $Pi = P_{imin}$,

b. If $\lambda j \geq \lambda_{imax}$ then set $Pi = P_{imax}$

c. If $\lambda_{imin} < \lambda_j < \lambda_{imax}$ then calculate

$$Pi = (\lambda_j - \alpha_i)/\beta_i$$

STEP *6. Calculate Pre-Prepared Demand (PPD) =*

$$\sum_{i=1}^{k} Pi \qquad (3)$$

STEP *7. Check j=2*k i.e. all λ values are considered if yes go to step 9.*

STEP *8. j = j+1 i.e., consider next higher λ value and go to step 5.*

STEP *9. Calculate slope m_j for two successive λ values $m_j = (\lambda_{j+1} - \lambda_j) / (PPD_{j+1} - PPD_j)$ for j=1 to 2k.*

STEP *10. Read Power Demand Pd value.*

STEP 11. If it lies within the limits goto step 12 otherwise go to step 18.

STEP 12. Find j and j+1 such that $PPD_j < P_d < PPD_{j+1}$.

STEP 13. Calculate $\Delta P = P_d - PPD_j$.

STEP 14. Calculate $\lambda_{new} = m_j * \Delta P + \lambda_j$.

STEP 15. Calculate P_i by using step 5 for λ_{new} i=1.

STEP 16. Print the result Pi λ_{new}, Total Fuel Cost.

STEP 17. Want to change Power Demand go to step 10.

STEP 18. Print that the "demand is not in between the limits".

STEP 19. Stop.

III. RESULTS AND DISCUSSIONS:

The effectiveness of proposed methods are tested with two different test data. The data consists of 3 generators and 38 generator systems. Considering 3 units systems, the data of the system is given in [19] and results are given in the table (3.1). Considering 38 units systems, the data of the system is given in [19] and results are given in the table (3.2)

	Heuristic Method	Genetic Algorithm	NON-Iterative
Number of Iterations	8	10	1
Initial Guess Value (λ.0)	8	λmin=8 λmax=10	No need
Final Value (λ. actual)	8.66781	8.667725	8.66781
P1	516.834	516.8045	516.836
P2	210.775	210.7538	210.777
P3	72.3873	72.3781	72.3873
Pgen	800	799.94	800
Total Fuel Cost ($/Hr.)	7341.49	7340.94	7341.49

TABLE 3.2: Comparison of test results for 38 units (Power values are in MW)

	Heuristic Method	Genetic Algorithm	Non-Iterative
Number of iterations	3999	5	1
Initial Guess Value(λ_{actual})	1060	$\lambda_{min \to 1060}$ $\lambda_{max \to 1070}$	No need
Final value(λ_{actaul})	1064.211	1064.216	1064.21
P_1	426.605	426.613	426.606
P_2	426.605	426.613	426.606
P_3	429.663	429.67	429.663
P_4	429.663	429.67	429.663
P_5	429.663	429.67	429.663
P_6	429.663	429.67	429.663
P_7	429.663	429.67	429.663
P_8	429.663	429.67	429.663
P_9	114	114	114
P_{10}	114	114	114
P_{11}	119.767	119.771	119.768
P_{12}	127.072	127.076	127.073
P_{13}	110	110	110
P_{14}	90	90	90
P_{15}	82	82	82
P_{16}	120	120	120
P_{17}	159.598	159.598	159.598
P_{18}	65	65	65
P_{19}	65	65	65
P_{20}	272	272	272
P_{21}	272	272	272
P_{22}	260	260	260
P_{23}	130.648	130.651	130.649
P_{24}	10	10	10
P_{25}	113.304	113.307	113.305
P_{26}	88.066	88.068	88.0666
P_{27}	37.505	37.505	37.505

P_{28}	20	20	20
P_{29}	20	20	20
P_{30}	20	20	20
P_{31}	20	20	20
P_{32}	20	20	20
P_{33}	25	25	25
P_{34}	18	18	18
P_{35}	8	8	8
P_{36}	25	25	25
P_{37}	21.7782	21.782	21.062
P_{38}	21.062	21.062	21.062
P_{gen}	5999.999	6000.077	6000.001
Total fuel cost($/Hr)	91417234	9417317	9417236.9

From the results of table 3.1 reveals the followings observations. All the three proposed methods give λ_{actual} value same but number of iterations taken to converge the solution is different. For a guess value of (λ^0) 8 for ED (ECONOMIC DISPATCH) of units for power demand 800MW,The Heuristic method has taken 8 iterations, Genetic Algorithm has taken 10 iterations and Non-Iterative method though it is not given any initial guess value (λ^0).It is converged in one iteration only. Here the power demand must be specified in pre-prepared data (PPD_1 to PPDj) limits only. If we assume the worst guess value of (λ^0), Heuristic and Genetic Methods may take more number of iterations to converge into solution. Sometimes this may lead to divergence of the solution. If we observe, the total power generation and the Fuel cost, there is no considerable difference in results. As the λ_{actual} value is same for all proposed methods, load sharing among 3 units for 3 methods are almost same.

From the results of table 3.2 reveals the followings observations.

All the three proposed methods give λ_{actual} value same but number of iterations taken to converge the solution is different. For a guess value of (λ^0) 1060 for ED (ECONOMIC DISPATCH) of units for power demand 6000MW,The Heuristic method has taken 3999 iterations, Genetic Algorithm has taken 5 iterations and Non-Iterative method though it is not given any initial guess value (λ^0).It is converged in one iteration only. If we assume the worst guess value of (λ^0), Heuristic and Genetic Methods may take more number of iterations and sometimes divergence of the solution may take place. As calculations are more in 38 unit system, the computation time is very large. By using Genetic Algorithm, to converge the solution very fastly and to reduce the number of iteration. The search space(λ limits),search points,mutation,cross-over and elitism probabilities must be appropriately selected.Therefore,an expert is needed to use GA method. By using non-iterative method, though it is initially calculating all the necessary data(Pre-Prepared),it is calculating only once If we specify the power demand within the pre-prepared data limits(i.e.PPD_1 to PPDj),the problem is converged into solution in only one iteration.Finally,we can observe the total power and total fuel cost that there is no considerable difference in results. As the λ_{actual} value is same for all proposed methods, therefore load sharing among 38 generators for 3 methods are almost same.

IV CONCLUSION

The paper has been an attempt to solve the Economic Dispatch problems using Iterative technique, Genetic Algorithm and Non-Iterative Technique.

Using any conventional method such as λ- updation method the disadvantages are a worst initial guess value which leads to divergence of the solution, slow convergence with large number of iterations and experienced persons are required to choose a good guess value. The paper then deals with Genetic Algorithm technique which is better than Heuristic method. The final stage of paper as explained the "Non- Iterative λ-based" method.

The paper has compared the results obtained by using the above three methods and views out the superiority of “Non-Iterative λ – logic based" method and it was the best method when compared with conventional and GA methods.

REFERENCES

[1] T.Yalcinoz, M.J.Short, “Large Scale Economic Dispatch using an improved Hopfield Neural Network”.IEE Proc.Gener. Tran .Disturb Vol.144 No.2. March 1997,PP 181-185.

[2] Hong-Tzer Yang Pai-Chuan yang, Ching-Lien Haang. “A Parallel Genetic Algorithm Approach to solving the unit commitment problem : Implementation on the Transpoter Networks,”IEEE transactions on Power Systems,Vol 12 No 2,May 1997.

[3] Kumar .J.and Sheble,G.B "Clamped State Solution of Artificial Neural Network for Real-Time Economic Dispatch", IEEE Transactions on Power Systems,1995,10 (2),PP 925-931.

[4] Park J.H.KIM,Y.S, ECM.I.K, and LEE, K.Y.,"Economic Load Dispatch for Piecewise Quadratic Cost Function using Hopfield Neural Network", IEEE Transaction on Power Systems,1993,8(3),PP 1030-1038.

[5] Sendaula M.H., Biswas,.S.K., Eltom.A, Parten.C. and Kazibwe W., "Simulatneous Solution of Unit Commitment and Economic Dispatch Problems using Artificial Neural Networks". Electrical Power Energy and Systems. 1993,15(3), PP 193-199.

[6] Luis Vargas. Victor H. Quintana,Anthony Vanneli. "A Tutorial Description of an Interior Point method and its application to Sevurity Constrained Economic Dispatch", IEEE Transactions on Power Systems. Vol.8, No.3, August 1993,PP 1315-1324.

[7] Chowdhury, B.H. and Rahman, S., "A Review of Recent Advances in Economic Dispatch", IEEE Transactions on Power Systems. Vol. , No.4,PP 248-1259,Nov 1990.

[8] Aoki.K and Satoh T., "New Algorithm for classic Economic Dispatch", IEEE Transactions on Power Apparatus and Systems. Vol. PAS-103. No.6. PP 1423-1431 , June 1984

[9] Mota-Palomino,R., and Quintana, V .II., "A Penalty Function Linear Programming Method for Solving Power System Constrained Economic Operation Problems", IEEE Transactions on Power Apparatus and Systems, Vol. PAS-103, No-6, Ppp.1414-14222. June 1984.

[10] Happ M.M "Optical Power Dispatch –A Comprehensive Survey", IEEE Transactions on Power Apparatus and Systems. Vol. PAS-91, No3.PP.841-854, May/June 1977.

[11] Wood A.J and Wollenberg . B.F. "Power Generation Operation and Control".(John Wiley and Sons ,New York,1984).

[12] C.L. Wadhwa, "Generation,Distribution and Utilisation of Electrical Energy", New Age International Publishers.

[13] M.L. Soni, P.V. Gupta, U.S Bhatnagar and A.Chakrabarti. "A Text Book On Power Systems Engineering",Dhanpat Rai and Sons (P) Ltd.

[14] J.B Gupta. "Course in Power Systems".S.K Kataria and Sons (P) Ltd.

[15] D.P. Kothari and I.J.Nagarath. "Modern Power System Analysis" Tata McGraw-Hill Publishing Company Ltd.

[16] S.Rajashekharan and G.A Vijayalaxmi Pai. "Neural Networks, Fuzzy Logic and Genetic Algorithm(Synthesis and Application)". Prentice-Hall of India(P) Ltd.

[17] John J.Grainger and William D. Stevenso, JR. "Power System Analysis".McGraw-Hill International Editions.

[18] Arthor R.Bergen and Vijay Vittal. "Power System Analysis".Pearson Education.

[19] Maheswarapu Sydulu. "A Very Fast and Effective Nom-Iterative λ-Logic Based Algorithm for Economic Dispatch of Thermal Units". IEEE Transactions on Power Systems. June 1999,PP 1434-1437.

◈◈◈

Alternate Derivation of Condition for Minimum Angle of Deviation

Molla Ramizur Rahman

Department of Electrical & Electronics Engineering,
Dayananda Sagar College of Engineering, Bangalore, India
E-mail: ramizurscience@yahoo.com

Abstract - In optics, the condition for minimum angle of deviation for light passing through a prism has been derived using maxima and minima, a concept belonging to the topic of calculus from the branch of mathematics. Unlike the traditional method of using geometry for deriving the relation, a new approach has been adopted which explains the wide application areas of calculus and also links calculus to optics.

Keywords*-maxima; minima; calculus; minimum deviation.*

I. INTRODUCTION

Optics has become an integrated part of physics which deals with the behavior of light. Newton worked on the particle nature of light while Dutch physicist Christian Huygens worked on the wave nature of it. Optics finds its application in a wide range, from human eye (biological nature) to astronomical telescopes (cosmological scale). Many great scientists like Snell have contributed to this field alongside Huygen. The known interaction of light with matter is in the form of three phenomenon – reflection, refraction and absorption. While reflection is the bouncing back of light in the same media from where it comes, refraction is the passage of light through a media. Absorption is the phenomenon of the loss of light in a media.

Various laws were formulated as research on optics progressed with time. The basic law of this field is the Snell's law [1,2,5], which states that the ratio of sine function of angle of incidence to the sine function of angle of refraction for a pair of media is constant and is known as the refractive index of the second media with respect to first media which is being represented as μ. The other important law regarding this is that the incident ray, refracted ray and normal at the point of incidence, all are coplanar. By term coplanar, we mean a plane which contains all the three, that is, the incident ray, refracted ray and normal lie in the same plane. Snell's law is based on the phenomenon of refraction.

Here, the condition for minimum angle of deviation through a prism in a theoretical process using calculus, taking into consideration the concept of maxima and minima, has been obtained which was previously accomplished using geometry.

II. DERIVATION OF CONDITION FOR MINIMUM ANGLE OF DEVIATION USING CALUCULUS

Consider a rectangular base prism XYZ as shown in fig. 1, where angle a as the angle of prism. Let AB be

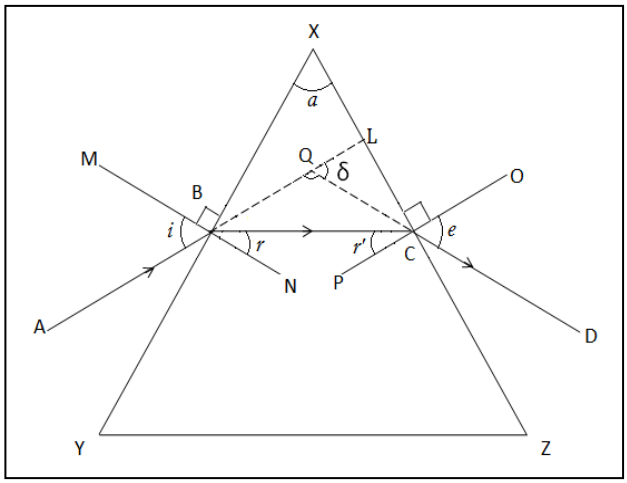

Figure 1: Diagram depicting the path of light refracting through a rectangular base prism.

the incident ray, BC be the refracted ray and CD be the emergent ray. Here, the angle of incidence is i and angle of emergence is e. MN and OP represent the normal drawn on the surface XY and XZ respectively. Let δ be the minimum angle of deviation. We need to find the

condition for which the angle of deviation, δ, is minimum.

From fig. 1

$$\angle ABM = i$$

$$\angle NBC = r$$
$$\angle OCD = e$$
$$\angle PCB = r'$$

$\angle NBL = \angle ABM$ [Vertically opposite angles are equal]

$\Rightarrow \angle NBL = i$

From the fig1,

$$\angle NBL = \angle NBC + \angle QBC$$
$$i = r + \angle QBC$$
$$\Rightarrow \angle QBC = i - r$$

$\angle QCP = \angle OCD$ [Vertically opposite angles are equal]
$\Rightarrow \angle QCP = e$

From the fig1,

$$\angle BCP + \angle QCB = \angle QCP$$
$$\Rightarrow r' + \angle QCB = e$$
$$\Rightarrow \angle QCB = e - r'$$

In ΔXBC,

$$\angle BXC + \angle XBC + \angle XCB = 180^0$$

[Sum of three angles in a triangle]

$\Rightarrow a + 90^0 - r + 90^0 - r' = 180^0$

$\Rightarrow a = r + r'$ (1)

In ΔQBC,

$\angle QBC + \angle QCB = \angle CQL$ [external angle of a triangle is equal to the sum of opposite interior angle]

$i - r + e - r' = \delta$

$\Rightarrow \delta = i + e - (r + r')$

substituting $a = r + r'$ [from (1)]

$\Rightarrow \delta = i + e - a$ (2)

Differentiating equation (1) with respect to r

$\Rightarrow \frac{da}{dr} = \frac{dr}{dr} + \frac{dr'}{dr}$

Since, 'a' is constant

$\therefore \frac{da}{dr} = 0$

$\Rightarrow 0 = 1 + \frac{dr'}{dr}$

$\Rightarrow \frac{dr'}{dr} = -1$ (3)

Differentiating equation (2) with respect to i

$\Rightarrow \frac{d\delta}{di} = \frac{di}{di} + \frac{de}{di} - \frac{da}{di}$

$\Rightarrow \frac{d\delta}{di} = 1 + \frac{de}{di}$ (4)

To get minimum angle of deviation,

$\frac{d\delta}{di} = 0$

Equating the above value in eq (4) we get

$\Rightarrow 0 = 1 + \frac{de}{di}$

$\Rightarrow \frac{de}{di} = -1$ (5)

From laws of refraction

$\frac{\sin i}{\sin r} = \mu$ and $\frac{\sin e}{\sin r'} = \mu$

$\therefore \sin i = \mu \sin r$ (6)

and, $\sin e = \mu \sin r'$ (7)

Differentiating equation (6) with respect to i, we get

$\cos i = \mu \cos r \frac{dr}{di}$

$\Rightarrow \cos i\, di = \mu \cos r\, dr$ (8)

Differentiating equation (7) with respect to e

$\cos e = \mu \cos r' \frac{dr'}{de}$

$\Rightarrow \cos e\, de = \mu \cos r'\, dr'$ (9)

Dividing equation (8) by equation (9)

$\frac{\cos i\, di}{\cos e\, de} = \frac{\cos r\, dr}{\cos r'\, dr'}$

$\Rightarrow \frac{\cos i\, dr'}{\cos e\, dr} = \frac{\cos r\, de}{\cos r'\, di}$

$\because \frac{dr'}{dr} = \frac{de}{di} = -1$ [from equation (3) and equation (5)]

$\therefore \frac{\cos i}{\cos e} = \frac{\cos r}{\cos r'}$

Squaring both sides of the above relation, we get the following,

$\Rightarrow \frac{\cos^2 i}{\cos^2 e} = \frac{\cos^2 r}{\cos^2 r'}$

$\Rightarrow \frac{1-\sin^2 i}{1-\sin^2 e} = \frac{1-\sin^2 r}{1-\sin^2 r'}$

$= \frac{\mu^2 - \mu^2 \sin^2 r}{\mu^2 - \mu^2 \sin^2 r'}$ [multiplying μ^2 in the numerator and denominator]

$\because \sin i = \mu \sin r$ and $\sin e = \mu \sin r'$ from eq (6) and

eq (7) respectively

$\therefore \frac{1-\sin^2 i}{1-\sin^2 e} = \frac{\mu^2-\sin^2 i}{\mu^2-\sin^2 e}$

From ratio and proportion [3], we say

if $\frac{a}{b} = \frac{c}{d}$, then $\frac{a}{b} = \frac{a-c}{b-d}$

$\Rightarrow \frac{1-\sin^2 i}{1-\sin^2 e} = \frac{1-\sin^2 i-\mu^2+\sin^2 i}{1-\sin^2 e-\mu^2+\sin^2 e}$

$\Rightarrow \frac{1-\sin^2 i}{1-\sin^2 e} = \frac{1-\mu^2}{1-\mu^2}$

$\Rightarrow \frac{1-\sin^2 i}{1-\sin^2 e} = 1$

$\Rightarrow 1-\sin^2 i = 1-\sin^2 e$

$\Rightarrow \sin^2 i = \sin^2 e$

$\Rightarrow \quad i = e$

III. RESULT AND DISCUSSION

As existent, Snell's Law, has been used as a base for obtaining the minimum angle of deviation using a combination of geometry and calculus. Whenever a ray of light is incident on refracting medium of higher refractive index than the medium from which the ray of light is coming, then it undergoes refraction and the light travels through the refracting medium by bending towards the normal while entering the medium. The ray of light exhibits deviation away from the normal when it passes from a medium of higher refractive index to a medium of lower refractive index. The deviation, that is, bending of light ray towards or away from the normal depends on the refractive indices of the two media and also on the angle of incidence. The above results show that when a ray of light travels through a rectangular base prism (of higher refractive index then the air), the condition for minimum angle of deviation is dependent on the angle of incidence and the angle of emergence. It has been shown here that when the angle of incidence is equal to the angle of emergence, the deviation of the light ray travelling through prism is minimum.

IV. APPLICATION OF CALCULUS BASED PROOF

As mathematics is the language of physics, different methods are used for to prove various theorem, results and formulae. So, herein calculus has been used to prove the above result which stands far apart from the traditional method of using geometry. The new approach uses a great combination of geometry and calculus. With the help of the obtained results, refractive index and other properties for which refractive index is the base can be determined very accurately. The knowledge of the refractive index can then be used as a base for studying the properties of light and deviation of the light and its components. This may also find its application in determining different combinations for various purposes as in case of cars, satellites, aircrafts, appropriate refractive index of glass for the human eye, glass made utensils and many others.

V. CONCLUSION

Snell's Law, already existent, has been used for obtaining the condition for minimum angle of deviation for a ray of light which is refracted through the rectangular base prism using a combination of geometry and calculus. It is seen from the derivation that the minimum angle of deviation is achieved when angle of incidence and angle of emergence are equal. The new proof opens up a new dimension of linking and forming new and strong foundations between physics and mathematics. This makes our understanding of physics all new more focused and better. This new approach also gives hope for new approaches of obtaining the established ideas and results in the form of laws and theorems.

REFERENCES

[1] Halliday/Resnick/Walker, "Fundamentals of Physics", 6th ed. Extended, Wiley Publication, pp 833-860.

[2] HC Verma , "Concepts of Physics",Vol I, 6th reprint ,Bharti Bhavan Publications, pp 385-400.

[3] Hall and Knight, "Higher Algebra",Essential Books, pp 1-10

[4] Sears/Zimansky/Young "University Physics",6th ed., Narosa Publishing House, pp 750-766

[5] DB Singh, "Arihant AIEEE Physics", 2007 edition, Arihant Prakashan, pp 699-744

◈◈◈